

I. ORBITAL INTERPRETATION AND PROPERTIES OF THE
 $X^1\Sigma^+$, $a^3\Pi$, $A^1\Pi$ AND $^3\Sigma^+$ STATES OF BH

II. GAS PHASE REACTIONS OF FLUOROMETHYL CATIONS
WITH ETHYLENE AND BENZENE

Thesis by
Richard Joseph Blint

In Partial Fulfillment of the Requirements

For the Degree of
Doctor of Philosophy

California Institute of Technology

Pasadena, California

1972

(Submitted March 8, 1972)

To Barbara, Liesl and David

ACKNOWLEDGMENTS

Deep expressions of gratitude go to my advisors Drs. W. A. Goddard III and J. L. Beauchamp who have taught me much. Also I wish to thank the entire present and past MQM group members for programs and helpful discussions. I especially wish to express my gratitude to D. L. Huestis, T. B. McMahon and Dr. W. E. Palke for all the personal assistance rendered. And last, but not least, I thank the typists, Joyce Lundstedt and Adria Larson, who have assisted me greatly in the compilation of this.

ABSTRACT

"Ab initio" calculations have been carried out on the states of $BH(X^1\Sigma^+, a^3\Pi, A^1\Pi, \text{ and } ^3\Sigma^+)$ which dissociate to the ground states of B and H. The application of the G1 method (which is a special case of the GI method) was extended to handle five- and six-electron systems, and this method along with SOGI, CI and the GVB method was used to investigate the BH states. The effect of restricting the orbitals of the wavefunction to be basis functions for the irreducible representations of the spatial symmetry group leads to noncontinuous changes in the orbitals as a function of internuclear distance. And further it is noted that the removal of this restriction on the atomic wavefunction of boron leads to simple predictions of the forms of the wavefunctions, geometries of the molecules and characteristics of the potential curves for the BH_N molecules. On the basis of this the potential curves for the $a^3\Pi$ and $A^1\Pi$ states are correctly predicted to have humps and the 2A_1 and 2B_1 states of BH_2 are predicted to be bent and linear, respectively. Molecular properties for many of these wavefunctions have been calculated and correlated with changes in the orbitals as a function of internuclear distance.

Gas phase reactions and properties of fluoromethyl cations have been investigated using the techniques of ion cyclotron resonance spectroscopy (icr). Fluoride transfer reactions between substituted methyl cations are observed to be rapid and permit the determination of relative fluoride ion affinities, defined as the negative of the enthalpy change for

the reaction $\text{CH}_N\text{F}_{3-N}^+ + \text{F}^- \rightarrow \text{CH}_N\text{F}_{4-N}$. By combining available thermochemical data and our experimental results the following order for the fluoride affinities of the methyl cations is constructed: CF_3^+ (256.3 kcal/mole) $>$ CH_3^+ (252.0 kcal/mole) $>$ CH_2F^+ (243.6 kcal/mole) $>$ CF_2H^+ (242.8 kcal/mole). A measurement of the equilibrium constant for the reaction ($\text{CF}_2\text{H}^+ + \text{CH}_2\text{F}_2 \rightleftharpoons \text{CH}_2\text{F}^+ + \text{CF}_3\text{H}$) between the latter two ions has permitted their relative fluoride ion affinities to be accurately determined. Fluoride ion affinities are a means of determining carbonium ion stabilities.

With the general goal of understanding reactions involving electrophilic addition to π -systems the reactions of the fluoromethyl cations with ethylene, ethylene- d_4 and benzene- d_6 were investigated. The important process in each case involves addition of the fluoromethyl cation to the substrate to form a chemically activated intermediate which decomposes with loss of HF or H_2 . Rate constants for the reactions of the fluoromethyl cations with ethylene were determined using icr trapped ion techniques. In conjunction with ion ejection double resonance, product distributions for the reactions involving ethylene- d_4 and benzene- d_6 have been determined. Only in the case of the reactions of fluoromethyl cations with benzene- d_6 is the possibility of a distinctive reaction mechanism revealed from the isotopic product distributions.

TABLE OF CONTENTS

	Page
DEDICATION	ii
ACKNOWLEDGMENTS	iii
ABSTRACT	iv
 PART	
I. Orbital Interpretation and Properties of the $X^1\Sigma^+$, $a^3\Pi$, $A^1\Pi$ and $^3\Sigma^+$ States of BH	1
A. Introduction	2
B. Summary	3
C. Generalized Valence Bond View of the BH_N Series	7
D. Orbital Description of the Lower Excited States of the BH Molecule	24
E. Appendix 1	72
F. Appendix 2	77
II. Gas Phase Reactions of Fluoromethyl Cations with Ethylene and Benzene	125
A. Introduction	126
B. Experimental Methods	127
C. Gas Phase Ion Chemistry of the Fluoromethanes	128
D. Fluoromethyl Cation Reactions with Ethylene	142
E. Fluoromethyl Cation Reactions with Benzene	148
F. Relative Reactivities of the Fluoromethyl Cations	150
G. Summary	160

I. ORBITAL INTERPRETATION AND PROPERTIES OF THE
 $X^1\Sigma^+$, $a^3\Pi$, $A^1\Pi$ AND $^3\Sigma^+$ STATES OF BH

A. Introduction

The very pleasing results derived from the application of MO (the Hartree-Fock method) theory to predicting the structure and geometry of molecules (Walsh's rules),¹ to similarly producing an Aufbau principle² and to predicting the products of organic reactions (Woodward-Hoffman rules)³ suggests the application of an improved method to the further investigation of these rules. As a portion of an overall study relating to these problems the GI⁴ (and SOGI)⁵ methods have been applied in a detailed study of the ground ($X^1\Sigma^+$) and excited ($a^3\Pi$, $A^1\Pi$ and $^3\Sigma^+$) states of BH. Both correct dissociation of the wavefunction and single occupancy of the orbitals are two of the advantages which the GI method has which are lacking in the Hartree-Fock method.⁶ Consequently the method has been employed to obtain an orbital description of the molecular building process in the BH system which gives new insights into the factors which influence the structure and geometry of related molecules. Molecular properties for these wavefunctions have been calculated and analyzed in terms of changes in the individual orbital properties.

Section B is a summary and discussion of all work accomplished on the project. Comments will be about programs written and ideas and methods developed in the course of the project. Discussion of the implications of the orbital description for the BH_N series are discussed in section C. The details and discussions on actual calculations of the ground and excited BH states are contained in section D, and Appendix 1

and 2 discuss previous work done on the symmetry restricted and non-symmetry restricted calculations on the ground ($X^1\Sigma^+$) state of BH.

B. Summary

Several relevant implications about the symmetry restrictions which must be placed on the basis set in a G1 (nonorthogonal GVB) approach⁷ to independent particle wavefunctions were brought out by the calculations on the ground state of the BH system. Also the calculations on two of the excited states of the BH system show a hump (maximum) in their potential curves which were predicted in advance of the calculation. Also developed is a method of partitioning the properties of the wavefunction in terms of contributions from the individual orbitals. Considerable programming was required to complete these projects.

Programming. The initial requirement for calculations on the BH system was the construction of the first five- and six-electron G1 program. The program required development of a rapid density matrix⁸-forming method and a series of auxiliary programs to form the Hamiltonians and variationally solve for the optimum orbitals. Also investigated in some detail were extrapolation methods to improve convergence and another method of solving the variational equations. Also a nonorthogonal G1 configurational generating program was written to calculate the projected G1 calculation discussed in Appendix 2. Also the program to calculate the GI properties and projected GI properties was written incorporating into it previously written integral properties programs.⁹ Various other small subsidiary programs were developed as needed.

Symmetry Restrictions. A critical result obtained from these calculations involved the symmetry restrictions placed upon the basis set expansion used to describe the molecular wavefunction. For non-degenerate, totally symmetric many-electron wavefunctions, the orbitals of the Hartree-Fock wavefunction must belong to irreducible representations of the total spatial symmetry group.¹⁰ This restriction, although valid for the HF wavefunction, produces extremely erratic results (see Appendix 2) in the orbital description of the GI wavefunction. Removal of the restriction that each orbital be a symmetry function allows the orbital to incorporate basis functions of whatever symmetry will minimize the energy of the system. Expanding the basis set for a boron atom calculation to include basis functions of a symmetry which could not normally be incorporated into a HF wavefunction allowed the GI wavefunction for the atom to incorporate angular correlation-like terms into the wavefunction. It is important to note that the angular correlation-like terms were introduced into the wavefunction variationally. The G1 boron atom symmetry restricted wavefunction,

$$\psi_{G1} = \mathcal{A}[(1s1s' + 1s'1s)(2s2s' + 2s'2s)2p_z \alpha\beta\alpha\beta\alpha] ,$$

adjusted variationally to mix p_x character into the 2s orbitals so that the wavefunction can then be written as

$$\psi_{G1} = \mathcal{A}[(1s1s' + 1s'1s)((2s + 2p_x)(2s - 2p_x) + (2s - 2p_x)(2s + 2p_x))2p_z \alpha\beta\alpha\beta\alpha] ,$$

where the admixture of angular correlation provides a rather unique interpretation for the wavefunction. The orbitals derived from this type of symmetry unrestricted wavefunction transform smoothly as a function of

internuclear distance in the construction of the $X^1\Sigma^+$ state (see Appendix 2) and provide an orbital interpretation which provides a means of predicting the geometries and the form of their potential curves (see section C).

BH Molecular States. The electronic wavefunction for the ground ($X^1\Sigma^+$) and low-lying excited states ($a^3\Pi$, $A^1\Pi$, $^3\Sigma^+$) of BH have been calculated using the SOGI method.⁵ The potential curve of the $A^1\Pi$ state in the zero rotational level is found to have a hump of 0.150 eV at $R = 3.89 a_0$ (experimentally a hump of unknown size is found at $3.9 \pm 0.4 a_0$);¹¹ a smaller hump (0.026 eV) at $R = 4.92 a_0$ is also found in the calculation of a $^3\Pi$ potential curve. The presence of these humps was predicted on the basis of an orbital recoupling process which must occur as a function of internuclear distance in order to minimize the energy at the equilibrium internuclear distance. The calculated binding energies of the BH states are 3.272 eV ($X^1\Sigma^+$), 2.216 eV ($a^3\Pi$), a 0.502 eV ($A^1\Pi$). The $^3\Sigma^+$ state is unbound although it does exhibit a small unbound minimum.

Properties. The dipole moment, molecular quadrupole moment and electric field gradient for the different states are calculated as a function of internuclear distance. The dipole moment of the $X^1\Sigma^+$ state is especially interesting because the property has a minimum at about $R = 4 a_0$ and changes sign as a function of internuclear distance. The dipole moment is negative (B^+H^-) for all $R > 3 a_0$; however at shorter internuclear distances it becomes positive and compares quite favorably with the experimental value of 1.27 ± 0.21 D (calculated value at

$R = 2.5 a_0$ is 1.25 D).¹² All the properties are discussed in terms of individual orbital contributions which are defined as

$$\langle P_i \rangle \equiv \langle \Phi P_i O_{11} \Phi \rangle / \langle \Phi | O_{11} \Phi \rangle$$

where Φ is the product of the spatial orbitals and P_i is the one-electron spatial operation associated with the property and operating only on electron index i . The total property $\langle P \rangle$ is the sum of each of the individual orbital contributions. In each case the changes in the properties can be correlated to changes in orbital contributions.

Implications. The form of the boron atom wavefunction allows the prediction of the two Σ states being bonding and repulsive due to the spin coupling of the unpaired orbital of B to the hydrogen 1s orbital. In the case of the two Π states, the two orbitals $s+p_x$ and $s-p_x$ of the boron must recouple with the s orbital so that the $s+p_x$ and H_s orbitals are coupled into a singlet. This recoupling causes a hump (maximum) in the potential curve. A discussion of this is contained in the following section.

C. Generalized Valence Bond View of the BH_N Series

I. INTRODUCTION

The Aufbau or building-up principle combined with the Mulliken and Hund orbital correlation diagrams [1] has been very successful in leading to useful predictions of the symmetries of excited states of molecules and when combined with the Walsh diagrams [2] has been quite useful in predicting qualitatively the geometries of polyatomic molecules. These important concepts were developed in terms of molecular orbitals and based on the Hartree-Fock (HF) method for wavefunctions. Despite these successes, there are some difficulties with these interpretations since the

Hartree-Fock method leads to very poor wavefunctions as atoms are pulled apart (bond dissociation).

An alternative approach, the valence bond (VB) method, provides a proper description of bond dissociation but generally leads to poor quantitative results. We have modified the usual VB method by solving for the orbitals self-consistently as in the Hartree-Fock method [3, 4]. This leads to energies better than the Hartree-Fock values and in addition leads to a proper description of bond dissociation. This method {called the generalized valence bond (GVB) method [4]} leads to an orbital description closely related to the usual VB description and hence allows convenient interpretation of the wavefunction.

We find that simple analyses of the GVB wavefunctions of atoms leads to an Aufbau-type principle that allows qualitative predictions of the symmetries and geometries of the excited states of molecules. However, this Aufbau principle does not involve the Mulliken-Hund or Walsh-type correlation diagrams. This principle, which was developed from the results of ab initio GVB calculations [5] on BH, will be illustrated here for the case of BH_n molecules.

II. WAVEFUNCTION

For a system with two bonds, a valence bond (VB) configuration has the form

$$\mathcal{Q}[\phi_a\phi_b\phi_c\phi_d(\alpha\beta - \beta\alpha)(\alpha\beta - \beta\alpha)]$$

which we denote as

$$\begin{array}{|c|c|} \hline a & b \\ \hline c & d \\ \hline \end{array}$$

(here a and b are singlet paired as are c and d). These orbitals can be bonded more than one way and the valence bond wavefunction may be taken as

$$C_1 \begin{array}{|c|c|} \hline a & b \\ \hline c & d \\ \hline \end{array} + C_2 \begin{array}{|c|c|} \hline a & c \\ \hline b & d \\ \hline \end{array} . \quad (1)$$

where the orbitals are generally taken as (hybridized) atomic orbitals. In the generalized valence bond (GVB) method [3, 4] we use wavefunctions of the form in (1) but allow every orbital (including nonbonding orbitals) to be singly occupied (but nonorthogonal) and solve variationally for the optimum such orbitals (analogous to the procedure in HF). In addition, the coupling coefficients of (1) are optimized. (This procedure is used for various numbers of electrons and spins and has also been referred to as the SOGI method [3].) In diagrams of the type in (1),

$$\begin{array}{|c|c|} \hline a & b \\ \hline \end{array}$$

indicates singlet pairing of the orbitals ϕ_a and ϕ_b , and

$$\begin{array}{|c|} \hline a \\ \hline b \\ \hline \end{array}$$

indicates triplet pairing of the orbitals.

A. The B Atom

The usual Hartree-Fock (and valence bond) wavefunction for the ground state (2P) of B atom has the form

$$Q(\phi_{1s}^{\alpha}\phi_{1s}^{\beta}\phi_{2s}^{\alpha}\phi_{2s}^{\beta}\phi_{2pz}^{\alpha}) \quad (2)$$

(where Q is the antisymmetrizer or determinant operator). In the generalized valence bond (GVB) method we allow all orbitals to be different and replace the Q by a suitable operator to retain the proper permutational (Pauli Principle) and spin symmetry. The final wavefunction can be written in the VB-type form

$$\begin{aligned} & Q[(\phi_{1s}\phi_{1s'} + \phi_{1s'}\phi_{1s})(\phi_{sx}\phi_{s\bar{x}} + \phi_{s\bar{x}}\phi_{sx})\phi_{pz}^{\alpha\beta\alpha\beta\alpha}] \quad (3) \\ & = \mathcal{A}[\phi_{1s}\phi_{1s'}\phi_{sx}\phi_{s\bar{x}}\phi_{pz}(\alpha\beta - \beta\alpha)(\alpha\beta - \beta\alpha)\alpha], \end{aligned}$$

which we will denote as

$$\begin{array}{|c|c|} \hline 1s & 1s' \\ \hline sx & s\bar{x} \\ \hline pz & \\ \hline \end{array} \quad (4)$$

The orbitals ϕ_{1s} and $\phi_{1s'}$ are referred to as core orbitals since they are similar to the usual 1s orbital (but radially split). These core orbitals are essentially unchanged upon bond formation and will be ignored in the following.

The pz orbital (Fig. 1c) is essentially the same as the HF 2pz orbital, however the (2s) HF pair changes drastically upon going to GVB. These orbitals, sx and $s\bar{x}$, build in p character so as to attain the form

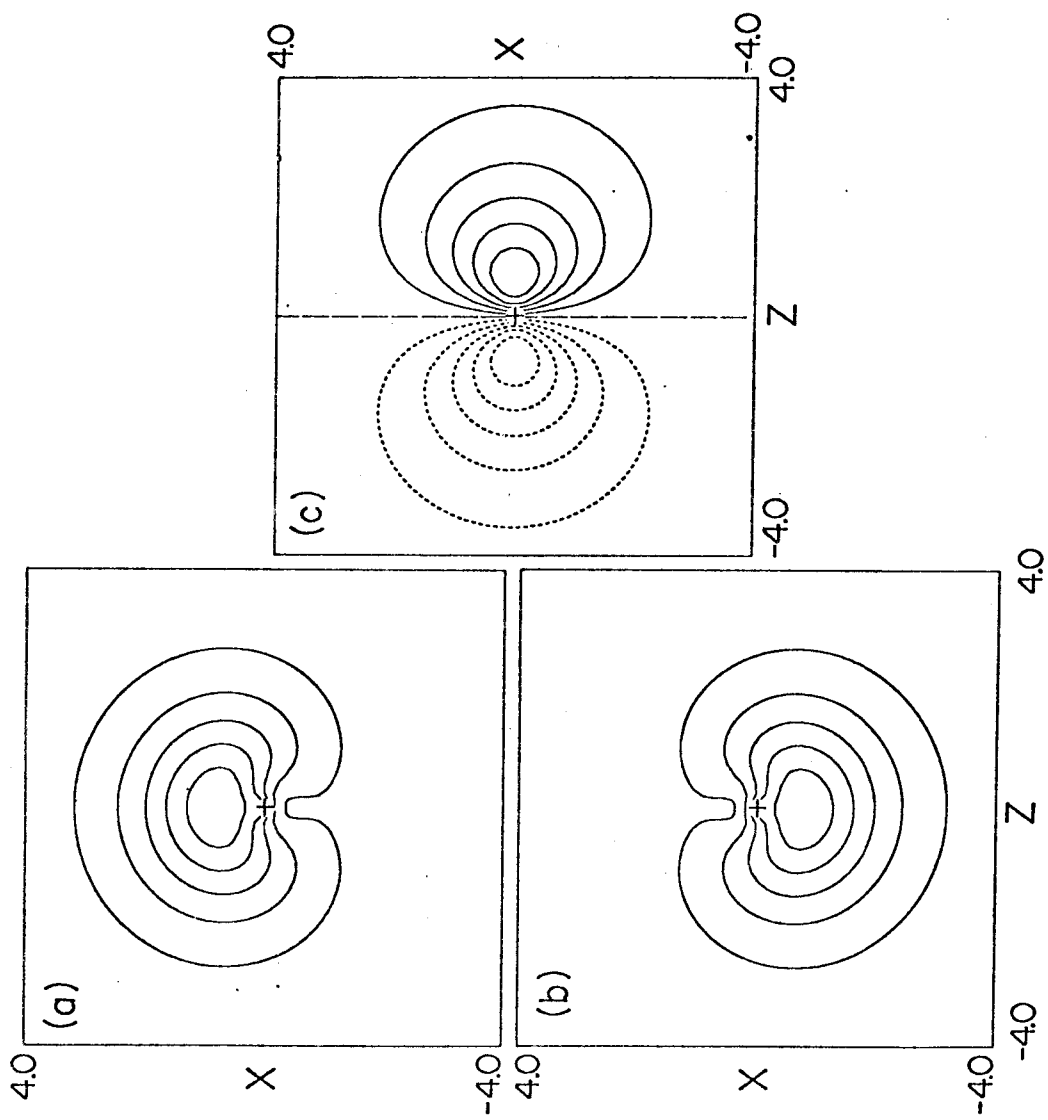


Fig. 1. The GVB valence orbitals of B atom (all quantities in atomic units).

$$\phi_{sx} = C_1\phi_{2s} + C_2\phi_{2px} \quad (5)$$

$$\phi_{s\bar{x}} = C_1\phi_{2s} - C_2\phi_{2px}$$

as shown in Fig. 1ab[5].

Combining the orbitals of (5) together, as in the many-electron wavefunction, leads to terms of the form [6]

$$\begin{aligned} \Psi_{(1,2)}^{\text{GVB}} &= \phi_{sx}\phi_{s\bar{x}} + \phi_{s\bar{x}}\phi_{sx} \\ &= C_1^2\phi_{2s}(1)\phi_{2s}(2) - C_2^2\phi_{2px}(1)\phi_{2px}(2) \end{aligned} \quad (6)$$

Consequently, when both electrons 1 and 2 are on the same side of the atom (say in the +x direction) the terms of (6) subtract, whereas they add when the electrons are on opposite sides of the atom. Thus the probability of the two electrons being on the same side is smaller than the probability of their being on opposite sides. This angular correlation [7] reduces the electron-electron repulsion energy (from that in HF) between these electrons and leads to a significant decrease in the energy {0.015h = 0.41 eV using (6) and 0.024h = 0.65 eV using the full symmetry [6]}.

In discussions of the B atomic orbitals it is convenient to represent them schematically as in Fig. 2a. Here the lobe orbitals sx and s \bar{x} are shown pointing away from each other and perpendicular to the pz orbital.

B. BH Molecule

Starting with the atomic orbitals of B and H we can form a $^1\Sigma$ state [8]

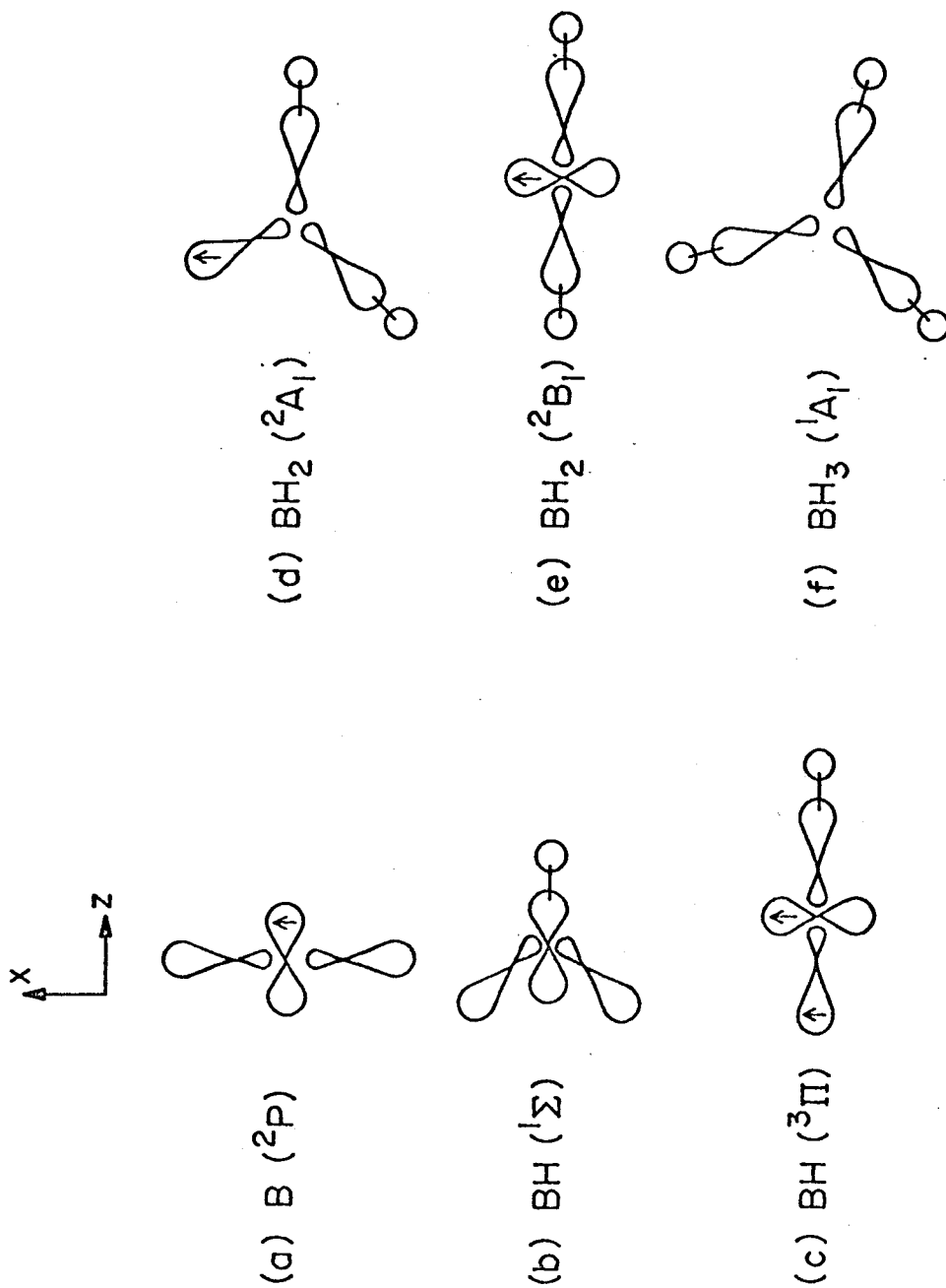


Fig. 2. Schematic representation of the orbitals of BH_n. A line connecting two orbitals indicates singlet pairing. An arrow indicates an unpaired orbital.

sx	s \bar{x}
pz	Hz

(7)

or a $^3\Sigma$ state

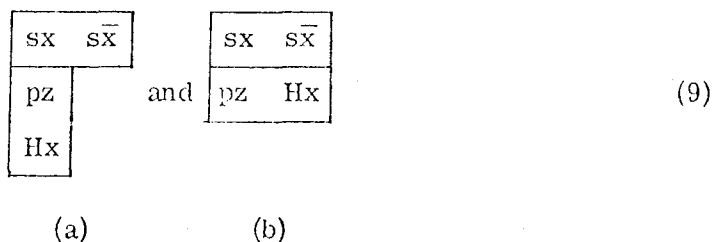
sx	s \bar{x}
pz	
Hz	

(8)

Since the pz and Hz orbitals have the same symmetry, the one-electron exchange terms should dominate the interaction energy, leading to a strongly bonding $^1\Sigma^+$ state and a repulsive energy curve for the $^3\Sigma^+$ state [9].

In Fig. 3 we show the orbitals for $^1\Sigma^+$ as a function of internuclear distance, R. Here we see that the Bpz orbital gradually delocalizes and hybridizes as the bond forms. As the bond is forming the nonbonding pair [sx, s \bar{x}] rotates out of the way of the bond. This serves to reduce the overlap between the bonding and nonbonding pairs and hence to reduce the repulsive interactions between these pairs. The final angle between each lobe and the bond is 125° . These orbitals are indicated schematically as in Fig. 2b.

Bringing the H in along the x axis leads from the atomic orbitals in (3) and (4) to



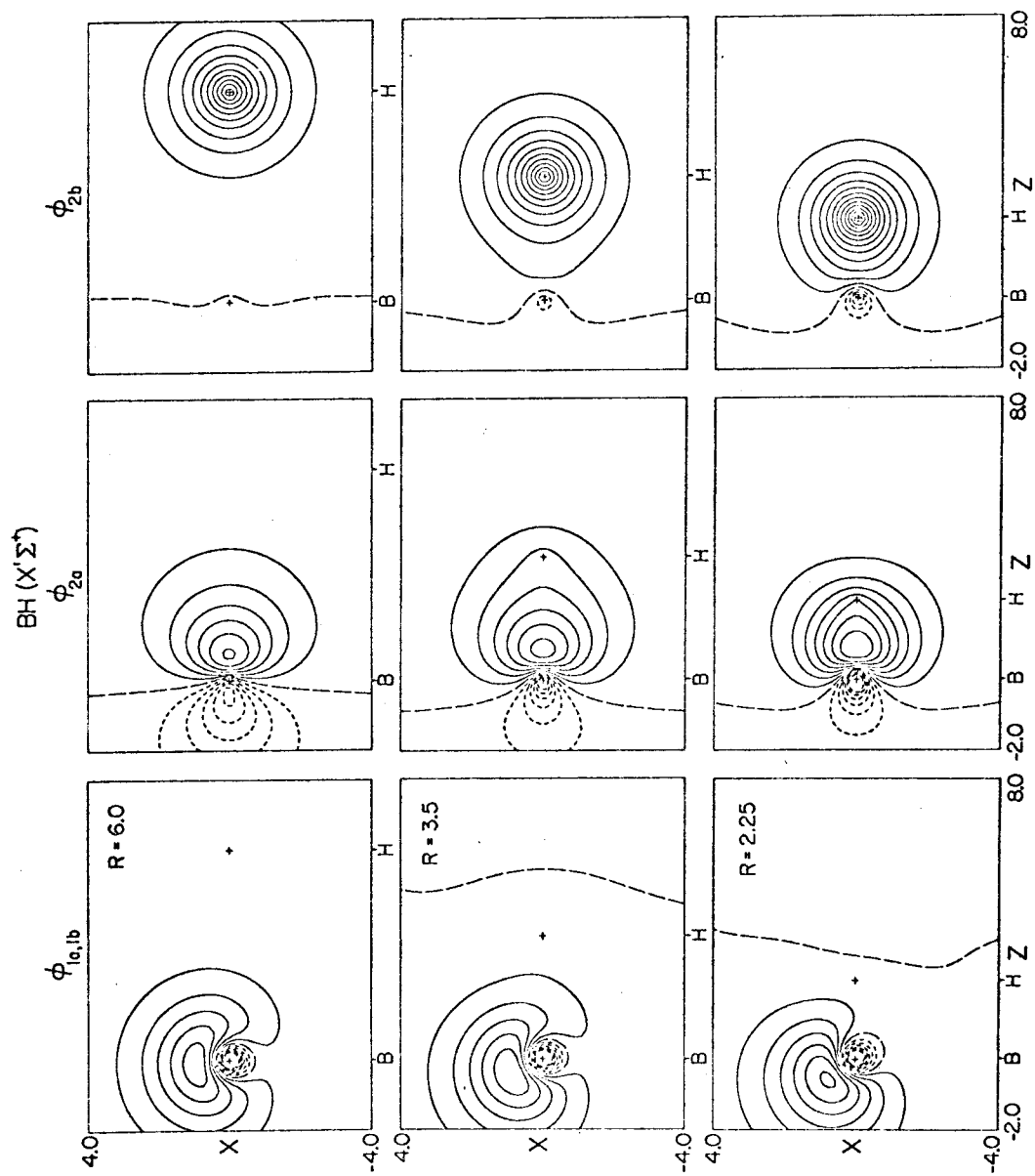


Fig. 3. The valence orbitals of the 1Σ state of BH as a function of R .

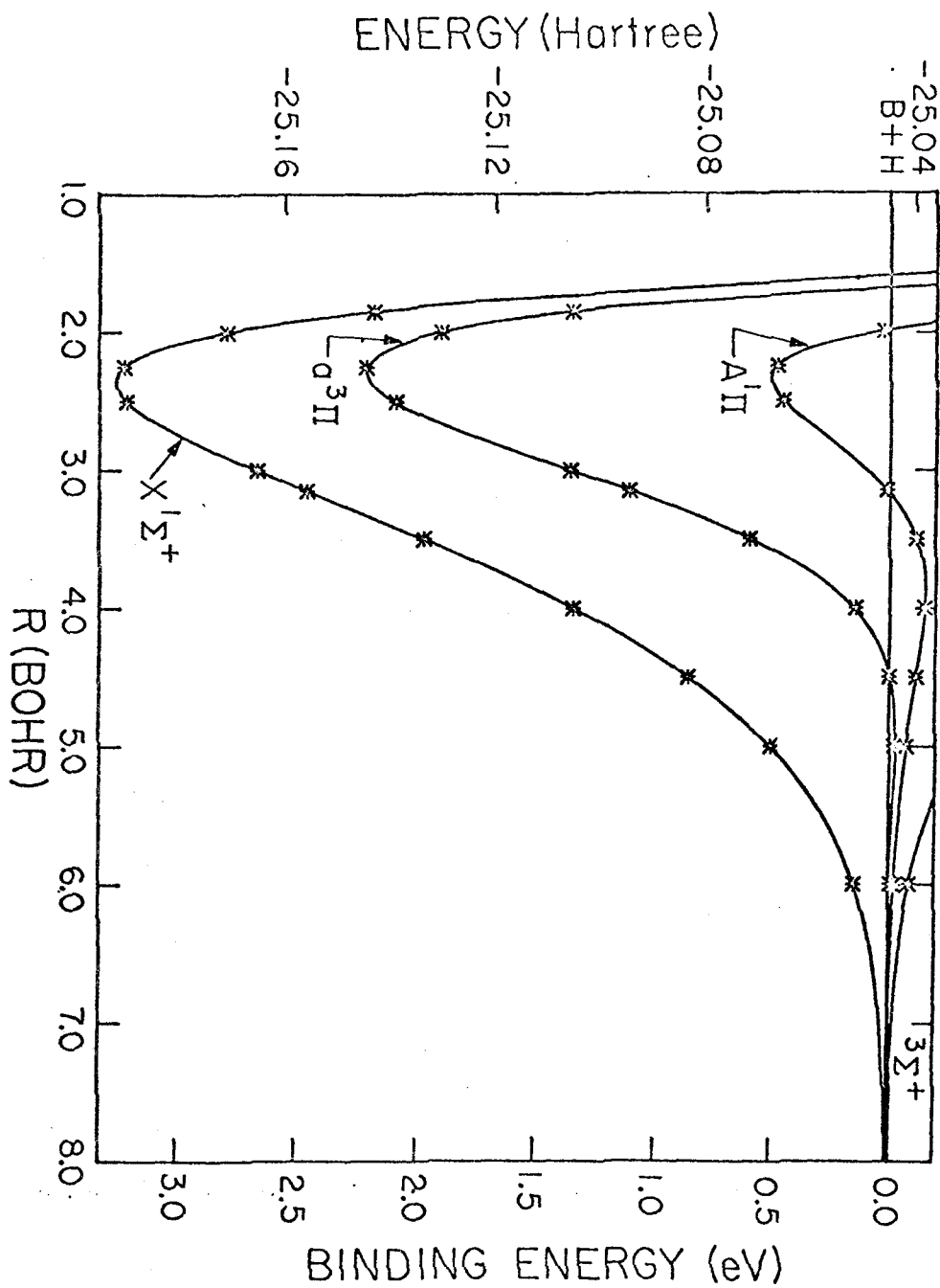


Fig. 4. The GVB energy curves for the low-lying states of BH.

which describe the $^3\Pi$ and $^1\Pi$ states, respectively. At large R , these couplings lead to repulsive energy curves since the overlapping orbitals Hx and sx are not singlet-paired (the repulsive terms are approximately proportional to the square of the overlap between ϕ_{Hx} and ϕ_{sx} [10] and are quite analogous to the repulsions between different pairs of orbitals that are responsible for rotational barriers in molecules.) However, for small R we can recouple the orbitals [11] of (9) as

$$\begin{array}{|c|c|} \hline \text{sx} & \text{Hx} \\ \hline \text{pz} & \\ \hline \text{s}\bar{\text{x}} & \\ \hline \end{array}
 \quad \text{and} \quad
 \begin{array}{|c|c|} \hline \text{sx} & \text{Hx} \\ \hline \text{pz} & \text{s}\bar{\text{x}} \\ \hline \end{array}
 \quad (10)$$

These couplings lead to attractive interactions between ϕ_{sx} and Hx that are approximately proportional to the square of their overlap. However, (10) also leads to repulsive interactions (approximately proportional to the square of the overlap) between $\phi_{\text{s}\bar{\text{x}}}$ and Hx (and between $\phi_{\text{s}\bar{\text{x}}}$ and ϕ_{sx}). Thus (10) can lead to bonding only if sx and $\text{s}\bar{\text{x}}$ are sufficiently different so that $S_{\text{sx}, \text{Hx}}$ is large while $S_{\text{s}\bar{\text{x}}, \text{Hx}}$ is small. However, as shown in Fig. 1, the atomic angular correlation leads to just such splittings in ϕ_{sx} and $\phi_{\text{s}\bar{\text{x}}}$, and hence we may expect bonding in the $^3\Pi$ and $^1\Pi$ states of BH. Indeed, these states are bound as shown in Fig. 4.

For large R the couplings in (10) cannot describe the ground state of the B atom. Consequently, the recoupling and concomitant bonding do not occur until R decreases enough so that the bonding interactions of sx and Hx overcome the effect of promoting the state of the B atom.

The orbitals for the $^3\Pi$ state are shown as a function of R in Fig. 5 (and indicated schematically in Fig. 2c). Here we see continuous changes in the orbitals with R . Indeed, comparing the orbitals at $R = 2.25 a_0$ (near R_e) with those at $R = \infty$, we see that the GVB orbitals of the molecule are rather close in shape to the GVB atomic orbitals, which justifies the analysis above [e.g., (9) and (10)].

Examining Fig. 5 closely we see that the singlet coupled pair (ϕ_{2a} and ϕ_{2b}) of the atom changes continuously into the bonding pair of the molecule while the nonbonding orbital on the H becomes the non-bonding orbital of the molecule. These changes are quite comparable to those that occur in chemical reactions (see ref. 4). Even the phase change expected (see refs. 4 and 12) in the nonbonding orbital (ϕ_{3a}) occurs. The potential humps in the Π states are quite analogous in origin to the activation energies of chemical reactions, and indeed the process $B + H \rightarrow BH$ corresponds to a highly exothermic addition reaction.

C. BH₂ and BH₃ Molecules

Starting with the orbitals of the ground state of BH, Fig. 2b, we must ask whether BH₂ should be stable and if so what geometry and symmetry should it have. Just as for the Π states of BH, we can form a strong bond by pairing the second H with one of the lobe orbitals of Fig. 2b, leading to Fig. 2d. Thus, we would expect BH₂ to be a 2A_1 state with a bond angle of about 125°. Some increase in this angle should occur due to overlapping of orbitals in different bonding pairs, and indeed the experimental bond angle [13] is 131° (theoretical calculations [14, 15] have led to 129°). A second state of BH₂ is obtained by starting with BH (${}^3\Pi$) and bonding the second H to the lobe orbital as indicated in Fig. 2e. This leads to the 2B_1 state of BH₂ which is indeed linear [13].

Starting with the 2A_1 state of BH₂ we would expect BH₃ to be planar with D_{3h} symmetry (after allowing for slight readjustments of the orbitals due to the new bond-bond interactions). At this point there are no more valence orbitals for bonding further H's. (However, we do have an empty π orbital that can be involved in coordinate bonds.)

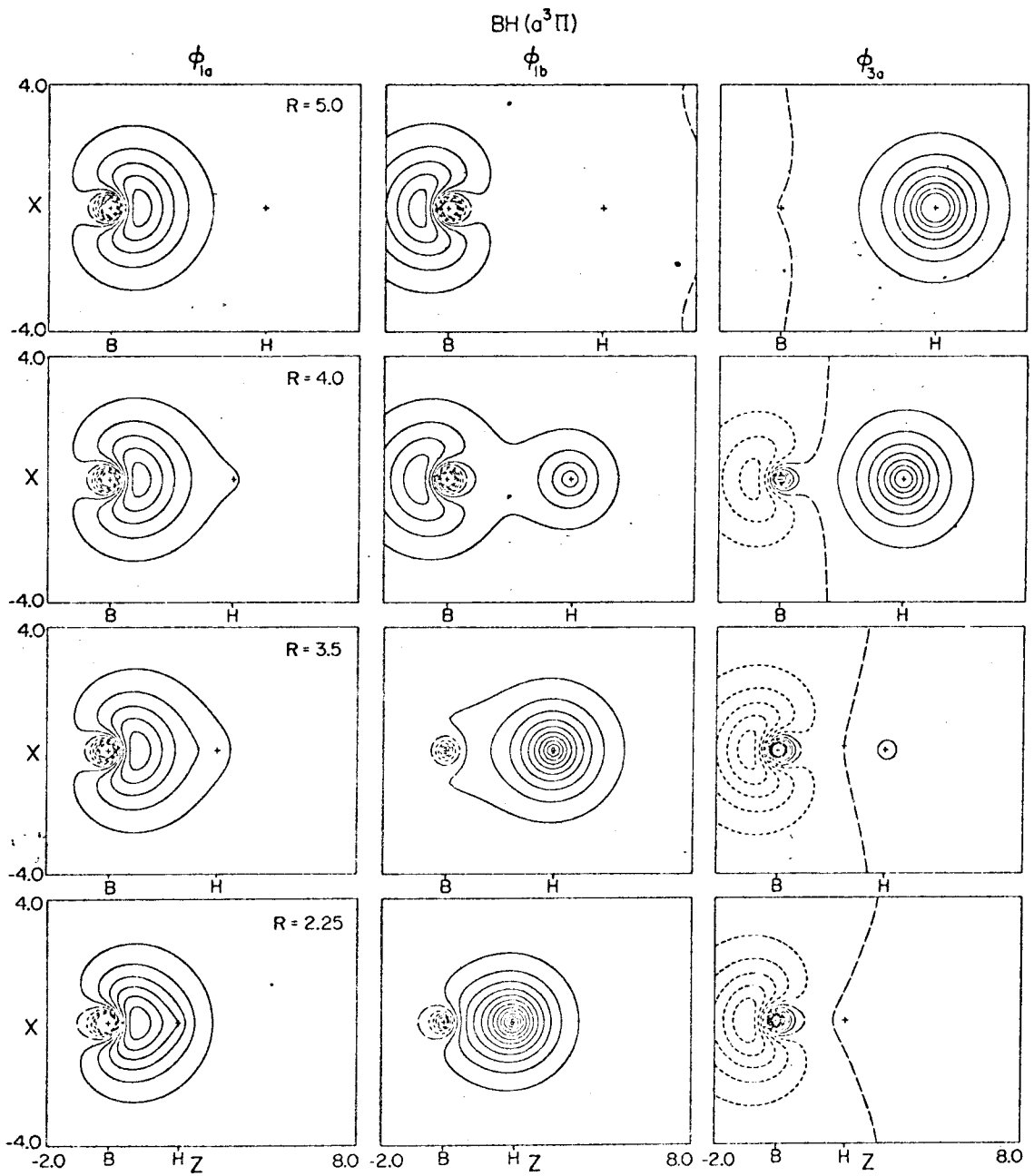


Fig. 5. The valence orbitals of the $\sigma^3\Pi$ state of BH as a function of R .

D. Energy Humps

Because of the recoupling involved in proceeding from (9) to (10), we expected and found an energy hump at large R . This hump is 0.15 eV for ${}^1\Pi$ and 0.03 eV for ${}^3\Pi$ and occurs at $3.9 a_0$ and $4.9 a_0$, respectively. The difference in the humps for these states is due to the difference in the exchange interactions between the nonbonding σ and π orbitals. By averaging, we obtain an exchangeless hump of about 0.09 eV at $4.4 a_0$.

In proceeding from $BH({}^1\Sigma)$ to $BH_2({}^2A_1)$ we have a similar recoupling. Thus for large R ($> 4.4 a_0$) we expect a repulsive energy curve regardless of orientation. However, for an angle of $\sim 125^\circ$ with respect to the bond axis and a second BH bond length of $\sim 4.4 a_0$, there should be a saddle point of about 0.03 to 0.09 eV in height. Inside this distance the energy should drop rapidly to that of BH_2 . On the other hand, for $BH({}^3\Pi) + H \rightarrow BH_2({}^2B_1)$, and $BH_2({}^2A_1) + H \rightarrow BH_3({}^1A_1)$, we expect no humps along the minimum energy path.

From the form of the rotational breakoffs for $A {}^1\Pi \leftrightarrow X {}^1\Sigma$ in BH , it has long been presumed that the $A {}^1\Pi$ state has a hump (at about $3.9 a_0$); however, the experiments do not yield the magnitude of the barrier [16]. No experimental results are available concerning humps in BH_2 and BH_3 .

III. DISCUSSION AND SUMMARY

From the GVB orbitals of B atom we can obtain qualitative predictions of the symmetries, geometries, and potential curves of the low-lying states of BH_n . Thus, the trivalent nature of B is already apparent in the orbitals of the ground state (2P) of B atom. There is no need to consider the presence of higher spectroscopic states to account for this trivalent character.

Similar analyses can be carried out for molecules formed from other atoms and lead to systematic predictions of the symmetries and geometries of large classes of polyatomic molecules. Thus valence-bond-type ideas can be used for predicting the sorts of things usually done with molecular orbitals in terms of Mulliken-Hund and Walsh-type correlation diagrams. In addition, the valence-bond ideas can be used for discussing processes involving bond dissociation. For example, this approach leads to correct predictions of the occurrences of energy humps.

REFERENCES

- [1] R. S. Mulliken, *Phys. Rev.* 32 (1928) 186, 761; *idem*, *Rev. Mod. Phys.* 4 (1932) 1; F. Hund, *Z. Physik* 40 (1927) 742; *ibid.* 42 (1927) 93; *ibid.* 51 (1928) 759; *ibid.* 63 (1936) 719.
- [2] A. D. Walsh, *J. Chem. Soc.* (1953) 2260, 2266, 2288, 2296, 2301, 2306, 2321, 2325.
- [3] (a) W. A. Goddard III, *Phys. Rev.* 157 (1967) 73; (b) R. C. Ladner and W. A. Goddard III, *J. Chem. Phys.* 51 (1969) 1073.
- [4] W. A. Goddard III and R. C. Ladner, *J. Amer. Chem. Soc.* 93 (1971) 6750.
- [5] R. J. Blint and W. A. Goddard III, *J. Chem. Phys.* 56 (1972) 000; these calculations used Gaussian basis functions with a primitive (11s5p3d/6s3p) set contracted to (7s3p1d/3s1p).
- [6] To retain the proper 2P symmetry of B, the second term of (6) must be replaced by

$$\frac{1}{\sqrt{3}} [\phi_{2p_x}^{(1)}\phi_{2p_x}^{(2)} + \phi_{2p_y}^{(1)}\phi_{2p_y}^{(2)} + \phi_{2p_z}^{(1)}\phi_{2p_z}^{(2)}].$$

However, the optimum orbitals using this form are essentially the same as those obtained using (5); hence no change occurs in the interpretation of the wavefunction.

- [7] J. Lennard-Jones and J. A. Pople, *Phil. Mag.* 43 (1952) 581.
- [8] To have the proper rotational symmetry (Σ) the $[sx, s\bar{x}]$ pair function of (7) and (8) should have the form $\{C_1^2\sigma(1)\sigma(2) - C_2^2[\pi_x(1)\pi_x(2) + \pi_y(1)\pi_y(2)]\}$. However, inclusion of π_y terms led to little change in the shape of the orbital, and they were not included in the calculations reported here.
- [9] As mentioned above, the splitting of the $(1s^2)$ core orbital has a negligible effect upon the bonding or interpretation of the wavefunctions. For this reason the core orbitals were kept doubly occupied in the calculations reported herein on BH. However, the orbitals shown in Fig. 1 come from a wavefunction in which the $1s$ pair was allowed to split. As a result the sx and $s\bar{x}$ orbitals in Fig. 1 are smooth in the core region whereas the corresponding orbitals of Figs. 3 and 5 have an orthogonality node.
- [10] C. W. Wilson, Jr. and W. A. Goddard III, *Chem. Phys. Letters* 5 (1970) 45; C. W. Wilson, Jr., Ph.D. thesis, California Institute of Technology, 1970.
- [11] In the GVB calculations reported here, we optimized the spin coupling (SOGI [3]) which leads to admixtures of other couplings [as in (1)] noted in (9) and (10). However, the qualitative interpretation is not changed.
- [12] W. A. Goddard III, *J. Amer. Chem. Soc.* 92 (1970) 7520; *ibid.* 94 (1972) 793.
- [13] G. Herzberg, *Molecular Spectra and Molecular Structure. III. Electronic Spectra and Electronic Structure of Polyatomic Molecules* (D. Van Nostrand Co., Inc., Princeton, New Jersey, 1967).

- [14] Calculations by L. R. Kahn and R. J. Blint; see L. R. Kahn and W. A. Goddard III, *J. Chem. Phys.* 56 (1972) 0000.
- [15] C. F. Bender and H. F. Schaefer III, *J. Mol. Spectrosc.* 37 (1971). 423.
- [16] G. Herzberg and L. G. Mundie, *J. Chem. Phys.* 8 (1940) 263; J. W. C. Johns, F. A. Grimm, and R. F. Porter, *J. Mol. Spectrosc.* 22 (1967) 435.

D. Orbital Description of the Lower Excited States of the BH Molecule

I. INTRODUCTION

A major objective in calculating electronic wavefunctions is to obtain qualitative concepts which allow one to predict the origins of the bonding and properties of various electronic states of molecules. A particularly useful approach leading to several important concepts has been the Hartree-Fock method which allows the wavefunction to be understood in terms of molecular orbitals occupied by the various electrons. Unfortunately the method often leads to erratic and inconsistent results (especially improper dissociation) for large internuclear separations, resulting in some difficulties in interpretation and in relating atomic and molecular properties.

The GI (and SOGI) (2) method is similar to Hartree-Fock in that the variational principle is applied and the orbitals are solved self-consistently; however, it places no overt restrictions on the many-electron wavefunction (especially double occupancy) and allows the wavefunction to dissociate properly. The SOGI wavefunction is similar to a valence bond wavefunction except that the orbitals are solved for self-consistently. Consequently, it is well suited for investigating the characteristics of a system from the separated-atom limit to the united-atom limit. In the past we have found these orbitals to be particularly useful in analyzing and interpreting the properties associated with the wavefunction. Here then we are particularly interested in

correlating changes in the individual orbitals (which exhibit an independent-particle formalism) with the changes in various properties of the wavefunction as a function of internuclear distance. For the $A^1\Pi$ state a smooth transition of the wavefunction from ∞ to R_e required a spatially projected SOGI wavefunction which was constructed from a CI wavefunction with specially selected configurations.

In this paper we consider the four electronic states of the BH molecule that dissociate to a B atom in the 2P state and a hydrogen atom in the 2S state. Three states are bound ($X^1\Sigma^+$, a $^3\Pi$, and $A^1\Pi$, in order of decreasing binding energy) and one is unbound ($^3\Sigma^+$). Calculations on these states have been carried out for internuclear distances (R) in the range of $1.85 a_0$ to ∞ . (3) In both the $^1\Pi$ state and the $^3\Pi$ state, the potential curves exhibit a maximum between R_e and ∞ which we find to result from changes in the spin coupling of the wavefunction (see Sec. III.C).

As discussed in Section II, we find that the B core orbitals ($1s, 1s'$) can be replaced by the HF doubly occupied core orbitals without seriously affecting the properties. This reduces the complexity of the calculations to essentially that of a four-electron system. Also discussed in Section II are some of the other relevant aspects of the wavefunctions and the calculational details. The wavefunctions and the potential curves are discussed in Sec. III in conjunction with some general concepts of bonding that have been abstracted from these calculations. In Sec. IV we report as a function of R some properties (dipole moment, quadrupole moment, and electric field gradient) for these wavefunctions.

II. THE WAVEFUNCTION

A. The Frozen Core Restriction

The six-electron SOGI wavefunction has the form

$$G_1^{\gamma L} [(\phi_c \phi'_c \phi_{1a} \phi_{1b} \phi_{2a} \phi_{2b}) \alpha \beta \alpha \beta \alpha \beta], \quad (1)$$

where $G_1^{\gamma L}$ is a group operator based on the Wigner projection operators for the symmetric group [and includes only permutation operators involving spatial and spin coordinates (2, 4)] and where each ϕ_k is a one-electron spatial function. The orbitals in (1) are solved self-consistently to yield the best possible energies. However, previous SOGI calculations on BH (5) and LiH (6) have shown that ϕ_c and ϕ'_c remain essentially the same as the atomic 1s core orbitals (that is, these orbitals change only slightly with R). In addition we have found that forcing

$$\phi_c = \phi'_c \quad (2)$$

(i. e., double occupancy) results in only very small changes in the calculated potential curves and properties. Since the complexity of the calculations is reduced significantly by assuming (2) and, since this restriction does not have a significant effect upon the molecular properties of interest (7), we have assumed (2) and taken ϕ_c to be the 1s Hartree-Fock orbital from the B(²P) wavefunction. Thus the wavefunction is taken as

$$G_1^{\gamma L} [\phi_c \phi_c \phi_{1a} \phi_{1b} \phi_{2a} \phi_{2b} \alpha \beta \alpha \beta \alpha \beta], \quad (3)$$

where the four valence orbitals (ϕ_{1a} , ϕ_{1b} , ϕ_{2a} , and ϕ_{2b}) are solved

self-consistently. This restriction in the wavefunction will be referred to as the frozen core restriction. Replacing a valence orbital ϕ_j with

$$\phi_j - \gamma \phi_c$$

(where γ is an arbitrary number) leads to no net change in the wavefunction (3) because of (2). Thus the valence orbitals may all be taken orthogonal to ϕ_c without making any additional restrictions upon the many-electron wavefunction (1). This orthogonality will result in the incorporation into the variational orbitals of nodes that would not appear in the 'ab initio' (six-electron) wavefunction; however, these nodes appear only in the region of the boron nucleus and do not alter the interpretation of the wavefunction.

In the variational equations

$$H_k \phi_k = \epsilon_k \phi_k \quad k = 1, 2, 3, 4 \quad (4)$$

for the valence orbitals of (3), the Hamiltonian has the form

$$H_k = \left(\frac{1}{2} \nabla^2 + 2J_{1s} - K_{1s}\right) + U_k \quad (5)$$

which is exactly the same form as for the four-electron wavefunction

$$G_1^{\gamma L} [(\phi_{1a} \phi_{1b} \phi_{2a} \phi_{2b})^{\alpha\beta\alpha\beta}] , \quad (6)$$

except for the presence of an additional term of the form $2J_{1s} - K_{1s}$ resulting from the interaction with the core orbitals. Consequently, the SOGI effective field term U_k of (5) is just the same as would be obtained from (6).

The most costly part of the SOGI calculations on BH is the computation of U_k repeatedly as the orbitals are being iterated to convergence. But from (5) we see that because of (2) we need only calculate the U_k for a four-electron system, which is much less time consuming than for a six-electron system. The $2J_{1s} - K_{1s}$ term then serves as an effective potential replacing the core orbitals (8). However, we should emphasize that the $2J_{1s} - K_{1s}$ appearing in (5) is not an approximation but results directly from the application of the variational principle to (3). That the core orbitals have not been allowed to readjust as a function of R is the only approximation in our procedure.

B. Spin Coupling

There are two linearly independent ways of combining the spins of four electrons together to get a singlet state. For example, the two valence bond (VB) wavefunctions

$$\psi_1 = \mathcal{Q}[(\phi_{1a}\phi_{1b} + \phi_{1b}\phi_{1a})(\phi_{2a}\phi_{2b} + \phi_{2b}\phi_{2a})\alpha\beta\alpha\beta] \quad (7)$$

$$\psi_2 = \mathcal{Q}[(\phi_{1a}\phi_{2b} + \phi_{2b}\phi_{1a})(\phi_{2a}\phi_{1b} + \phi_{1b}\phi_{2a})\alpha\beta\alpha\beta]$$

correspond to one choice of the two linearly independent wavefunctions.

Furthermore, wavefunction (6) can be expanded as

$$G_1^{\gamma L}[\phi_{1a}\phi_{1b}\phi_{2a}\phi_{2b}\alpha\beta\alpha\beta] = c_1\psi_1 + c_2\psi_2 \quad (8)$$

where optimizing the spin coupling in the SOGI wavefunction is equivalent to optimizing the linear coefficients in (8). Thus the SOGI method

corresponds to solving self-consistently for the optimum orbitals in (7) simultaneously with optimizing the coefficients in (8).

For convenience of discussion the orbital couplings in (7) are represented as

$$\begin{aligned} \psi_1: & \begin{array}{|c|c|} \hline 1a & 1b \\ \hline 2a & 2b \\ \hline \end{array} \\ \psi_2: & \begin{array}{|c|c|} \hline 1a & 2b \\ \hline 2a & 1b \\ \hline \end{array} , \end{aligned} \tag{9}$$

where elements in the same row are symmetrically coupled (as for a singlet). [Note in (9) and below an orbital ϕ_{1a} is often denoted as 1a.]

In discussing the SOGI wavefunction (6), a convenient choice for the pair of linearly independent wavefunctions is often ψ_1 plus

$$\psi_f: \begin{array}{|c|c|} \hline 1a & 1b \\ \hline 2a & 2b \\ \hline \end{array} , \tag{10}$$

where in ψ_f orbitals 1a and 2a are antisymmetrically (triplet) coupled as also are 1b and 2b. The wavefunctions ψ_1 and ψ_f are often referred to as G1 and GF coupled, respectively. The GF wavefunction can be expressed as a linear combination of ψ_1 and ψ_2 ,

$$\begin{array}{|c|c|} \hline 1a & 1b \\ \hline 2a & 2b \\ \hline \end{array} = \begin{array}{|c|c|} \hline 1a & 2b \\ \hline 2a & 1b \\ \hline \end{array} - \begin{array}{|c|c|} \hline 1a & 1b \\ \hline 2a & 2b \\ \hline \end{array} . \tag{11}$$

For a four-electron triplet state, the three linearly independent VB wavefunctions can be taken as

$$\begin{array}{ccc}
 \psi'_1: & \begin{array}{|c|c|} \hline 1a & 1b \\ \hline 2a & \\ \hline 3a & \\ \hline \end{array} & \psi'_2: & \begin{array}{|c|c|} \hline 2a & 1b \\ \hline 3a & \\ \hline 1a & \\ \hline \end{array} & \psi'_3: & \begin{array}{|c|c|} \hline 3a & 1b \\ \hline 1a & \\ \hline 2a & \\ \hline \end{array} \\
 & & & & & & (12)
 \end{array}$$

Again the SOGI method corresponds to optimizing a linear combination of these wavefunctions while solving self-consistently for the optimum orbitals. The special couplings used in describing SOGI wavefunctions are $\{\psi''_1, \psi''_2, \psi''_f\}$ where

$$\psi''_1 = \psi'_1$$

$$\psi''_2 = \frac{2}{3}\psi'_1 + \frac{4}{3}\psi'_3$$

$$\psi''_f = \frac{1}{2}\psi'_1 - \frac{1}{2}\psi'_2 - \frac{3}{2}\psi'_3 .$$

In the case of the $^1\Sigma^+$ and $^3\Sigma^+$ states of BH, we find that the optimum wavefunction involves only the first type (G1) of coupling. However, for both the $^1\Pi$ and $^3\Pi$ states, we find that the other possible spin couplings become quite important.

C. Projected SOGI Wavefunction

In the case of the BH($A^1\Pi$) state it is found that two unique SOGI wavefunctions are necessary to properly describe the wavefunction as a function of internuclear distance. Consequently a

selected configuration interaction wavefunction was constructed which incorporates both forms of the SOGI wavefunction. This wavefunction can be described as

$$\psi_{\text{PSOGI}} = c_1 G_1^{\gamma L}(\phi_{1a} \phi_{1b} \phi_{2a} \phi_{2a} \alpha\beta\alpha\beta) + \\ c_2 G_1^{\gamma L}(\phi_{3a} \phi_{3b} \phi_{2a} \phi_{2b} \alpha\beta\alpha\beta)$$

or

(13)

$$\psi_{\text{PSOGI}} = G_1^{\gamma L}[(c_1 \phi_{1a} \phi_{1b} + c_2 \phi_{3a} \phi_{3b}) \phi_{2a} \phi_{2b} \alpha\beta\alpha\beta]$$

where orbitals $\phi_{1a} \phi_{1b}$ and $\phi_{3a} \phi_{3b}$ are the orbitals which correspond to the different SOGI wavefunctions which are important to the molecular wavefunction. The ψ_{PSOGI} wavefunction is constructed by selecting all configurations which describe the wavefunctions in (7) and (8). (9) In addition certain single and double excitations are allowed into the wavefunction to give approximately the same freedom of wavefunction adjustment as a self-consistent approach would provide.

D. Computational Details

The SOGI equations (3) were solved self-consistently using a basis set expansion in terms of nuclear-centered Gaussian-type basis functions. For each R the molecular integrals (ab initio) were evaluated

using a general set consisting of 42 basis functions (called the primitives); these basis functions were then contracted into 16 functions for use in solving the SOGI equations.

On the boron we used the 11s set of boron of Huzinaga and Sakai (10), the 5p set of boron of Huzinaga (11), and a set of polarization functions (three each of d_{x^2} , d_{y^2} , d_{z^2} , and d_{xz}) based on a fit to the optimum Slater basis functions of Cade and Huo (12). The s and p primitives were contracted on the basis of uncontracted SOGI calculations on the boron atom (using the frozen core restriction) ———— |
| ———— and using the Dunning principles. The contraction coefficients for the d functions were obtained from a previous set of ab initio (six-electron) calculations on the $^1\Sigma^+$ state (5).

Six primitive Gaussian 1s functions from Huzinaga (11) and a p_z orbital (along the molecular axis) based on Cade and Huo (12) were centered on the hydrogen nucleus. The s functions were contracted into three basis functions suitable for describing the hydrogen atom at R_e and $R = \infty$ (13).

The coefficients for the contractions are given in Table I. (14) The SOGI calculations were carried out using the Ladner quadratically convergent SOGI program and the Blint G1 program. The projected SOGI calculation was carried out using the Ladner-Hay spin eigenfunction CI program. The Hunt version of the Basch Polyatom Integrals program was used to calculate the Gaussian molecular integrals (partly contracted). The integrals for the contracted functions were obtained using the Huestis N^5 -integral transformation program. The Gaussian properties integrals were carried out using the Neumann-Moskowitz NYU program. The contour plots were made using the Huestis-Guberman-Parr Contour Plotting program.

Table I. Contraction coefficients for BH calculations where each χ is orthogonalized to the core orbital.

α_i	Type	Disjoint Contraction	Core Orbital	Contraction Coefficients	
10324.650	S(B)	0.0014191	0.17617112	- - - -	- - - -
1587.2834	S	0.0106715	0.17617112	- - - -	- - - -
358.64641	S	0.0567633	0.17617112	- - - -	- - - -
99.421167	S	0.2366461	0.17617112	- - - -	- - - -
31.5161170	S	0.7696531	0.17617112	- - - -	- - - -
10.9185210	S	1.0	0.32132155	-0.0032(χ_4)	- - - -
4.0434363	S	1.0	0.43507210	-0.0146(χ_4)	- - - -
1.6000069	S	1.0	0.20250098	-0.0388(χ_4)	- - - -
0.4230671	S	1.0	0.00964005	1.0(χ_5)	- - - -
0.1648581	S	1.0	-0.00224001	1.0(χ_6)	- - - -
0.0661828	S	1.0	0.0006900	1.0(χ_7)	- - - -
11.341300	X	1.0	- - - - -	0.0059(χ_8)	0.0143(χ_8^*)
2.43599	X	1.0	- - - - -	0.0279(χ_8)	0.0873(χ_8^*)
0.68358	X	1.0	- - - - -	0.1535(χ_8)	0.3031(χ_8^*)
0.21336	X	1.0	- - - - -	0.2470(χ_9)	0.5144(χ_8^*)
0.070114	X	1.0	- - - - -	0.0266(χ_9)	1.0(χ_9^*)
11.3413	Z	1.0	- - - - -	0.0143(χ_{10})	0.0059(χ_{10}^*)
2.43599	Z	1.0	- - - - -	0.0874(χ_{10})	0.0279(χ_{10}^*)
0.68358	Z	1.0	- - - - -	0.3031(χ_{10})	0.1535(χ_{10}^*)
0.21336	Z	1.0	- - - - -	1.0(χ_{11})	1.0000(χ_{11}^*)
0.070114	Z	1.0	- - - - -	1.0(χ_{12})	1.0000(χ_{11}^*)
1.23148	XX	0.1836481	- - - - -	-1.7600(χ_{14})	3.550(χ_{15})
0.36852	XX	0.8872685	- - - - -	-1.7600(χ_{14})	1.000(χ_{15})
0.13582	XX	1.0	- - - - -	-0.5000(χ_{14})	-3.5500(χ_{15})
1.23148	YY	0.1836481	- - - - -	-1.7600(χ_{14})	-1.0000(χ_{15})
0.36952	YY	0.8872685	- - - - -	-1.7600(χ_{14})	- - - -
0.13582	YY	1.0	- - - - -	-0.5000(χ_{14})	- - - -

Table I. (Continued)

α_i	Type	Disjoint Contraction	Core Orbital	Contraction Coefficients
1.23148	ZZ	0.1836481	- - - - -	3.5200(χ_{14}) - - - -
0.36952	ZZ	0.8872685	- - - - -	3.5200(χ_{14}) - - - -
0.13582	ZZ	1.0	- - - - -	1.0000(χ_{14}) - - - -
1.23148	XZ	0.1836481	- - - - -	1.7100(χ_{16}) - - - -
0.36952	XZ	0.8872685	- - - - -	1.7100(χ_{16}) - - - -
0.13582	XZ	1.0	- - - - -	1.0000(χ_{16}) - - - -
82.4736	S(H)	0.0068959	- - - - -	1.0(χ_1) - - - -
12.3983	S	0.0521466	- - - - -	1.0(χ_1) - - - -
2.83924	S	0.2536880	- - - - -	1.0(χ_1) - - - -
0.814717	S	0.7680501	- - - - -	1.0(χ_1) - - - -
0.271838	S	1.0	- - - - -	1.0(χ_2) - - - -
0.099482	S	1.0	- - - - -	1.0(χ_3) - - - -
3.89655	Z	0.1736019	- - - - -	1.73(χ_{13}) - - - -
0.92283	Z	0.8940545	- - - - -	1.73(χ_{13}) - - - -
0.28535	Z	1.0	- - - - -	1.0(χ_{13}) - - - -

* Contracted functions which are different for the Π states.

III. THE WAVEFUNCTIONS AND ENERGIES

The four states that arise from the coupling of the 2S state of hydrogen plus the 2P state of boron are discussed in the following sections.

A. Potential Energy Curves and Energy-Related Properties

The calculated potential curves (15) of BH are shown in Fig. 1. The $X\ ^1\Sigma^+$ state is the ground state of the system; it has only one minimum. The $^3\Pi$ and $^1\Pi$ are the next two states, each of which is slightly repulsive at large R and attractive for small R . The resulting maximum at intermediate R is henceforth referred to as a hump. Finally, the $^3\Sigma^+$ state leads to a highly repulsive potential curve possessing a small (unbound) minimum near $R = 2.1\ a_0$. The R 's and energies of the humps and minima are given in Table II, and a tabulation of the energies calculated for each internuclear distance are shown in Table III.

It was first noted by Herzberg and Mundie that the potential curve for the $A\ ^1\Pi$ state of BH must have a hump. This was indicated by the linearity of the breaking off points in the absorption spectra of the visible bands ($X\ ^1\Sigma^+ \rightarrow A\ ^1\Pi$, transitions). Rotational break-off is caused by predissociation of the vibrational-rotational levels of the $A\ ^1\Pi$ state. In the case that the rotationless potential curve has a hump (as in Fig. 1) at $R = R_{\max}$, the rotational hump in the effective potential curve $[E + J(J + 1)/2mr^2]$ is also essentially at R_{\max} (i.e., $R_{\max}^J \approx R_{\max}^0$). Hence the energy of break-off is approximately proportional to $J(J + 1)$. In this case extrapolation of the break-off energy to $J = 0$ yields the sum

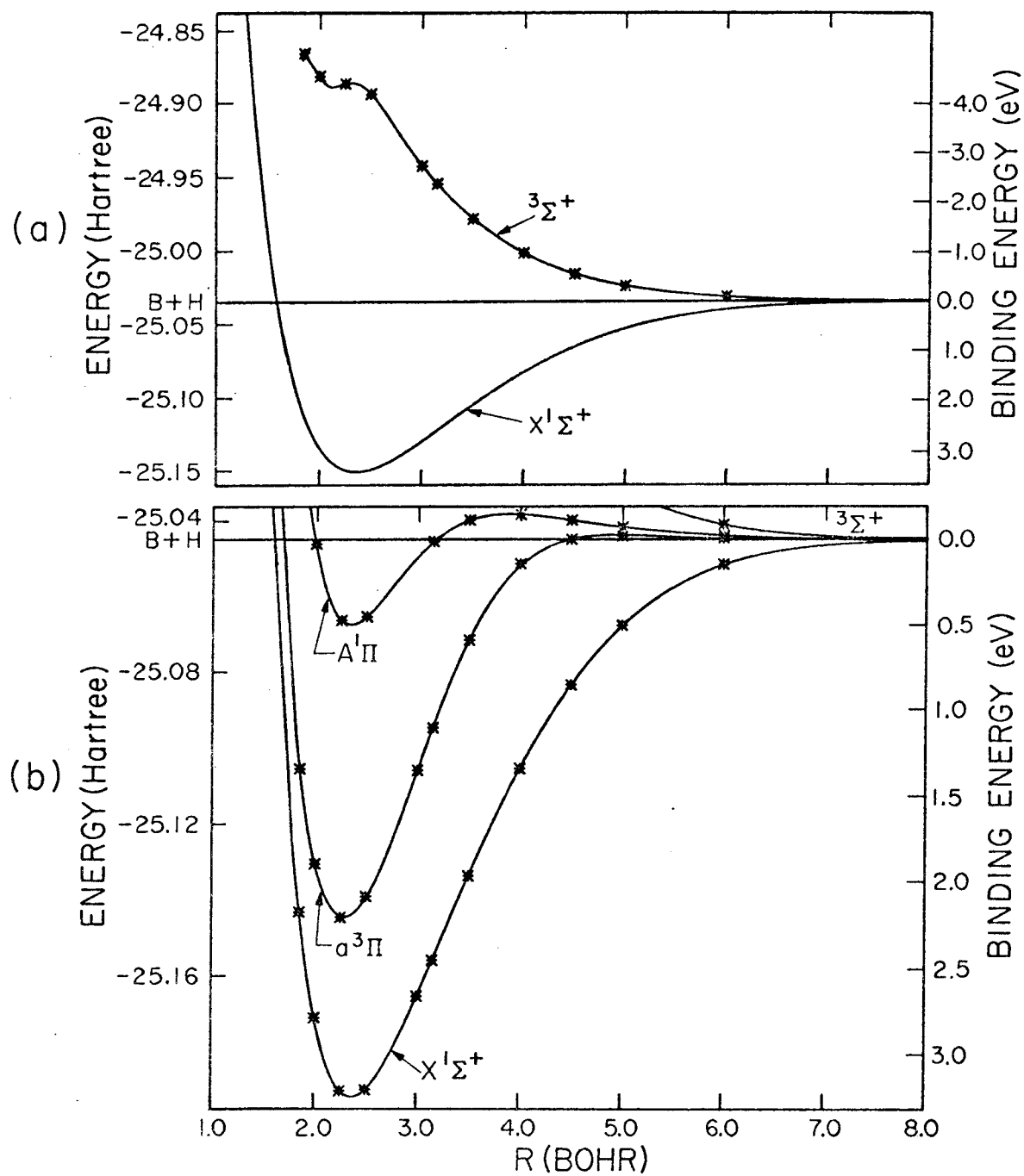


Fig. 1. SOGI potential curves for each of the excited states.

TABLE II. Potential minima and maxima of the ground and lower excited states of BH.

State	Calculated		Experimental	
	Potential Minimum	Potential Maximum	Potential Minimum	Potential Maximum
	D_e (eV) r_e (Å)	E_{\max} (eV) r_{\max} (Å)	D_e (eV) r_e (Å)	E_{\max} (eV) r_{\max} (Å)
X $^1\Sigma^+$	3.272 1.250	-----	3.572 1.2324	-----
a $^3\Pi$	2.216 1.211	0.026 2.60 1.201
A $^1\Pi$	0.502 1.240	0.150 2.057	0.704 1.219 2.05 ± 0.2
$^3\Sigma^+$	-4.35 ₁ 1.131	4.36 ₅ 1.177

TABLE III. Ab initio energies of the four states at each calculated point. (All energies are in Hartree and R is in Bohr.)

R	X $^1\Sigma^+$	$^3\Sigma^+$	a $^3\Pi$	A $^1\Pi$
∞	-25.047120	-25.047120	-25.047120	-25.047120
6.0	-25.052582	-25.043930	-25.046860	-25.046326
5.0	-25.065720	-25.036235	-25.046417	-25.044525
4.5	-25.078552	-25.027634	-25.047119	-25.042999
4.0	-25.096619	-25.012787	-25.052414	-25.041702
3.2	-25.119766	-24.988342	-25.068939	-25.042938
3.15	-25.137970	-24.963577	-25.087845	-25.047653
3.0	-25.145752	-24.950806	-25.096985	-25.050896 ^a
2.5	-25.165833	-24.899826	-25.124237	-25.063828
2.25	-25.166077	-24.886826	-25.128738	-25.064636
2.0	-25.159345	-24.883484	-25.117142	-25.048111
1.85	-25.127518	-24.868912	-25.096573	-25.026169

^a SOGI angle ($\theta/2$) equals 29.358; a converged SOGI angle was not obtained for this state.

$$D_0(X \ ^1\Sigma^+) + E_{\max}(A \ ^1\Pi) \quad (14)$$

which is referred to as the predissociation limit. In addition, the slope of the break-off energy curve yields an estimate of R_{\max} .

Since only the first three vibrational levels of the $X \ ^1\Sigma^+$ state are known, $D_0(X \ ^1\Sigma^+)$ cannot be reliably obtained from a Birge-Sponer extrapolation and the presence of E_{\max} (14) does not allow a separate estimate of $D_0(X \ ^1\Sigma^+)$. Thus, it has not yet been possible to obtain separate experimental determinations of $D_0(X \ ^1\Sigma^+)$, $D_0(A \ ^1\Pi)$ and $E_{\max}(A \ ^1\Pi)$. The most recent experimental determination (17) of the predissociation limit (14) is $28,850 \pm 150 \text{ cm}^{-1}$ ($3.577 \pm 0.0186 \text{ eV}$) as extrapolated from emission break-off points. From the slope of the break-off curve, $R_{\max}(A \ ^1\Pi)$ is estimated to be $3.9 \pm 0.4 a_0$ (the R_e for the $A \ ^1\Pi$ state is $2.303 a_0$). The experimental separation between the two states [$D_e(X \ ^1\Sigma^+) - D_e(A \ ^1\Pi)$] is $23,135 \text{ cm}^{-1}$ (2.868 eV).

In order to obtain $D_0(X \ ^1\Sigma^+)$, it has been necessary to estimate $E_{\max}(A \ ^1\Pi)$. The only previous estimate for this quantity was made by Hurley (18). Hurley carried out a semi-empirical valence-bond calculation on the $A \ ^1\Pi$ state and found that it produced a purely repulsive potential curve; using the semi-empirical i. c. c. correction for correlation errors in atomic and ionic limits, he obtained a corrected potential curve with a hump of 0.155 eV at $4.32 a_0$ and a minimum at $2.7 a_0$. He then estimated that the hump from the i. c. c. calculation should not be more than twice the size of the exact hump. He thus estimated $E_{\max} = 0.12 \pm 0.04 \text{ eV}$, and obtained a $D_0(\text{BH})$ of $3.39 \pm 0.04 \text{ eV}$ [using the older predissociation limit ($28,350 \text{ cm}^{-1}$) reported by Herzberg and Mundie(16)]. Wilkinson assumed E_{\max} to be $0.08 \pm 0.08 \text{ eV}$, leading to $D_0(X \ ^1\Sigma^+) = 3.43 \pm 0.08 \text{ eV}$. (19)

occurs at $2.13_7 a_0$ and it is 4.25_1 eV above the dissociation limit. As we will see below, the inner minimum arises from the B 2S Rydberg state of B atom.

Since our basis set does not contain the diffuse basis functions needed to describe a Rydberg state, we do not expect to obtain a good description of the region near the inner minimum. Recently Schaefer (21) has carried out configuration interaction (CI) calculations using a basis including diffuse functions and finds a deeper well centered at $2.217 a_0$ with the maximum occurring at $2.73 a_0$.

B. The Orbitals

The three valence orbitals of B(2P) are shown in Fig. 2 where the coupling is

$$\begin{array}{|c|c|} \hline 1a & 1b \\ \hline 2a & \\ \hline \end{array} \quad (15)$$

Taking the p orbital (ϕ_{2a}) along the z axis these orbitals have the form

$$\begin{aligned} 1a &\sim s + cp_x \sim sx \\ 1b &\sim s - cp_x \sim s\bar{x} \\ 2a &\sim p_z \end{aligned} \quad (16)$$

where s denotes the spherically symmetric part of ϕ_{1a} (or ϕ_{1b}) and p_x and p_z denote functions with the angular symmetry of a p orbital but no special radial behavior (in particular, the self-consistent orbitals lead to a different radial form for p_x than for p_z). [The orbitals of

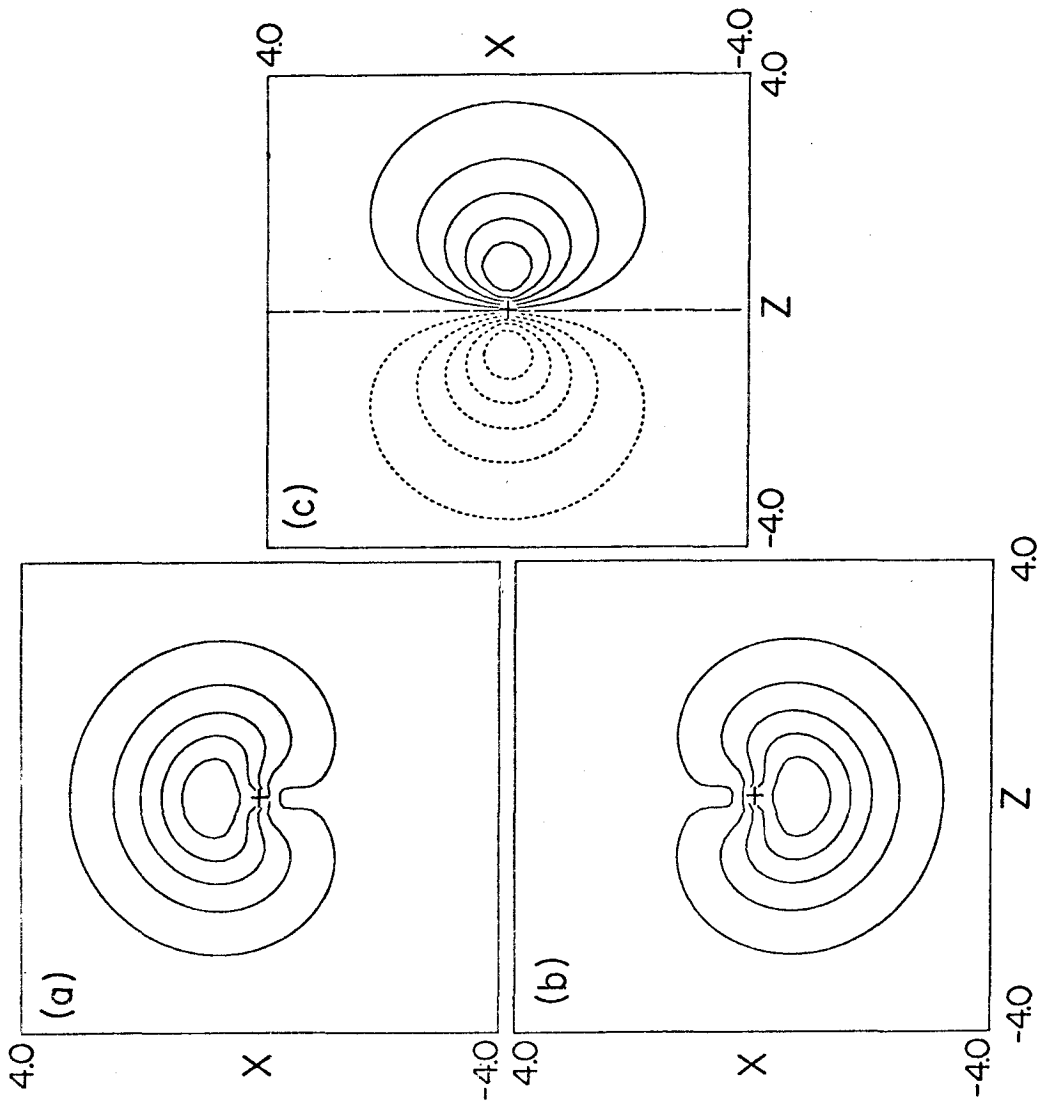


Fig. 2. $B(^2P)$ valence orbitals (s_x , $s_{\bar{x}}$, p_x).

(16) will sometimes be denoted as sx , $s\bar{x}$, and p_z although, of course, nothing is special about the axes chosen, i.e., we could just as well have used sy , $s\bar{y}$ and p_x .] In (14) $1a$ and $1b$ are hybridized functions (c is about 0.185 if s and p_x are normalized) pointing in opposite directions and perpendicular to the p orbital, ϕ_{2a} . We should make it clear that $1a$ and $1b$ are not forced to have the form in (16), they are solved self-consistently, yielding the form in (16).

In discussing these orbitals we will represent them schematically as



where the dot indicates that orbital $2a$ is not paired with any other orbitals.

1. The Σ States

Starting with the orbitals of (15) and bringing the H in along the z axis



we can couple the pz and Hz orbitals in either of two ways, obtaining the two states

$$\begin{array}{|c|c|} \hline sx & s\bar{x} \\ \hline pz & Hz \\ \hline \end{array} \equiv {}^1\Sigma^+ \quad (19)$$

$$\begin{array}{|c|c|} \hline sx & s\bar{x} \\ \hline pz & \\ \hline Hz & \\ \hline \end{array} \equiv {}^3\Sigma^+, \quad (20)$$

where (19) leads to a ${}^1\Sigma^+$ state and (20) leads to a ${}^3\Sigma^+$ state. The Hz orbital has a much larger overlap with pz than with the sx, $s\bar{x}$ functions, so that the dominant term in the interatomic potential should be the exchange term between pz and Hz,

$$K_{pz, Hz}$$

which should be large and negative. But for singlet coupling of pz and Hz as in (19), $K_{pz, Hz}$ enters with a plus sign, whereas for triplet coupling as in (20) it comes in with a minus sign. Thus the ${}^1\Sigma$ state is attractive and the ${}^3\Sigma$ state is repulsive. The interactions between Hz and the (sx, $s\bar{x}$) pair are repulsive since the corresponding exchange terms (e.g., $-\frac{1}{2}K_{sx, Hz}$) enter with a negative sign and hence are positive.

Upon solving for the orbitals self-consistently, we would expect that in the ${}^1\Sigma$ state they would adjust so as to increase the overlap between Hz and pz, while at the same time decreasing the overlap between Hz and the (sx, $s\bar{x}$) pair (thereby decreasing the repulsive terms while increasing the bonding terms). In Fig. 3, we show the self-consistent SOGI orbitals

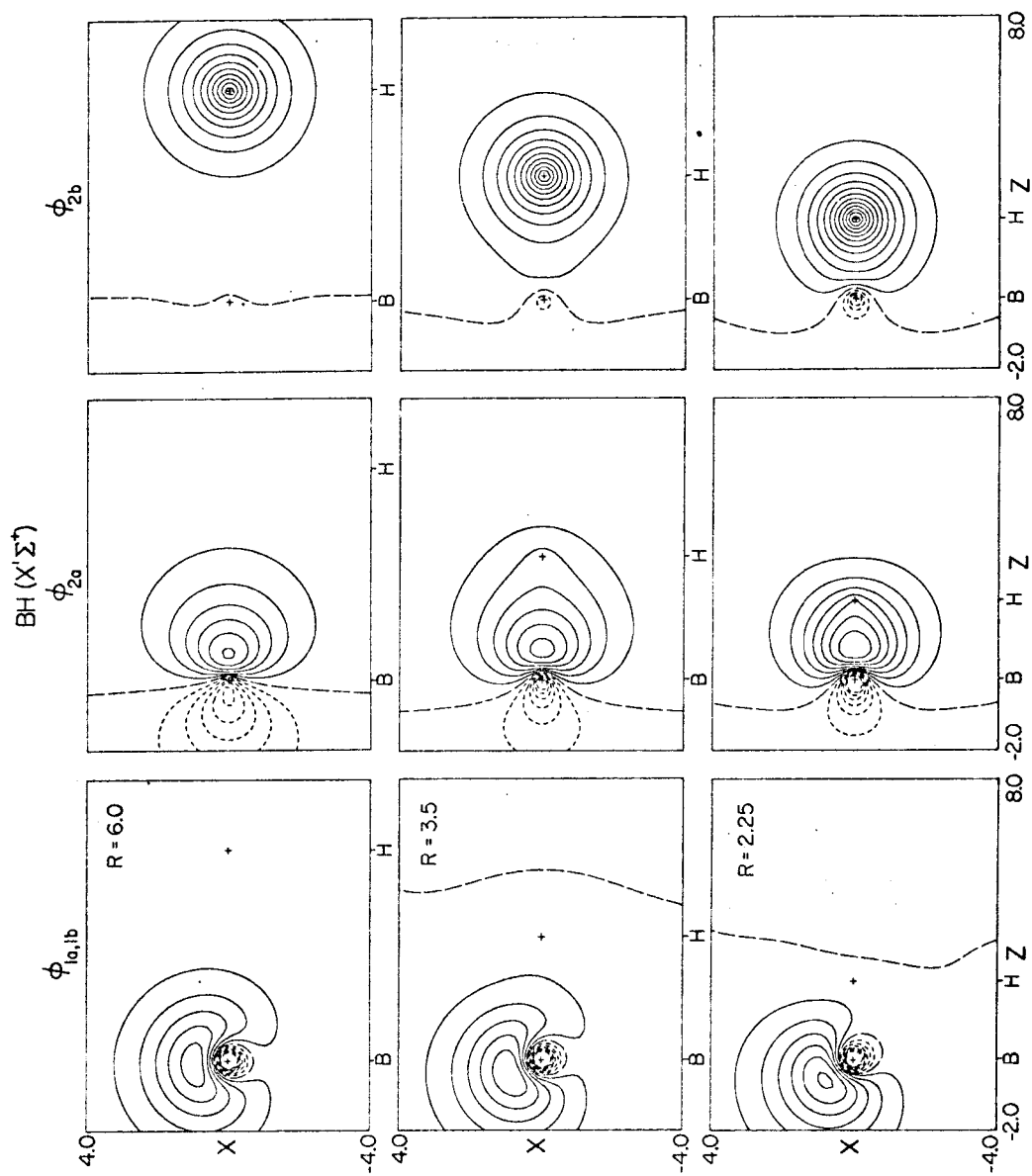
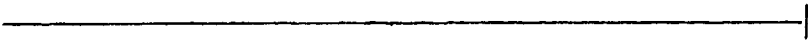


Fig. 3. Contour plots of the optimum SOGI orbitals for the $X^1\Sigma^+$ state.

as a function  of R, where we see that the orbitals readjust about as expected. The pz orbital hybridizes a bit, delocalizing toward the H, and the (sx, s \bar{x}) pair rotates away from the newly forming bond.

For the $^3\Sigma$ state the pz and H orbitals readjust minimizing the overlaps at all R. Primarily this results in the pz orbital hybridizing away from the H. The interactions between pz and the (sx, s \bar{x}) pair then favors a rotation of this pair toward the H despite an unfavorable interaction with the H orbital.

The orbital energies of the Σ states are shown in Fig. 4. For the $^1\Sigma$ state ϵ_{pz} drops monotonically from $R = \infty$ to $R = R_e$, but ϵ_{Hz} increases as R decreases to about $5a_0$ and then decreases rapidly for smaller R. On the other hand, ϵ_{sx} decreases as R decreases to $5a_0$ and increases for smaller R. The rapid decrease of ϵ_{Hz} and ϵ_{pz} for $R < 3a_0$ reflects their strongly bonding effect in this region. The increase of ϵ_{sx} in this region probably reflects the repulsive interactions between them as they are rotated into each other. Part of this increase in ϵ_{sx} could also be due to the shielding of the B nucleus from the ϕ_{sx} and $\phi_{s\bar{x}}$ orbitals due to the presence of the ϕ_{Hz} orbital. For large R ($> 5a_0$), the main change in the orbitals is a delocalization of pz partly onto the H.

In Fig. 4, the $^3\Sigma^+$ orbital energies strongly reflect the crossing of the Rydberg state ($B^2S + H^2S$) with the initially repulsive valence state ($B^2P + H^2S$). For large R we find that all the orbital energies increase smoothly as R decreases with the 2b orbital ($B2p\sigma$) increasing most rapidly. However, at about $2.5a_0$ the two states cross and orbitals 1a, 1b, and 2b start decreasing rapidly as one would expect for BH^+ orbitals while the 2a orbital keeps on increasing smoothly.

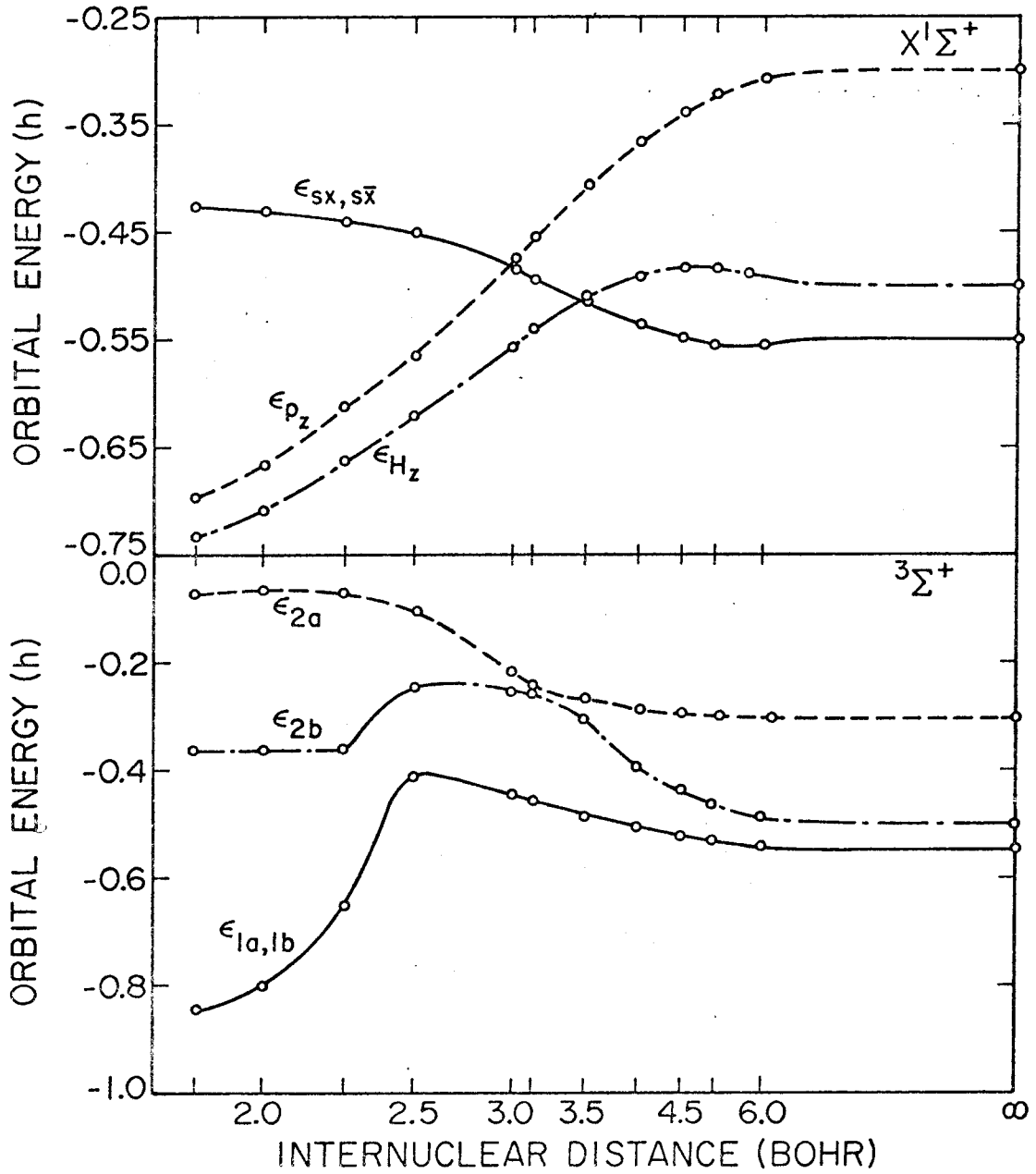


Fig. 4. Orbital energies for the two Σ states of BH. The internuclear axis is scaled to include the point at infinity as $z = 16.28/R$.

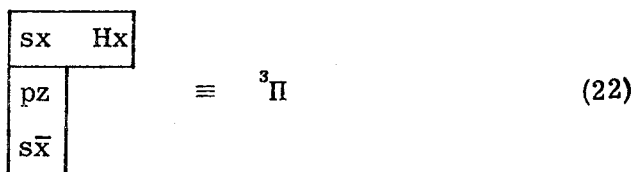
2. The Π States

Besides the Σ states discussed above we can get other states by starting with $B(^2P)$ plus $H(^2S)$.

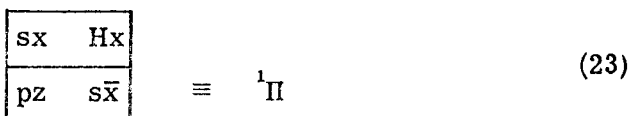
In Fig. 5 we show a plot of the sx and $s\bar{x}$ orbitals along the x axis. Considering an H atom at about $R = 2.5a_0$, we see that Hx has a much larger overlap with sx than with $s\bar{x}$. Thus we should consider the possibility that strongly bound states could be formed by bringing the H along the x axis and bonding to sx ,



In this case we can couple the orbitals in either of two ways,



and



depending upon how the nonbonding orbitals ($s\bar{x}$ and pz) are paired.

Since the pz orbital is perpendicular to the molecular axis, we obtain

${}^3\Pi$ and ${}^1\Pi$ states. Both of these states have a bonding interaction

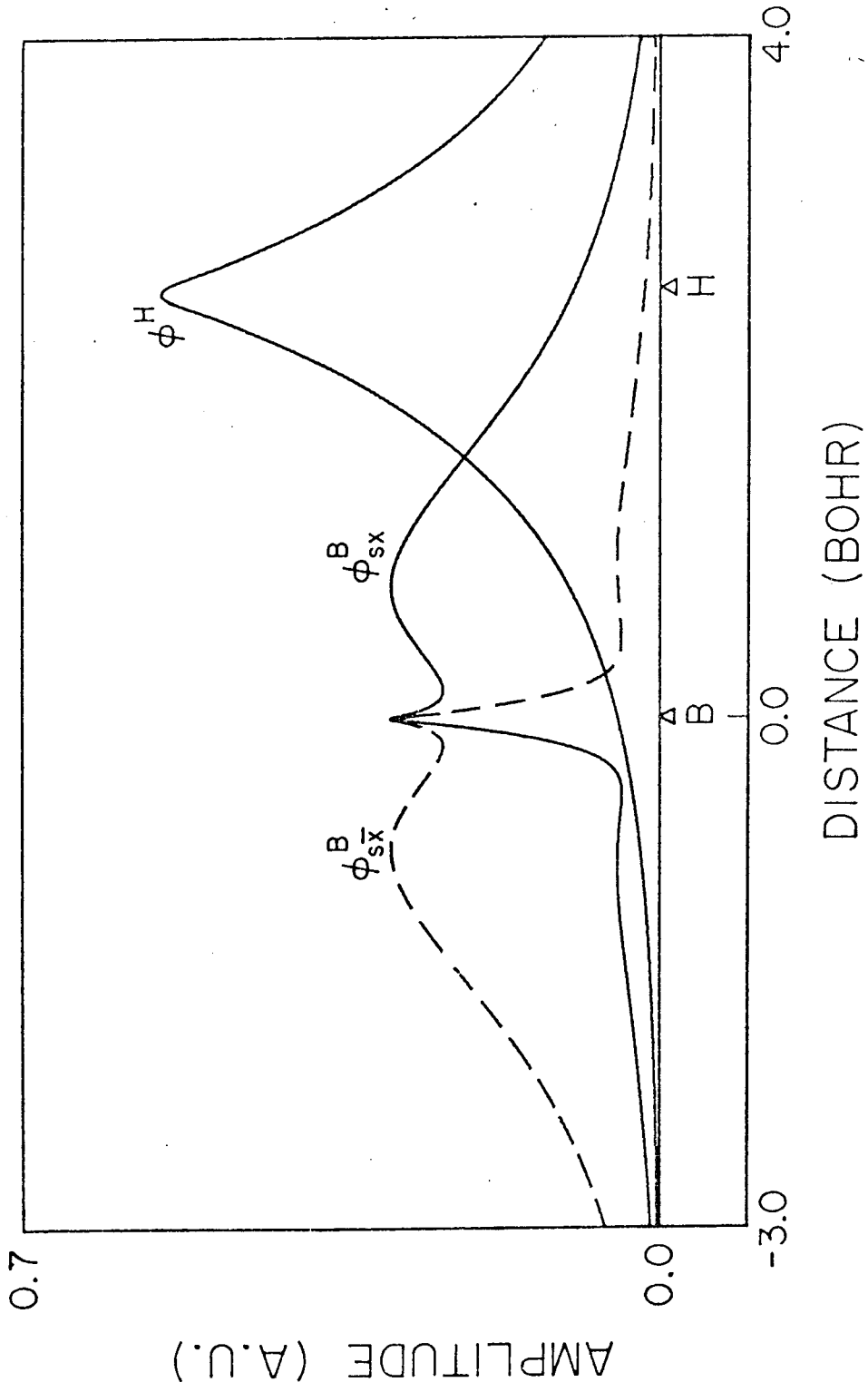


Fig. 5. Line plots of the unperturbed atomic orbitals at $R = 2.5 a_0$.

between sx and H ; they differ in that the exchange term $K_{pz, s\bar{x}}$ comes into the energy with a negative sign for (22) and a positive sign for (23). Since pz and $s\bar{x}$ are orthogonal, the exchange term is positive and the $^3\Pi$ state should be lower.

At large R the orbitals of the $^3, ^1\Pi$ states are not coupled as in (22) and (23) but rather as



and



But in (24) and (25) the Hx orbitals have negative exchange interactions with both orbitals of the $(sx, s\bar{x})$ pair, and hence both the $^3\Pi$ and $^1\Pi$ potential curves should be repulsive for large R .

The recoupling of orbitals that occurs for these states as R decreases from ∞ to R_e is similar to that occurring in the radical exchange reactions



and indeed forming BH in a Π state is in many ways quite analogous to the highly exothermic reaction (26b). Indeed for the same reason that an activation energy (energy barrier) is involved in each reaction of (26), we expect a hump to occur in the potential curves for each of the Π states.

The changes of the orbitals in such reactions have been discussed in detail elsewhere (22) and we will note here the implications relevant for BH. In such reactions the singlet pair [for BH, the pair (sx, s \bar{x})] stays somewhat paired during the reaction, becoming the bonding pair of the product. The orbital starting out in the middle (ϕ_{sx}) stays there during the reaction, changing little in the process. The orbital ($\phi_{s\bar{x}}$) starting out coupled with ϕ_{sx} delocalizes onto the other center, becoming of the form

$$\phi_{s\bar{x}} + \phi_{Hx} \quad (27)$$

in the transition region (keeping a high overlap with ϕ_{sx}). Concomitantly, the nonbonding orbital of the reactants (ϕ_{Hx} in this case) switches centers and becomes the nonbonding orbital ($\phi_{s\bar{x}}$) of the product. In the transition region this orbital has the form

$$\phi_{Hx} - c\phi_{s\bar{x}} \quad (28)$$

(keeping a low overlap with the other two orbitals) and hence changes phase during the reaction.

The self-consistent orbitals of the $^3\Pi$ state are shown in Fig. 6 where we see that the orbital changes are just as expected. The orbitals of the $^4\Pi$ state vary in a somewhat more complicated manner and are discussed further in the next section.

For both the $^3\Pi$ states and $^4\Pi$ states (Figs. 7 and 8) we see that the self-consistent orbitals at R_e are quite similar to those at $R = \infty$ except that they have been recoupled. This justifies the above qualitative discussions making use of the atomic orbitals.

Similar qualitative discussions can be used to predict the bonding and geometries of polyatomic molecules, as will be discussed elsewhere.

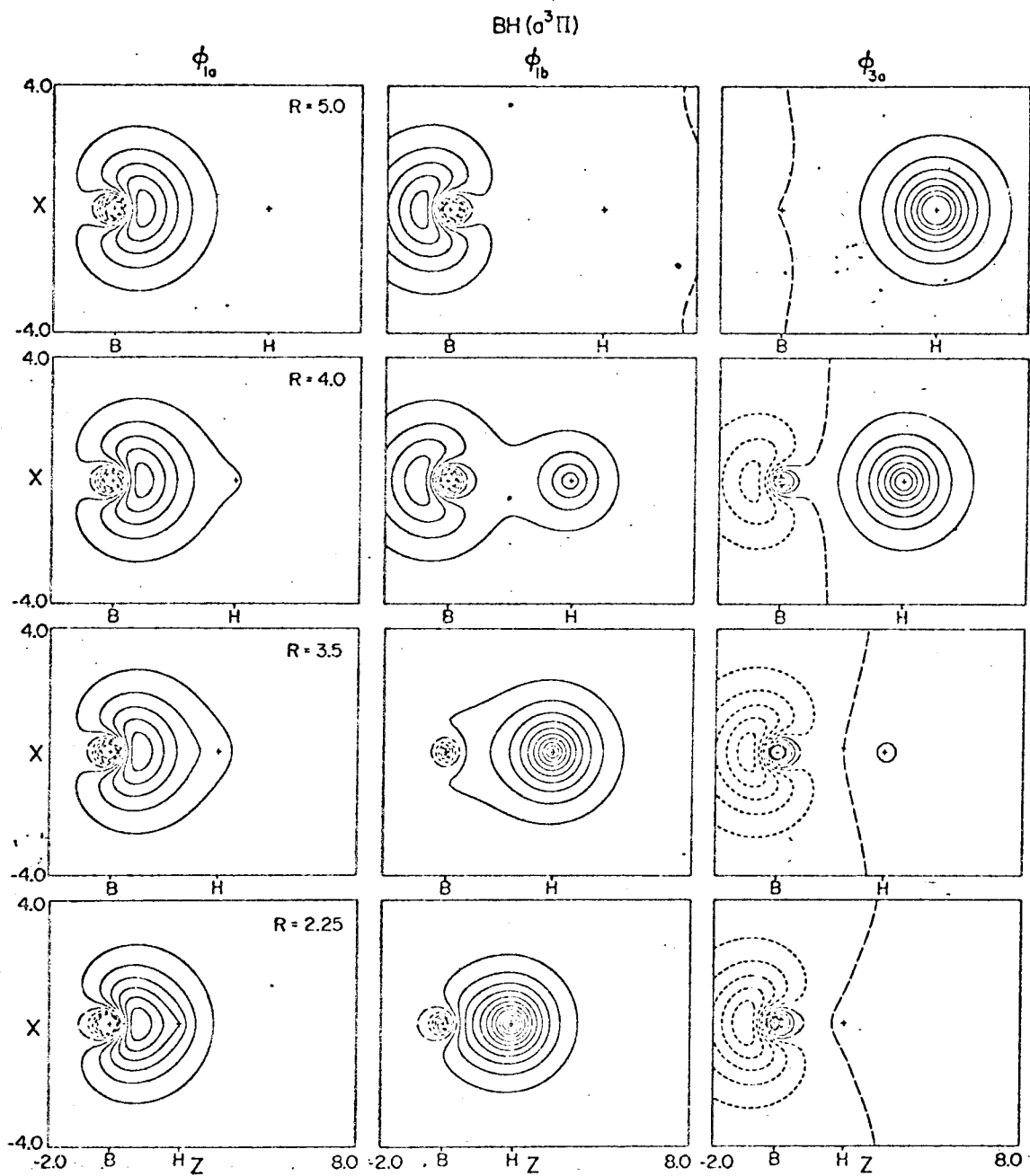


Fig. 6. The valence orbitals of the $\sigma^3\Pi$ state of BH as a function of R .

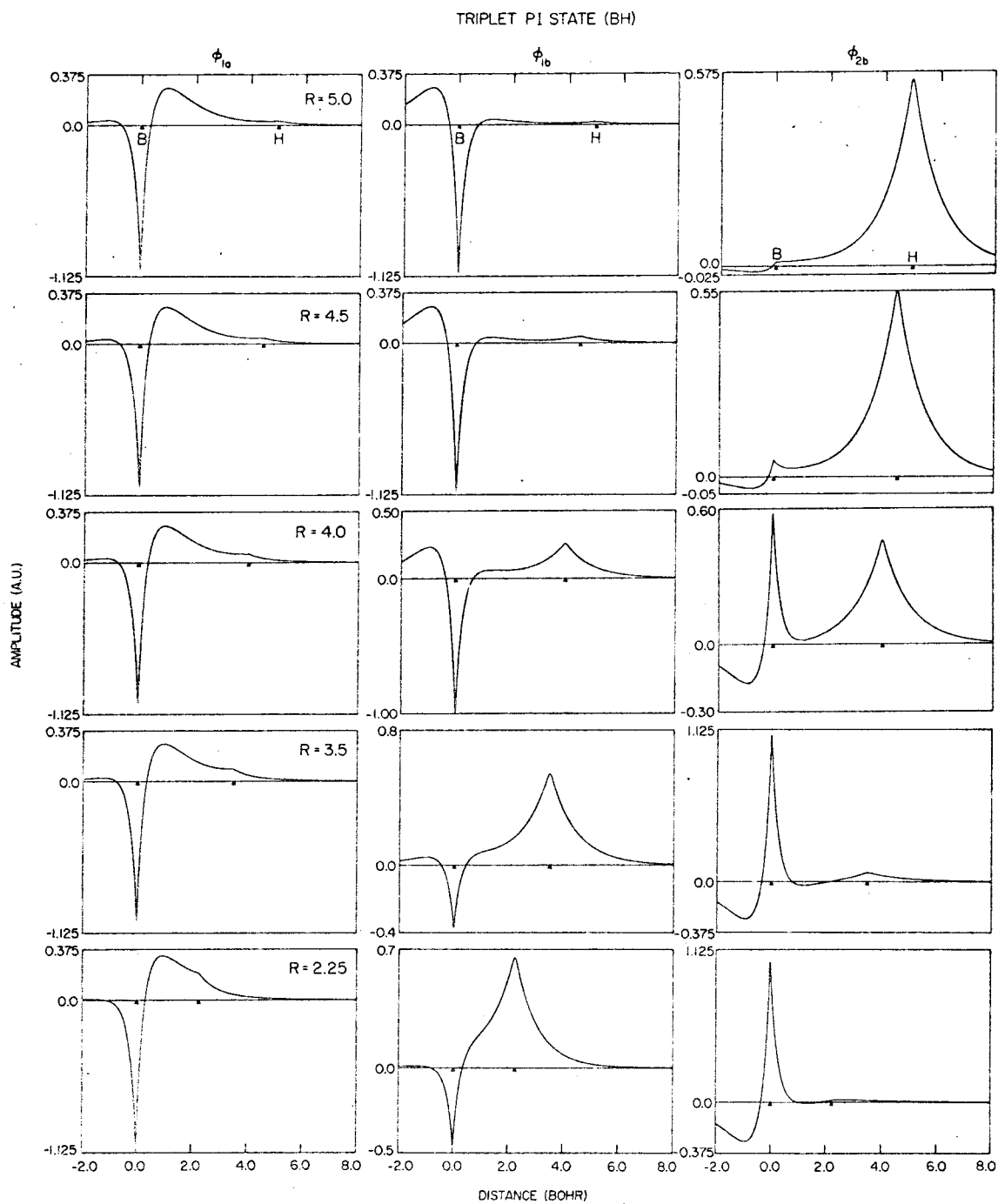


Fig. 7. Line plots of the $a^3\Pi$ SOGI orbitals as a function of internuclear distance.

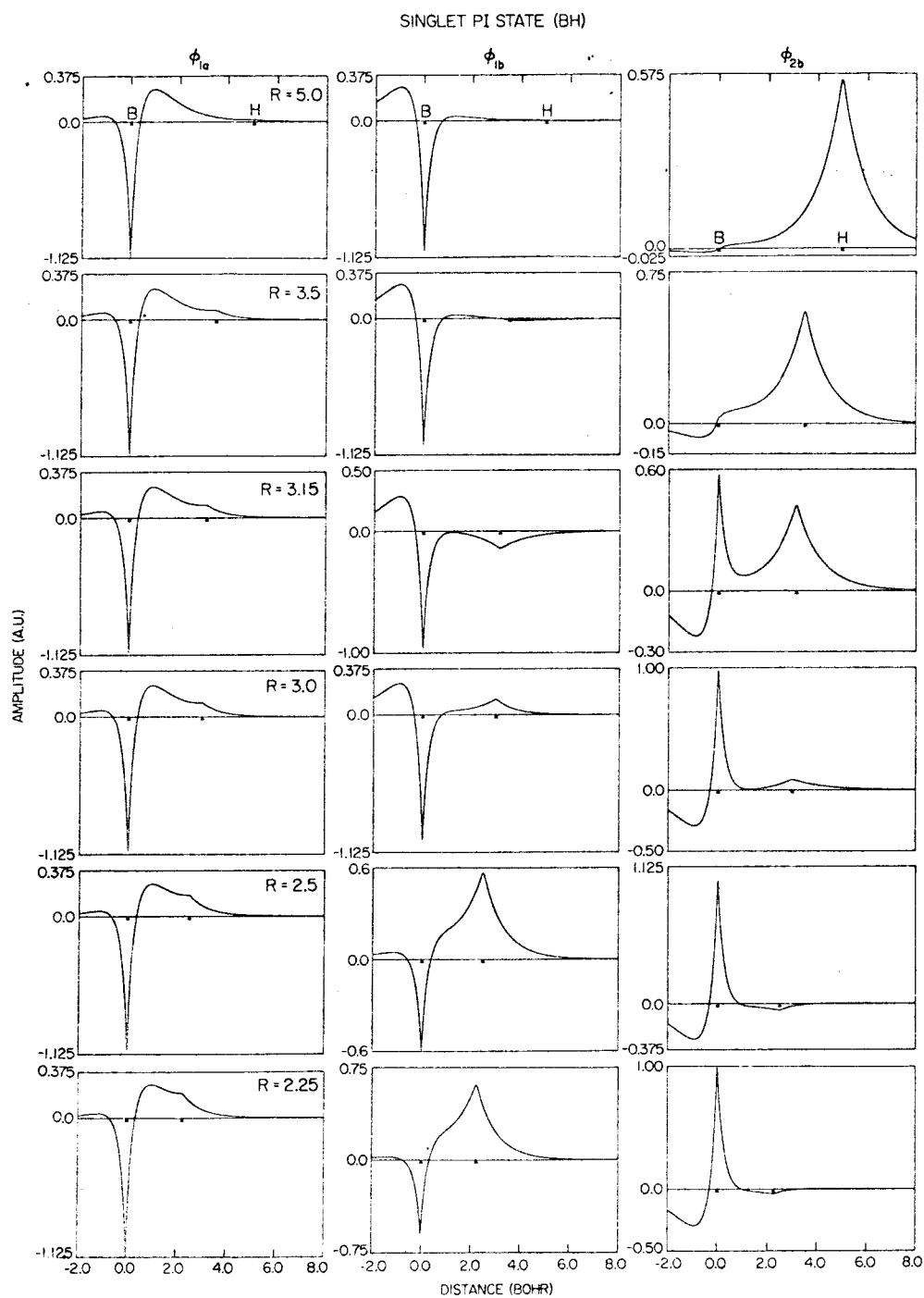


Fig. 8. Line plots of the $A^1\Pi$ SOGI orbitals as a function of internuclear distance.

The rapid decrease with R in the orbital energies of the 1a and 1b orbitals (see Fig. 9) of the $^3\Pi$ state indicates that these orbitals are bonding orbitals. Orbital 2a (the π -orbital) exhibits only a slight dip in the bonding region and otherwise is essentially constant. This is consistent with ϕ_{2a} being a nonbonding orbital. Orbital 1a has basically the same shape as the bonding orbitals of the $X^1\Sigma^+$ except that for the $^3\Pi$ state the orbital energy has a hump in the region where the spin coupling is changing rapidly ($5.0 a_0$ to $3.5 a_0$). (This hump is due to strong interactions with the 1b and 2b orbitals, both of which have high overlap with 1a.) The changes in orbitals 1b and 2b are discussed in detail in the next section; however, it should be noted that the 1b is basically a bonding orbital at all R and 2b is essentially a nonbonding orbital at all R .

The orbital energies for the $^1\Pi$ state are quite erratic in the region ($3.5a_0$ to $2.5a_0$) of large spin coupling changes. The π -orbital 2a is nonbonding and for $R < 4.0 a_0$, ϵ_{2a} increases slowly with decreasing R due to increased interactions with the other orbitals. Orbital 1a is a bonding orbital at all R and ϵ_{1a} behaves similarly to that for the $X^1\Sigma^+$ and $^3\Pi$ states. The behavior of the 1b and 2b orbitals is discussed in more detail in the following section. At large R , ϵ_{1b} increases as R decreases, as expected, since in this region there is no net binding; however, for $R < 3.0a_0$, ϵ_{1b} decreases rapidly with R as a bonding orbital would be expected. For large R , ϵ_{2b} decreases with R ; however, for $R < 3.0 a_0$, ϵ_{2b} increases rapidly.

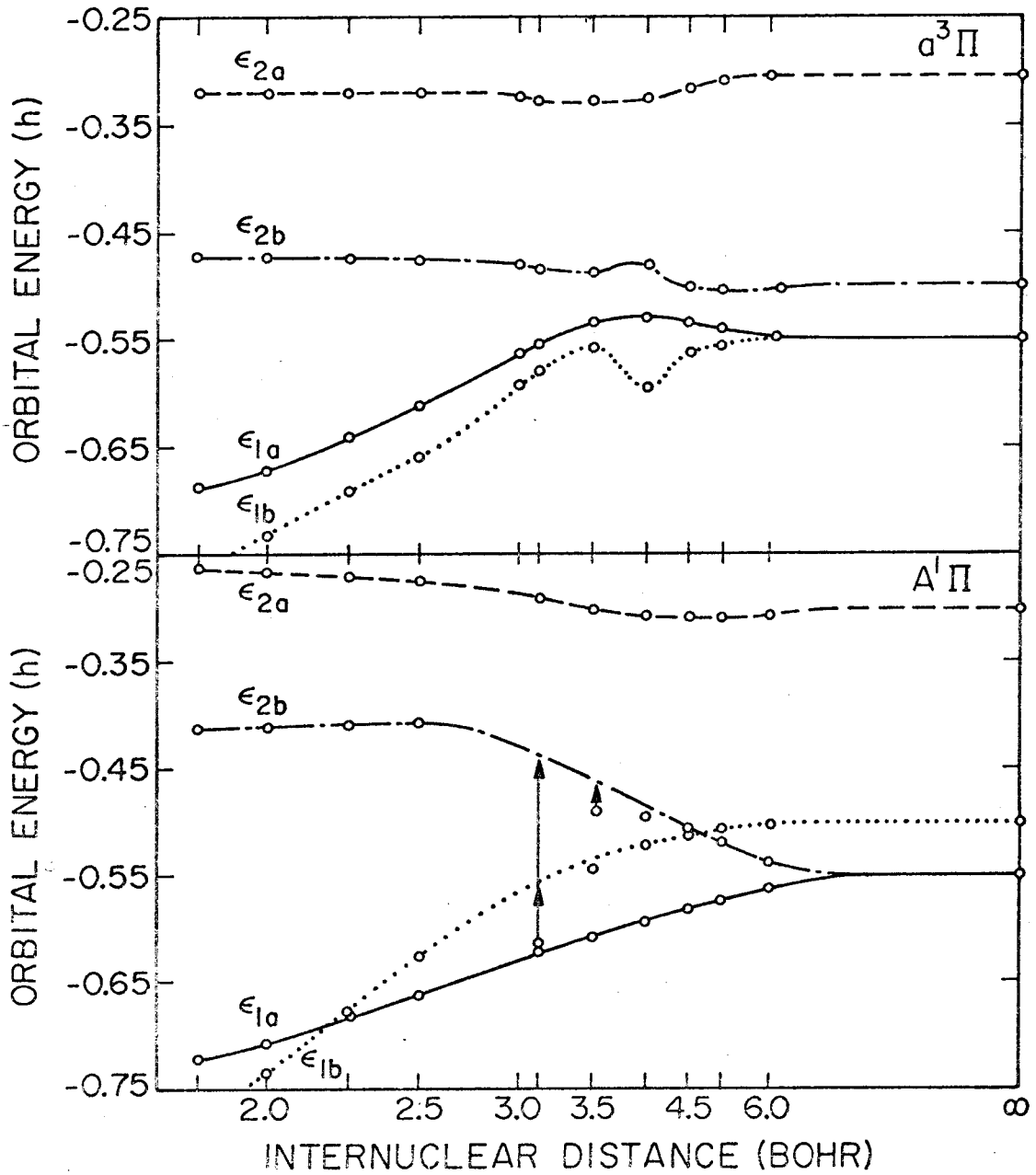


Fig. 9. Orbital energies for the two Π states of BH. The internuclear axis is scaled as in Fig. 4.

3. Angular Correlation in the Π States

The proper description of the boron atom wavefunction at the separated atom limit for the Π states is the three-configurational wavefunction (29) which has the same symmetry ($C_{\infty v}$) as does

$$\psi = [1s^2(2s^2 - \frac{1}{2}(p_x^2 + p_y^2))p_z \alpha\beta\alpha\beta\alpha] \quad (29)$$

the BH molecule. The inclusion of the term $(p_x^2 + p_y^2)$ in the wavefunction is an angular correlation effect which corresponds to double excitations from the $2s^2$ orbital into the p orbitals perpendicular to the p_z orbital. As discussed previously these correlation terms, although not the major configuration of the wavefunction, significantly lower the energy of the wavefunction.⁽⁷⁾ However, the wavefunction (29) can not be expressed in a non-spatially projected independent particle method. The Hartree-Fock method is capable of handling only one configuration per pair of electrons and the G1 method which corresponds to a self-consistently optimized valence bond wavefunction is equivalent to only two configurations per pair of electrons. Consequently the G1 wavefunction for the boron atom can be expressed as

$$\psi = [1s^2(2s^2 - p_x^2)p_z \alpha\beta\alpha\beta\alpha] \quad (30)$$

which does have an independent particle interpretation, but does not have $C_{\infty v}$ symmetry. This wavefunction has an energy which is only slightly above that for fully correlated wavefunction (29). The difference in the energies is due only to the interactions of p_x and p_y . For the calculations on the Σ states the situation remains exactly the same

where an independent particle wavefunction exactly analogous to (30) can be written and where the only difference in energy between the completely correlated wavefunction and the partially correlated wavefunction is the interaction term between π_x and π_y which has been shown to be small.

The situation is considerably different for the Π states where the hydrogen atom is oriented along one of the lobes of the p correlated orbitals (16) rather than the p_z orbital. Self-consistent optimization of the SOGI wavefunction will then require a recoupling of the orbitals so that the singlet coupled pair of orbitals in the BH bond will have the maximum overlap. This recoupling of the orbitals require the orbitals, ϕ_{1b} and ϕ_{2b} , to change character as described in the previous section and the wavefunction to incorporate additional VB configurations into the wavefunction [see (7) and (8)]. In order to minimize the energy orbital ϕ_{2b} retains as small an overlap with ϕ_{1a} and ϕ_{1b} as possible. However, since each of the orbitals ϕ_{1b} and ϕ_{2b} contain significant portions of the other there is a point in the transition region where their overlap reaches a maximum. Also maximum inclusion of secondary valence bond structures (high SOGI spin coupling angles) will occur at this point. The maximum in the potential hump will occur at approximately this point also because a high overlap of the ϕ_{1b} and ϕ_{2b} orbitals maximizes the effect of the positive energy contributions arising from the coupling of these two orbitals. Neither of the Π wavefunctions can incorporate the configuration (π_y^2) corresponding to the py^2 configuration which appears in (29).

The erratic variations in the orbital energies for the $A^1\Pi$ wavefunction in the region around $R = 3.0 a_0$ are attributed to the energetic interactions caused by the high overlap of the ϕ_{1b} and ϕ_{2b} orbitals. The incorporation of the π_y^2 configurations into the wavefunction would allow orbitals ϕ_{1b} and ϕ_{2b} to split outside the xz plane and would, therefore, minimize their overlap in the transition region. This would allow the orbitals to transform smoothly through the transition region. This effect should be the most pronounced in the $A^1\Pi$ state which also has the nonbonding orbitals coupled into a singlet. The combination of high overlap and singlet coupling maximizes the exchange contributions to the energy. The $a^3\Pi$ state should also show this effect; however, it should be much less pronounced because the nonbonding orbitals are coupled into a triplet where the exchange contributions improve the energy.

The effect of including this angular correlation remains to be determined; however, a projected SOGI calculation was done on the $A^1\Pi$ correlation term (29). (23)

$$\psi_{SCI} = c_1 G_1^L [\phi_{1a} \phi_{1b} \phi_{2a} \phi_{2b} \alpha\beta\alpha\beta] + c_2 \mathcal{L} [\Pi_y \Pi_y \phi_{2a} \phi_{2b} \alpha\beta\alpha\beta]. \quad (29)$$

A comparison of these energies to those in Table III shows that the Π correlation improvement in the wavefunction is a decreasing effect and consequently would actually enhance the maximum of the hump by as much as 26%. So, although the orbital description of the $A^1\Pi$ state is improperly described within the transition region, the description at R_e and at ∞ are unaffected.

IV. PROPERTIES

The dipole moment, electric field gradient on both centers and the quadrupole moment calculated at the boron center are shown in Figs. 10-11 for all four states as a function of the internuclear distance (see also Table IV). The behavior of these properties will be examined in the light of the changes which occur in the individual orbitals which we shall qualitatively discuss in terms of individual orbital contributions which are defined as

$$\langle P \rangle_i = \langle \Phi | P_i O_{11}^{\gamma L} | \Phi \rangle / \langle \Phi | O_{11}^{\gamma L} | \Phi \rangle$$

where Φ is the product of spatial orbitals and P_i is the one electron spatial operator associated with the property and operating only on electron index i . The total property $\langle P \rangle$ is the sum of the orbital contributions.

A. Dipole Moment

The $X^1\Sigma^+$ dipole moment has a particularly interesting shape which can be related to the changes which occur in the individual orbital contributions. The initial negative character (B^+H^-) arises because of the large and decreasing negative contribution from the $2a(Bp_z)$ orbital which is hybridizing significantly onto the hydrogen atom. The upturn and eventual change to a positive (B^-H^+) dipole moment occurs when the $2a$ orbital contribution reaches a minimum and begins to increase and when the steadily increasing positive contributions from the other three orbitals become significant and then dominate the dipole moment. The nonbonding orbitals have a positive contribution

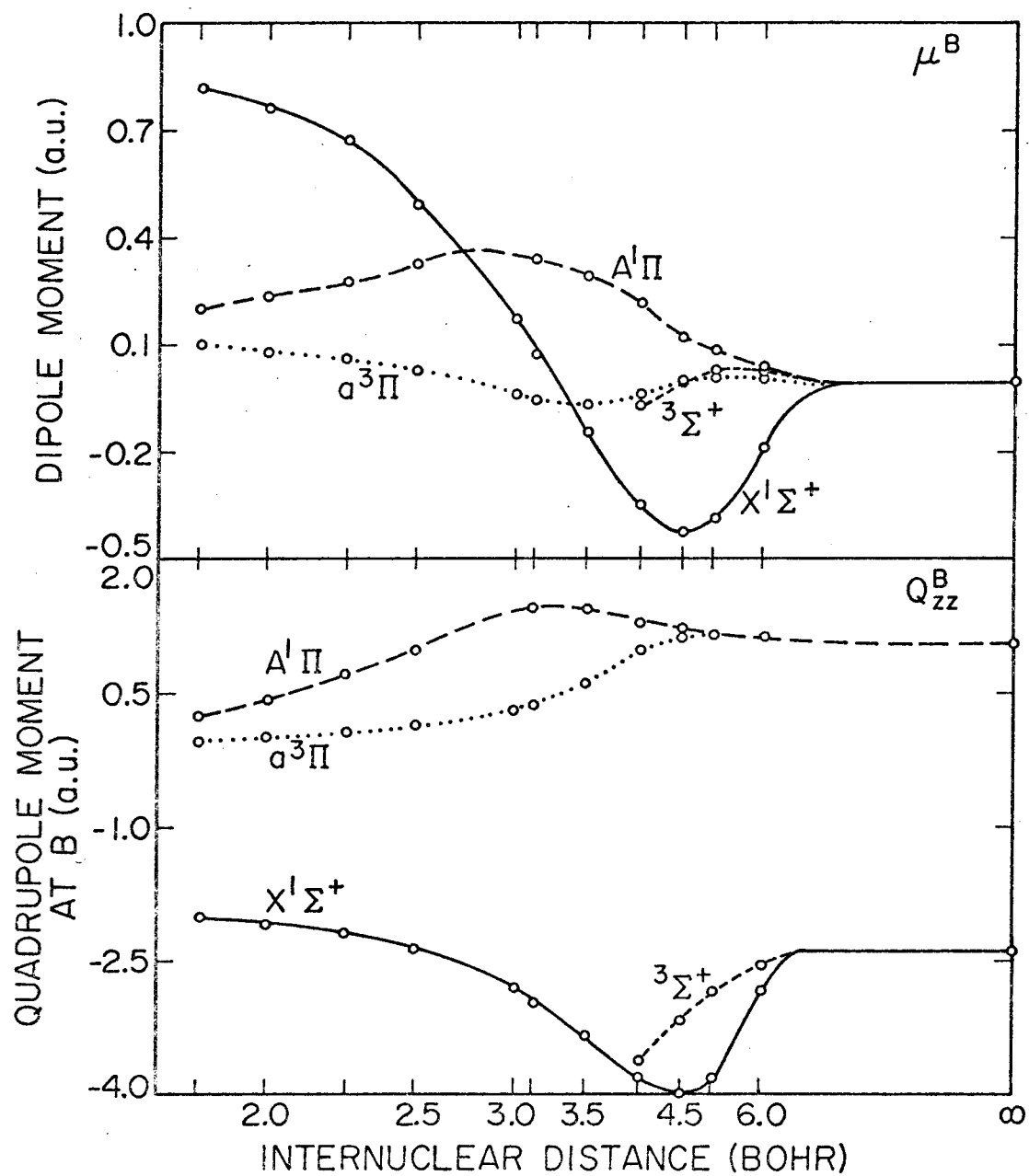


Fig. 10. Dipole and quadrupole moments for each of the BH states as a function of internuclear distance. Abscissa is scaled as in Fig. 4.

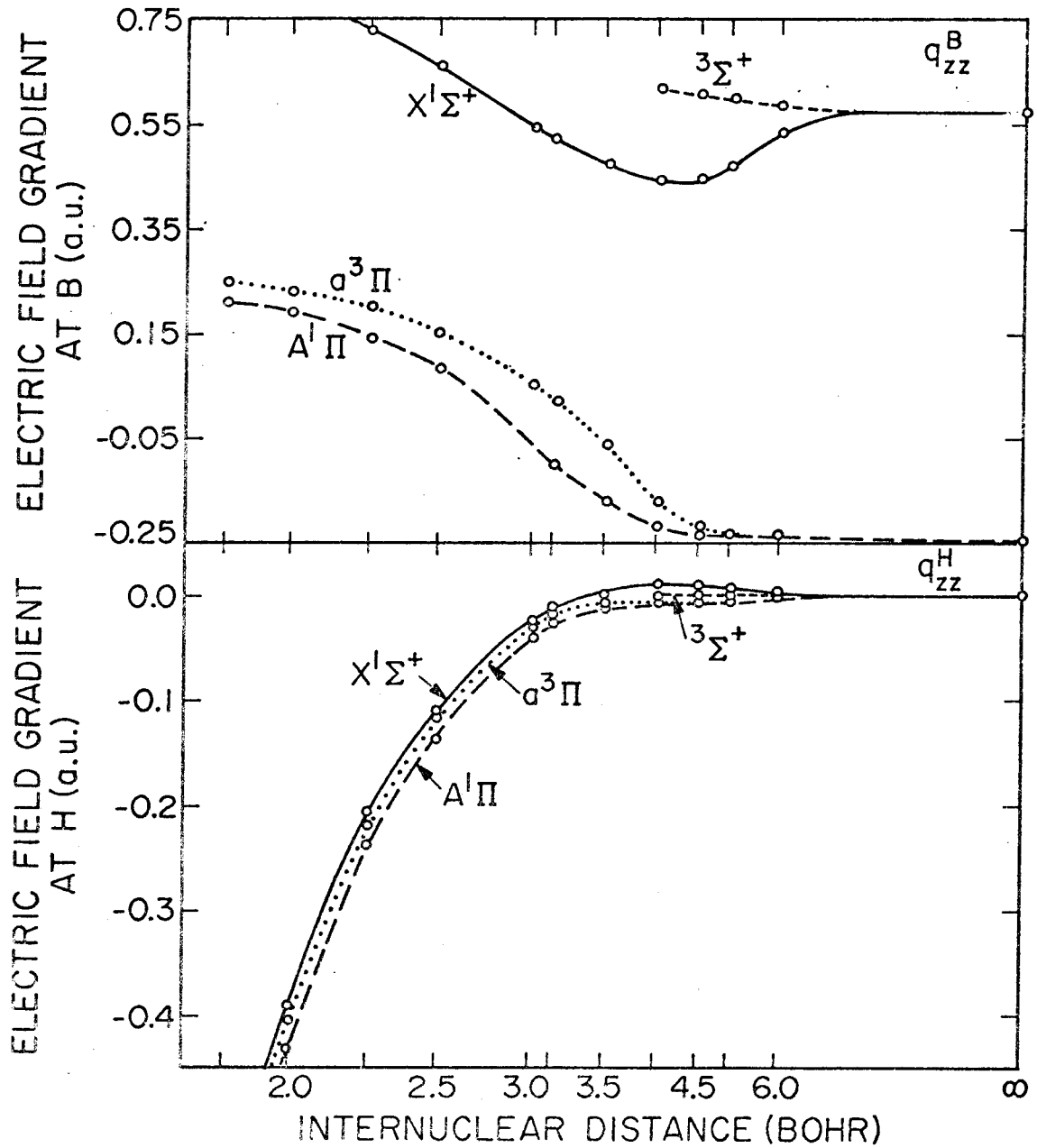


Fig. 11. Electric field gradient on each nuclei for each of the BH states as a function of internuclear distance. Abscissa is scaled as in Fig. 4.

Table IV. Calculated properties as a function of internuclear distance for each of the four states. (All properties are reported in atomic units.)

μ^B					Q_{zz}^B			
R	$X^1\Sigma^+$	$^3\Sigma^+$	$a^3\Pi$	$A^1\Pi$	$X^1\Sigma^+$	$^3\Sigma^+$	$a^3\Pi$	$A^1\Pi$
∞	0.000	0.000	0.000	0.000	-2.398	-2.398	1.025	1.025
6.0	-0.184	0.024	0.011	0.036	-3.132	-2.554	1.103	1.081
5.0	-0.379	0.023	0.010	0.090	-3.829	-2.857	1.129	1.131
4.5	-0.419	-0.002	0.003	0.138	-3.982	-3.154	1.123	1.205
4.0	-0.342	-0.071	-0.031	0.210	-3.821	-3.631	0.967	1.325
3.5	-0.132	- - -	-0.066	0.300	-3.376	- - -	0.606	1.444
3.15	0.074	- - -	-0.051	0.346	-2.988	- - -	0.394	1.431
3.0	0.170	- - -	-0.036	- - -	-2.824	- - -	0.326	- - -
2.5	0.490	- - -	0.029	0.319	-2.359	- - -	0.146	0.980
2.25	0.634	- - -	0.059	0.277	-2.188	- - -	0.068	0.717
2.0	0.759	- - -	0.084	0.230	-2.053	- - -	-0.002	0.460
1.85	0.822	- - -	0.095	0.210	-1.985	- - -	-0.037	0.282
q_{zz}^B					q_{zz}^H			
R	$X^1\Sigma^+$	$^3\Sigma^+$	$a^3\Pi$	$A^1\Pi$	$X^1\Sigma^+$	$^3\Sigma^+$	$a^3\Pi$	$A^1\Pi$
∞	0.574	0.574	-0.246	-0.246	0.000	0.000	0.000	0.000
6.0	0.530	0.585	-0.243	-0.244	0.004	0.002	-0.002	-0.002
5.0	0.472	0.599	-0.239	-0.245	0.009	0.002	-0.004	-0.005
4.5	0.447	0.608	-0.224	-0.240	0.011	0.002	-0.004	-0.008
4.0	0.443	0.617	-0.170	-0.222	0.011	0.001	-0.004	-0.014
3.5	0.472	- - -	-0.063	-0.170	0.004	- - -	-0.006	-0.025
3.15	0.518	- - -	0.017	-0.100	-0.013	- - -	-0.019	-0.042
3.0	0.544	- - -	0.049	- - -	-0.024	- - -	-0.030	- - -
2.5	0.657	- - -	0.150	0.081	-0.108	- - -	-0.113	-0.137
2.25	0.725	- - -	0.196	0.144	-0.206	- - -	-0.213	-0.238
2.0	0.794	- - -	0.234	0.194	-0.390	- - -	-0.405	-0.433
1.85	0.831	- - -	0.249	0.212	-0.574	- - -	-0.599	-0.628

to the dipole moment because they bend away from the hydrogen and back behind the boron, and the adjusted (the nuclear term has been added to this contribution) $2b(Hs)$ orbital contribution is positive because it hybridizes more onto the B as R is decreased.

The portion of the ${}^3\Sigma^+$ dipole moment curve calculated shows it as decreasing and negative (B^+H^-). (Only the initial parts of the ${}^3\Sigma^+$ curves were calculated because the highly repulsive character of the potential curve makes the properties at short R uninteresting.) Due to the triplet coupling the $2a$ orbital contribution is positive, but both the $1a(sx)$, $1b(s\bar{x})$, and $2b(Hs)$ orbitals come in with negative contributions. The sharp decrease of the moment is due to rapid drop in the nonbonding orbital contributions which occurs because the $1a$ and $1b$ orbitals are bending forward rapidly.

The $a^3\Pi$ dipole moment tends to be quite small and it changes sign twice as R is reduced. Basically we find that only one orbital $1a(sz)$, provides a negative contribution to the dipole moment; the remaining three orbitals all have positive (B^-H^+) contributions. Orbital $1a$ has a negative contribution because it is an sz orbital directed toward the hydrogen; while the remaining three orbitals, $s\bar{z}$, Hs , and π are all directed at or past the boron atom. Because the dipole moment is small (it is always less than 0.1 a. u.) indicates that the electron density is rather evenly distributed in the molecule which is nontypical of the other two bound states. One could predict that the dipole moment for the $a^3\Pi$ state would always be less than that of the $A^1\Pi$ state because coupling the two nonbonding orbitals into singlet

in the $A^1\Pi$ state causes a higher interaction between the two orbitals and causes them to spread out behind the boron increasing the dipole moment. In the $a^3\Pi$ state this is a bonding interaction so that these two orbitals would tend toward each other, thereby reducing the dipole moment. The $A^1\Pi$ dipole moment is always positive (B^-H^+) reaching a maximum at slightly less than $3.0 a_0$. Two orbitals, 1b and 2b, provide the impetus for the positive character of the dipole moment. As one would expect, these two orbitals tend to hybridize to or behind the boron atom causing a positive increasing behavior. The 1a(sz) orbital contributes negatively, as would be expected, due to its significant hybridization onto the hydrogen center. Finally the 2a(π) orbital has a small negative contribution indicating that it is bending in the direction of the hydrogen atom. The maximum found in the dipole moment curve occurs because the negative contributions from the 1a and 2a orbitals are steadily decreasing, while the contributions from 1b and 2b orbitals have begun to decrease slightly. This probably occurs because the high overlap of the 1b and 2b orbitals has begun to decrease and 1b has become significantly localized on the hydrogen center.

Experimentally the dipole moments of the $X^1\Sigma^+$ and $A^1\Pi$ states of BH have been determined by analyzing the Stark effects observed in the optical emission spectrum of BH. (24). The dipole moments were determined to be 1.27 ± 0.21 D. and 0.58 ± 0.04 D. for the $X^1\Sigma^+$ and $A^1\Pi$ states, respectively. This compares quite favorably with the calculated value of 1.25 D. for the $X^1\Sigma^+$ state at $2.5 a_0$. (25) The error limits of the experimental result include the R dipole

moment and extend somewhat past R_e . Other determinations of the $X^1\Sigma^+$ dipole moment are 1.733 D. (12) using the HF method and a VB-CI determination of 1.784 D. (26). The consistently too high values of these calculations result from the double occupancy restriction in HF which over emphasizes the description of the wavefunction on the boron at the expense of that on the H atom. The dipole moment for the $A^1\Pi$ state is experimentally determined to be 0.58 ± 0.04 D. The calculated dipole moment for the $A^1\Pi$ state at $R = 2.5 a_0$ is 0.810 D. at $R = 2.25 a_0$ is 0.705 D. and at $R = 2.0 a_0$ is 0.586 D. The too high dipole moment exhibited by the $A^1\Pi$ calculation is quite likely due to the inability of the wavefunction to adjust at long enough internuclear distance to the spin coupling change.

B. Quadrupole Moment

The molecular quadrupole moment, Q_{ZZ}^B , was evaluated with respect to the boron nucleus. A plot of Q_{ZZ}^B for each of the states is shown in Fig. 10. A negative quadrupole moment corresponds to an electron-charge distribution which is prolate along the bonding axis. For the $X^1\Sigma^+$ state the wavefunction becomes increasingly prolate as the internuclear distance is reduced until about $R = 4.5 a_0$ where the prolate character begins to decrease making the wavefunction more oblate. The orbital contribution from the $2a$ (Bp_z) orbital is the major contributing factor because it is hybridizing onto the hydrogen nucleus and consequently gives a very prolate contribution. However, as the internuclear distance is reduced this contribution decreases and the contributions from the other three orbitals which are more oblate in

character become important.

The portion of the ${}^3\Sigma^+$ quadrupole moment plotted shows an increasingly prolate character which is not unexpected because of the high repulsive character between the Bp_z orbital and the Hs orbital. The orbital contributions for the $1a(sx)$ and $1b(s\bar{x})$ orbitals are positive, equal and quite small compared to the orbital contributions from the $2a(Bp_z)$ and $2b(Hs)$ orbitals which are large and negative.

The molecular quadrupole moments for the $a^2\Pi$ and $A^1\Pi$ states are quite similar. For the $a^3\Pi$ wavefunction the molecular quadrupole moment increases slightly initially until it reaches a maximum in the region of the potential maximum and then it decreases smoothly and actually goes negative. The high oblate character of this wavefunction is completely attributable to the π orbital. The orbital contribution from the π orbital varies in the range from 1.24 a. u. to 1.87 a. u. and reaches its minimum at about $R = 3.15 a_0$. The contributions from the sx and $s\bar{x}$ orbitals are both negative and the contribution from the Hs orbital after correction for the nuclear contribution is positive (oblate).

For the $A^1\Pi$ state the molecular quadrupole moment is also very oblate; however this state exhibits a much greater oblate hump than did the $a^3\Pi$ wavefunction. The maximum of this hump also occurs at approximately the same region, as did the hump in the potential curve. Again as expected a major and essentially constant oblate contribution comes from the π orbital which ranges in value from $1.35 a_0$ to 1.23 a. u. The contributions from each of the sz and $s\bar{z}$ orbitals is

again prolate. The contribution from the Hs orbital is positive and increases from zero to a maximum of about 1.44 a.u. at short R. The major difference between the $a^3\Pi$ curve and the $A^1\Pi$ curve is the orbital contribution of $1a(sz)$ orbital. The sz orbital contribution has a much greater prolate character for the $a^3\Pi$ state than it does for the $A^1\Pi$ state. This indicates that the $1a$ orbital for the $a^3\Pi$ state is more highly polarized along the bond axis than is the $1a$ orbital for the $A^1\Pi$ state.

C. Electric Field Gradient

Electric field gradients at both nuclei are shown as a function of internuclear distance in Fig. 11. In interpreting the contributions to q_{ZZ}^B (electric field gradient at the boron nucleus) note that a $2p_z$ function leads to a positive q_{ZZ} while a $2p_x$ (or $2p_y$) function leads to a negative q_{ZZ} .

The q_{ZZ}^B for the $X^1\Sigma^+$ state remains positive for all R shown; however, it does reach a minimum near $4 a_0$ due primarily to the boron bonding orbital, $2a$, which is the major contribution to this property at all R. The contribution from the nonbonding orbitals is small and starts out negative as would be expected. However, as more and more p_z character is incorporated into the orbitals (the nonbonding orbitals bend back) this contribution becomes positive. The orbital contribution from the Hs function is a smoothly increasing positive term.

The $^3\Sigma^+$ state exhibits a positive, increasing function which is mainly due to the contribution from the Bp_z orbital. All other contributions to this field gradient are completely negligible.

Each Π states exhibit considerably different character. Each of them has essentially zero contributions to the electric field gradient on the boron, q_{ZZ}^B , until about $5.4 a_0$ when they both begin to increase smoothly. The $a^3\Pi$ state exhibits a slightly greater q_{ZZ}^B than does the $A^1\Pi$ state.

Two effects characterize the shape of the $a^3\Pi$ q_{ZZ}^B curve; one is the constant and predominate effect at long R of the contribution from the π orbital which varies between -0.30 and -0.31 a. u. The other effect is the growing positive contributions from the remaining three orbitals; $1a$, $1b$, and $2b$. Each of these functions are polarized along the bonding axis and consequently make positive contributions to the electric field gradient. Both the $1a$ and $1b$ (sx and $s\bar{x}$) orbitals start out with a small positive contribution and increase while the $2b(Hs)$ orbital starts out from zero and also increases.

q_{ZZ}^B for the $A^1\Pi$ state exhibits quite similar characteristics. The major negative orbital contribution again comes from the π orbital which remains essentially constant at all R ; while the effect which causes the increase in the q_{ZZ}^B is the increasing positive contributions from each of the remaining three orbitals. The major difference between the two curves is the magnitude of the contribution from the $1a$ (sz) bonding orbital. The contribution from the $A^1\Pi$ for this orbital is much less than that of the $a^3\Pi$ state. The electric field gradient could be considered as a measure of the amount of p-like character in an orbital and as was also observed in the contribution to the molecular quadrupole moment the $1a(sz)$ orbital hybridization is more pronounced for the $a^3\Pi$ state than it is for the $A^1\Pi$ state.

From Fig. 11 the q_{ZZ}^H , electric field gradient on the hydrogen nucleus, for all four states looks quite similar. Clearly the dominate effect for this property is the nuclear contribution which makes $q_{ZZ}^H < 0$ at all distances less than $R = 3.0$. Similarity of shape and value of q_{ZZ}^H for all states indicates that the character of each of the wavefunctions in the vicinity of the hydrogen-nucleus are quite alike with respect to the p-like character in the wavefunction. In each case the orbital contributions from each of the four orbitals show a gradually and smoothly increasing value which is rapidly dominated by the Z/R^3 nuclear term especially at short internuclear distances.

REFERENCES

1. (a) Partially supported by a grant from the National Science Foundation (GP-15423); (b) Contribution No.
2. (a) W. A. Goddard III, Phys. Rev., 157, 73 (1967); ibid. 157, 81 (1967); R. C. Ladner and W. A. Goddard III, J. Chem. Phys., 51, 1073 (1969).
3. $1 a_0 = 0.52917715 \times 10^{-8}$ cm; $1 \text{ h} = 27.211652 \text{ eV} = 219,474.07 \text{ cm}^{-1}$.
4. W. A. Goddard III, Int. J. Quant. Chem., 3S, 593 (1969).
5. R. J. Blint and W. A. Goddard III, J. Chem. Phys., in press.
6. W. E. Palke and W. A. Goddard III, J. Chem. Phys. 50, 4524 (1969).
7. The frozen core would not allow proper calculation of the spin density at the nucleus.
8. L. R. Kahn and W. A. Goddard III, J. Chem. Phys., 55, 0000 (1971).
9. Basis functions for these calculations were selected by orthogonalizing the optimum SOGI orbitals for each SOGI wavefunction.
10. S. Huzinaga and Y. Sakai, J. Chem. Phys., 50, 1371 (1969).
11. S. Huzinaga, J. Chem. Phys., 42, 1293 (1965).
12. P. E. Cade and W. M. Huo, J. Chem. Phys., 47, 614 (1967).
13. R. C. Ladner and W. A. Goddard III, Theoret. Chim. Acta, submitted for publication.
14. Due to the requirement of orthogonality to the core, the contraction for the basis set changes slightly at each internuclear distance. The contraction coefficients presented are those for

$R = \infty$ and at each internuclear distance the contraction coefficients are orthogonalized to the core orbital.

15. Potential curves were fit using a Morse potential multiplied by a polynomial in $R - R'$, where R' was not necessarily the R_e for the potential curve.
16. G. Herzberg and L. G. Mundie, J. Chem. Phys. 8, 263 (1940).
17. J.W.C. Johns, F. A. Grimm, and R. F. Porter, J. Mol. Spectry., 22, 435 (1967).
18. A. C. Hurley, Proc. Roy. Soc. (London), A261, 237 (1961).
19. P. G. Wilkinson, Astrophys. J., 138, 778 (1963).
20. Zero-point energy of 0.148 eV (1195.8 cm^{-1}) calculated from the spectroscopic constants of Ref. 17.
21. P. K. Pearson, C. F. Bender, and H. F. Schaefer III, to be published.
22. W. A. Goddard III and R. C. Ladner, J. Amer. Chem. Soc., 93, 6750 (1971).
23. Projected SOGI calculation at $R = \infty$, $E = -25.062603 \text{ h}$ and at $R = 4.0 a_0$, $E = -25.055187 \text{ h}$.
24. R. Thomson and F. W. Dalby, Can. J. Phys., 47, 1155 (1969).
25. 1 a.u. = 2.54177 D.
26. J. F. Harrison and L. C. Allen, J. Mol. Spectry. 29, 432 (1969).

Appendix 1

1. INTRODUCTION

We report here the wavefunctions and properties of the BH molecule as obtained using the recently developed G1 [1-3] and spin-coupling optimized G1 [4] (SOGI) methods. The G1 method can be viewed as a generalization of the valence bond (VB) method in which all orthogonality conditions are removed, the orbitals are allowed to be of any shape and spread over all the atoms, and the orbitals are functionally optimized in ab initio calculations [3,4]. Thus for BH there are six orbitals, none of which are orthogonal to another. However, the orbitals still divide into three groups: two core orbitals, two nonbonding orbitals, and two bonding orbitals. The SOGI method is a generalization of the G1 method in which the spin-coupling is optimized simultaneously with the orbital optimization rather than forced to be the spin coupling appropriate for the G1 or VB wavefunction [4].

The G1 wavefunction has the form

$$G_1^Y \Phi \chi, \quad (1)$$

where

$$\Phi = \phi_{1a}(1) \phi_{1b}(2) \phi_{2a}(3) \phi_{2b}(4) \phi_{3a}(5) \phi_{3b}(6) \quad (2)$$

and

$$\chi = \alpha(1)\beta(2)\alpha(3)\beta(4)\alpha(5)\beta(6)$$

are products of spatial and spin functions respectively. (In the following, electron numbers will be omitted from functions such as Φ and χ ; it will be understood that all functions are ordered by electron number.) Here G_1^Y is the group operator [5] (involving spatial and spin permutation operators) which ensures that for any Φ and χ , (1) describes a singlet state and satisfies Pauli's principle. The wavefunction in (1) can be re-expressed as [2,4]

$$\begin{aligned} & cA[(\phi_{1a} \phi_{1b} + \phi_{1b} \phi_{1a})(\phi_{2a} \phi_{2b} + \phi_{2b} \phi_{2a}) \times \\ & (\phi_{3a} \phi_{3b} + \phi_{3b} \phi_{3a}) \alpha\beta\alpha\beta\alpha\beta] = \\ & cA[\phi_{1a} \phi_{1b} \phi_{2a} \phi_{2b} \phi_{3a} \phi_{3b} \times \\ & (\alpha\beta - \beta\alpha)(\alpha\beta - \beta\alpha)(\alpha\beta - \beta\alpha)], \quad (3) \end{aligned}$$

which has the form of a generalized valence-bond wavefunction (c is just an arbitrary constant dependent upon normalization). In the G1 method it is required that each orbital, ϕ_k , be optimum (that is, that the energy be stationary under variations of ϕ_k). The result is a set of self-consistent equations analogous to the Hartree-Fock equations. However, the ϕ_k 's are allowed to be completely general (no double occupancy or orthogonality restrictions) and the G1 wavefunctions dissociate to the correct atomic limits.

In the usual valence bond [6] (VB) or extended valence bond [7] (EVB) method, the wavefunction for BH would have the form in (3) except that we would take ϕ_{1a} and ϕ_{1b} to be identical core-like orbitals and ϕ_{2a} and ϕ_{2b} to be identical non-bonding orbitals. In this case (3) differs from the form of the Hartree-Fock wavefunction only by having a split ϕ_3 pair. Thus the G1 wavefunction is a generalization of the VB and EVB wavefunctions in which *all* orbitals are allowed to split and where the orbitals are allowed to be of any shape and spread over all the atoms, and the orbitals are functionally optimized in *ab initio* calculations.

Given a product of orbitals as in (2) we can construct five linearly independent many-electron wavefunctions satisfying Pauli's principle and describing a singlet state. These can be taken as [5]

$$G_i^\gamma \Phi \chi, \quad i = 1, 2, \dots, 5,$$

where the group operator G_i^γ simultaneously takes care of the Pauli and spin symmetries. The different i just correspond to the different spin couplings of 6 electrons to form a singlet, one of which is presented in (1) and (3). However the G_i^γ are expressed in terms of representation matrices for the symmetric group, and any linear combination of the operators $\sum_i C_i G_i^\gamma$ can be expressed as $G_1^{\gamma L}$ using a new set representation matrices [4],

$$U_\tau^L = L U_\tau L^{-1}.$$

Thus the optimum wavefunction constructable from the product of orbitals Φ in (2) can be written as [4]

$$G_1^{\gamma L} \Phi \chi. \quad (4)$$

The orbitals of (4) are optimized in the same way (using the same programs) as are the orbitals of (1) except that now we must also optimize the transformation matrices L in order to optimize the spin coupling. In order to distinguish these approaches the latter is called the spin-coupling optimized GI (SOGI) method [4]. The SOGI orbitals can also be interpreted as the states of electrons moving in the average field due to the other electrons (the independent particle interpretation). In fact since the SOGI wavefunction is the best possible wavefunction using just the product of orbitals (1), these SOGI orbitals are the optimum independent particle orbitals. Hence the SOGI method can be viewed as the generalization and synthesis of the other orbital methods, such as Hartree-Fock, valence bond, and G1.

Previous calculations with the G1 and SOGI methods have been limited to molecules [3,4] and

atoms [2,4,8] with up to four electrons. Here we will report the first such calculations on larger systems. A matter of particular interest will be the description of the nonbonding orbitals of BH since VB and HF calculations take the nonbonding orbitals to be doubly occupied and since the systems previously considered with the G1 and SOGI methods did not have nonbonding orbitals.

2. CALCULATIONAL DETAILS.

The SCF calculations were carried out in the same way as described previously [1-4] except that each GI equation was expanded to first order in all six orbitals and the six coupled equations for the changes in all six orbitals were solved for the increments in each orbital each iteration. This generalized Newton-Raphson procedure [9] was found to lead to quadratic convergence in the orbitals*.

Only the first row of L is needed for constructing $U_{11}^L(\tau)$. In the case of a six-electron singlet state or a five-electron doublet state this row becomes

$$L_{11} = \cos \frac{1}{2}\Xi$$

$$L_{12} = \sin \frac{1}{2}\Xi_1 \cos \frac{1}{2}\Xi_2$$

$$L_{13} = \sin \frac{1}{2}\Xi_1 \sin \frac{1}{2}\Xi_2 \cos \frac{1}{2}\Xi_3$$

$$L_{14} = \sin \frac{1}{2}\Xi_1 \sin \frac{1}{2}\Xi_2 \sin \frac{1}{2}\Xi_3 \cos \frac{1}{2}\Xi_4$$

$$L_{15} = \sin \frac{1}{2}\Xi_1 \sin \frac{1}{2}\Xi_2 \sin \frac{1}{2}\Xi_3 \sin \frac{1}{2}\Xi_4.$$

Thus the spin-coupling is specified by the angles $\{\Xi_1, \Xi_2, \Xi_3, \text{ and } \Xi_4\}$. In some cases it is convenient to represent the spin-coupling in terms of the standard five spin-couplings (corresponding to the standard Young tableaux; these coefficients are denoted as $\{c_i\}$ and can be easily calculated from the $\{\Xi_i\}$).

The basis set consists of nine Slater orbitals on the boron (five s, three p, and one d) and two Slater orbitals on the hydrogen (one s and one p). The three core-like s functions of the B were chosen from a G1 B⁺⁺ calculation [2] and the other functions were chosen from Hartree-Fock [10,11] and GF [12] calculations. All SCF orbitals were *restricted* to be symmetry functions (σ for BH, s or p for B). Indeed, we have found that for

* Typically three to four iterations were required for the orbitals to converge to ten places. For six electrons and eleven basis functions this took 220 seconds/iteration on an IBM 360/75 computer.

Table 1
Calculated properties for the HF, G1 and SOGI wavefunctions of B and BH. Hartree atomic units are used unless otherwise specified

	B			BH		
	HF [13]	G1	SOGI	HF [10,14]	G1	SOGI
Total energy (E)	-24.52905	-24.54558	-24.54602	-25.13137	-25.16639	-25.16640
Kinetic energy (KE)	24.52837	24.53695	24.53800	25.11630	25.15858	25.15850
Virial ratio ($V/2E$)	0.99999	0.99982	0.99984	1.00030	0.99984	0.99984
Electric field gradient ^{b)}						
B nucleus	-0.62042	-0.62149	-0.63051	...	-0.74218	-0.74249
H nucleus	0.0	0.0	0.0	...	0.17671	0.17668
Dipole moment ^{c)}	0.0	0.0	0.0	0.682	0.70197	0.70200
Molecular quadrupole moment at boron ^{d)}	-2.45908	-2.44813	-2.42077	...	-2.32339	-2.32198
$\langle r^{-2} \rangle_B$ e)	15.853	15.90059	15.87240	22.75 ^{a)}	23.19517	23.19441
$\langle r^{-2} \rangle_H$ e)	3.0	3.0	3.0	47.70 ^{a)}	48.30235	48.30173
$\langle \frac{1}{r} \rangle_B$ f)	11.37930	11.37642	11.37727	11.81 ^{a)}	11.80471	11.80471
$\langle \frac{1}{r} \rangle_H$ f)	1.0	1.0	1.0	3.272 ^{a)}	3.26849	3.26847

a) Ref. [15].

b) 1 au = 3.24140×10^{15} esu/cm³.

c) 1 au = 2.54158 D.

d) 1 au = 1.34492×10^{-26} esu cm².

e) Multiply by -0.791985 to obtain diamagnetic susceptibility in ppm (cgs).

f) Multiply by 17.7497 to obtain diamagnetic shielding in ppm (cgs).

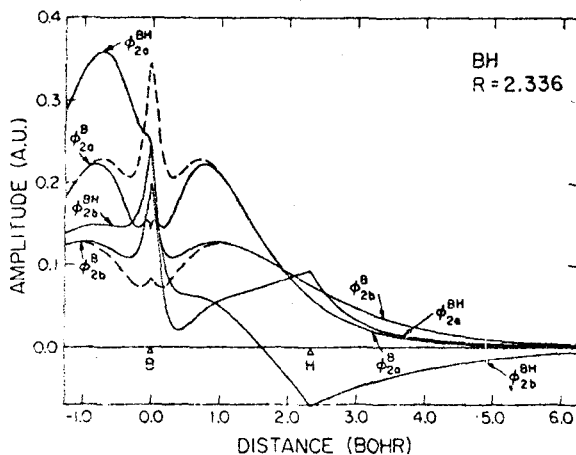


Fig. 1. The nonbonding SOGI orbitals of BH and the 2s valence pair SOGI orbitals of B. The dashed lines show the G1 orbitals of B, the G1 orbitals of BH superimposed upon the SOGI orbitals.

the UHF, GF, G1 and SOGI wavefunctions of such systems as Be, B, and BH, the SCF orbitals split so as to have lower symmetry than that of the atom and molecule. In this case, the spatial symmetry of the total wavefunction is not correct. The wavefunctions reported here are the optimum

ones leading to the correct spatial symmetry for the total wavefunction. These effects will be discussed more completely elsewhere.

Note in fig. 1 that the core parts of the non-bonding orbitals (2a and 2b) of B change significantly between SOGI and G1 (indicated by dashed lines in fig. 1). We have also noted that the shapes of the 2a and 2b orbitals in B for symmetry restricted calculations are quite sensitive to the description of the core potentials whereas this is not true for the unrestricted wavefunctions. Thus the changes in this B pair seem to be due to inadequacies in the basis being magnified by the symmetry restrictions. All the other orbitals of B and BH from the G1 and SOGI calculations nearly superimpose.

3. RESULTS AND DISCUSSION

The energies and properties of the (symmetry restricted) SOGI wavefunctions of B and BH are given in table 1. The optimum SOGI angles for BH are: $\frac{1}{2}\Xi_1 = 0.8165^\circ$, $\frac{1}{2}\Xi_2 = 94.65^\circ$, $\frac{1}{2}\Xi_3 = -39.44^\circ$, $\frac{1}{2}\Xi_4 = 23.1^\circ$ and the corresponding spin-coupling coefficients are:

$$c_1 = 0.99681, \quad c_2 = -0.01810, \quad c_3 = -0.07755,$$

$$c_4 = 0.00430 \text{ and } c_5 = 0.00169.$$

Table 2
The SOGI wavefunctions for BH molecule ($R = 2.336 a_0$) and B atom

BH molecule	ϕ_{1a}	ϕ_{1b}	ϕ_{2a}	ϕ_{2b}	ϕ_{3a}	ϕ_{3b}
B 1s 5.0	1.143 246	0.706 898	0.037 763	0.039 543	0.033 893	0.011 822
B 3s 7.9	-0.172 579	0.203 322	-0.028 390	-0.009 537	-0.022 257	-0.006 118
B 3s 4.84	0.004 488	0.172 874	-0.042 033	-0.011 014	-0.036 046	-0.018 877
B 2s 0.979 64	-0.001 731	-0.002 108	0.016 565	0.732 485	0.151 871	-0.076 912
B 2s 1.565 74	0.009 075	-0.043 706	0.882 057	0.184 435	0.663 363	0.106 787
B 2p 0.910 77	0.000 284	0.012 328	-0.007 938	0.690 080	0.089 509	0.053 472
B 2p 1.540 07	-0.001 014	-0.020 281	-0.382 704	0.451 711	0.275 117	0.016 676
B 2p 2.144 47	0.002 320	0.017 790	-0.023 835	-0.176 545	0.065 855	0.047 420
B 3d 1.080 34	0.000 511	-0.000 006	0.044 084	-0.146 639	0.066 574	0.005 197
H 1s 1.182 74	0.003 730	-0.000 816	0.102 911	-0.090 995	0.123 680	0.933 762
H 2p 1.699 99	-0.000 466	-0.001 868	-0.024 368	-0.002 887	-0.058 525	-0.013 321
ϵ	-7.887 418	-7.379 591	-0.492 456	-0.340 935	-0.619 464	-0.675 779
SOGI angles		$\frac{1}{2}\Xi_1 = 0.8165^\circ$	$\frac{1}{2}\Xi_2 = 94.65^\circ$	$\frac{1}{2}\Xi_3 = -39.44^\circ$	$\frac{1}{2}\Xi_4 = 23.13^\circ$	

B atom	ϕ_{1a}	ϕ_{1b}	ϕ_{2a}	ϕ_{2b}	ϕ_{3a}
B 1s 5.0	1.141 563	0.702 788	0.022 575	0.031 547	0.0
B 3s 7.9	-0.173 477	0.202 382	-0.034 825	-0.009 340	0.0
B 3s 4.84	0.002 680	0.172 992	-0.086 832	0.009 758	0.0
B 2s 1.11	0.004 485	0.013 193	0.121 019	1.109 207	0.0
B 2s 1.72	0.018 043	-0.032 001	0.054 425	-0.132 354	0.0
B 2p 0.931	0.0	0.0	0.0	0.0	0.691 758
B 2p 1.753	0.0	0.0	0.0	0.0	0.353 931
B 2p 4.558	0.0	0.0	0.0	0.0	0.017 740
ϵ	-7.916 911	-7.424 851	-0.588 972	-0.477 026	-0.312 538
SOGI angles		$\frac{1}{2}\Xi_1 = 4.673^\circ$	$\frac{1}{2}\Xi_2 = 76.00^\circ$	$\frac{1}{2}\Xi_3 = -3.748^\circ$	$\frac{1}{2}\Xi_4 = 21.56^\circ$

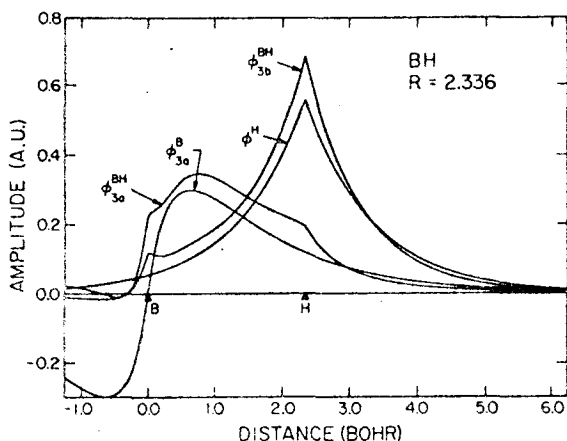


Fig. 2. The bonding SOGI orbitals of BH and the 2p valence SOGI orbital of B. The G1 orbitals superimpose upon the SOGI orbitals.

Thus we see that the SOGI wavefunction is essentially the G1 wavefunction. In fact, for BH the expansion coefficients of the G1 orbitals are the same as the SOGI coefficients (see table 2) to about four places and the plots of the G1 orbitals

would superimpose on the SOGI orbitals of figs. 1 and 2. The G1 energy is higher than the SOGI energy by 0.0004 for B and 0.00001 for BH and the G1 dipole moment of BH is lower by 0.0001 debye. This close comparison between G1 and SOGI was also observed for LiH [3] and is expected to occur often in the ground states of such stable, nonconjugated systems.

The SOGI energy of BH is 0.035 hartree lower than the best Hartree-Fock value [10] and the calculated dissociation energy is 91.5% of the experimental value as compared to 77.8% for Hartree-Fock. The Hartree-Fock and SOGI values for the dipole moment are nearly the same.

Next we will discuss the SOGI orbitals for B and BH, the expansion coefficients of which are given in table 2.

The boron atom ($2p$ state) has five orbitals. Two of these orbitals (ϕ_{1a} and ϕ_{1b}) are spherically symmetric s-like functions which are concentrated in the region close to the boron nucleus; these orbitals are similar to the Hartree-Fock core orbital and will be referred to as core functions. However, the SOGI orbitals are split significantly, that is, ϕ_{1a} is not equal to ϕ_{1b} as is

demonstrated by the 0.9625 overlap between the two orbitals. The second pair of orbitals, ϕ_{2a} and ϕ_{2b} , are also s-like functions, but are much more diffuse (see fig. 1), being concentrated in what will be called the valence region. These orbitals are similar to the Hartree-Fock 2s orbital in the valence region although they are significantly split (overlap 0.9084). However, in the core region they differ greatly from the HF 2s orbital since the HF 2s is forced to be orthogonal to the HF 1s whereas no orthogonality restrictions are imposed upon the SOGI orbitals. The remaining orbital, ϕ_{3a} (see fig. 2) is a p-type orbital which is nearly identical to the corresponding Hartree-Fock orbital. The resulting total energy for SOGI is 0.017 hartree lower than the Hartree-Fock value.

In the BH molecule ($^1\Sigma^+$ state at $R = R_e = 2.336 a_0$), the orbitals naturally group into three pairs. The first pair of orbitals, ϕ_{1a} and ϕ_{1b} , are s-type core functions concentrated mainly in the area of the boron nucleus and are essentially the same as in B atom. The pair of orbitals, ϕ_{3a} and ϕ_{3b} , are aptly termed as bonding orbitals and have evolved from the pairing of a boron atom orbital with the hydrogen 1s orbital (see fig. 2). We see that by $R = R_e$ these two orbitals have significantly increased their amplitude between the two nuclei. The ϕ_{3a} orbital has mixed in s character into the orbital so as to increase its amplitude between the two nuclei. The hydrogen orbital has also mixed in some s-like character from the boron center so as to increase its amplitude in the area between the nuclei. The remaining pair of orbitals, ϕ_{2a} and ϕ_{2b} , are clearly nonbonding orbitals (see fig. 1). Both of these orbitals have hybridized such that they have "moved" out of the area between the two nuclei. Additionally, these two orbitals have split more so that the overlap between the two orbitals is now 0.8350.

Although these changes in the orbitals from B to BH seem reasonable a more detailed comparison of the changes as a function of R shows disturbing features. Even for R as large as $7a_0$ the H 1s orbital is coupled to one of the 2s orbitals (ϕ_2) of B rather than with the 2p orbital. Furthermore between 7.0 and 3.5 the nonbonding orbitals change drastically where it appears that these orbitals flip from one type of coupling appropriate for large R to one appropriate for small R . A further investigation showed that these strange

features were due to the symmetry restrictions and that unrestricted GI and SOGI calculations lead to continuous changes of the orbitals for changing from ∞ to R_e .

The bonding orbitals of BH have shapes similar to the bonding orbitals of LiH and are closely related to what one might have guessed for hybridized valence-bond orbitals. However, the nonbonding orbitals are rather different from the previously discussed valence-bond orbitals primarily because the valence-bond nonbonding orbitals are usually taken as doubly occupied atomic orbitals. It will be of great interest to see what the nonbonding orbitals are like in larger molecules and perhaps determine how they affect and are affected by neighboring bonding orbitals.

ACKNOWLEDGEMENTS

We thank Luis R. Kahn for the use of his Diatomic Properties Integral program and Dr. A. D. McLean for the use of the McLean Integrals program (QCPE 104).

REFERENCES

- [1] W. A. Goddard III, Phys. Rev. 157 (1967) 81.
- [2] W. A. Goddard III, Phys. Rev. 169 (1968) 120.
- [3] W. E. Palke and W. A. Goddard III, J. Chem. Phys. 50 (1969) 4524.
- [4] R. C. Ladner and W. A. Goddard III, J. Chem. Phys. 51 (1969) 1073.
- [5] W. A. Goddard III, Phys. Rev. 157 (1967) 73.
- [6] H. Eyring, J. Walter and G. E. Kimball, Quantum chemistry (Wiley, New York, 1944); L. Pauling and E. B. Wilson, Introduction to quantum mechanics (McGraw-Hill, New York, 1935).
- [7] J. C. Slater, Electronic structure of molecules (McGraw-Hill, New York, 1963).
- [8] U. Kaldor and F. E. Harris, Phys. Rev. 183 (1969) 1.
- [9] J. Hinze and C. C. J. Roothaan, Progr. Theoret. Phys. (Kyoto) 40 (1967) 37.
- [10] P. E. Cade and W. M. Huo, J. Chem. Phys. 47 (1967) 614.
- [11] P. S. Bagus, T. L. Gilbert, H. D. Cohen and C. C. J. Roothaan, unpublished results.
- [12] L. R. Kahn and W. A. Goddard III, unpublished results.
- [13] W. A. Goddard III, Phys. Rev. 182 (1969) 48.
- [14] P. E. Cade and W. M. Huo, J. Chem. Phys. 45 (1966) 1063.
- [15] R. A. Hegstrom and W. N. Lipscomb, J. Chem. Phys. 45 (1966) 2378.

I. INTRODUCTION

The independent particle formalism of the Hartree-Fock method¹ has been extremely influential in the conceptual understanding of atomic and molecular systems. However, for molecules such as BH the Hartree-Fock method does not describe the system correctly as R becomes large.² Since this method does not describe properly the process of breaking a bond, it is not generally useful for describing chemical reactions and chemical binding.

The GI² (and SOGI)³ method resolves this difficulty by allowing each orbital to be different (no double occupation restriction) while retaining the correct spin symmetry in the many-electron wavefunction. The resulting orbitals change smoothly from the atomic orbitals at large internuclear distances to the optimum molecular orbitals at the equilibrium internuclear distance, R_e .

In this paper we consider the ground state ($X^1\Sigma^+$) of the BH molecular system as a function of R (from $2a_0$ to ∞) using the GI method. Since this particular system contains both bonding and non-bonding valence orbitals, we will be especially interested in how these orbitals interact and change as the molecule forms.

Some basic aspects of the GI method are described in Sec. II, and Sec. III contains some of the details of the calculations. Section IV contains a description of the optimum GI orbitals and wavefunctions as a function of R . Following sections

discuss the effects of symmetry restrictions in the atomic and molecular basis sets, the properties as a function of R , and the implications of this orbital description as applied to BH_2 and other systems. It is interesting to note that the properties of BH are typically non-monotonic and that the behavior of the properties can be easily understood in terms of qualitative changes in the orbitals.

II. THE WAVEFUNCTIONS

In the Hartree-Fock method the wavefunction for BH is taken as a Slater determinant with three doubly occupied orbitals

$$\mathcal{Q}[\phi_1\alpha\phi_1\beta\phi_2\alpha\phi_2\beta\phi_3\alpha\phi_3\beta] = \mathcal{Q}[\phi_1\phi_1\phi_2\phi_2\phi_3\phi_3\alpha\beta\alpha\beta\alpha\beta], \quad (1)$$

where \mathcal{Q} is the antisymmetrizer (or determinant operator), α and β are the usual one-electron spin functions, and electron number is implied by position (i. e., the first orbital is electron 1, the second is electron 2, etc.); on the right side of (1) we merely separate the orbitals from the spin terms. The spatial orbitals ϕ_i must be doubly occupied or the wavefunction is not an eigenfunction of \hat{S}^2 . For each internuclear distance, R , the orbitals $\{\phi_i\}$ are required to be the best possible ones, which results in the variational equations

$$H^{HF} \phi_k = \epsilon_k \phi_k, \quad (2)$$

where

$$H^{HF} = -\frac{1}{2}\nabla^2 + U^{HF} \quad (3)$$

and U^{HF} contains the usual Coulomb and exchange operators and the nuclear attraction terms.¹

The wavefunction (1) does relatively well⁴ for properties near R_e , the equilibrium internuclear distance. However, in order to describe the ground-state Hartree-Fock wavefunctions for B and H at $R = \infty$, we must have two doubly occupied and one singly occupied orbital localized on the B and one singly occupied orbital localized on the H. That is, we require at least two doubly occupied and two singly occupied orbitals at $R = \infty$. But (1) has only three doubly occupied orbitals at $R = \infty$ and hence cannot describe BH properly at large distances.⁵

An alternative type of wavefunction is the valence bond (VB) wavefunction,

$$\begin{aligned} & \mathcal{Q}[\phi_1 \phi_1 \phi_2 \phi_2 (\phi_{3a} \phi_{3b} + \phi_{3b} \phi_{3a}) \alpha \beta \alpha \beta \alpha \beta] \quad (4) \\ & = \mathcal{A}[\phi_1 \phi_1 \phi_2 \phi_2 \phi_{3a} \phi_{3b} \alpha \beta \alpha \beta (\alpha \beta - \beta \alpha)] \end{aligned}$$

in which ϕ_1 and ϕ_2 are doubly occupied B 1s and B 2s functions,

ϕ_{3a} is the Bp_z function (where z is the intermolecular axis), and ϕ_{3b} is the H 1s function. This wavefunction describes a singlet state and dissociates correctly to B and H atoms for $R = \infty$. However, since (4) uses atomic orbitals, the description near R_e is generally poor. It leads to an R_e that is too large and a binding energy that is too small. One way of improving the valence bond wavefunction (4) is to do a configuration interaction⁶ (CI) with a number of terms of the form (4). Unfortunately, the configuration interaction wavefunction does not lend itself to such a simple interpretation.

In the GI method^{2, 7} we consider a wavefunction of the form (1) except that the \mathcal{Q} (which takes care of Pauli's Principle) is replaced by the group operator,⁸ G_i^γ , which simultaneously takes care of both the spin symmetry and Pauli's principle. (Thus we obtain the correct spin symmetry without doubly occupying the orbitals.) The resulting wavefunction is

$$G_i^\gamma[\phi_{1a}\phi_{1b}\phi_{2a}\phi_{2b}\phi_{3a}\phi_{3b}\alpha\beta\alpha\beta\alpha\beta]. \quad (5)$$

The orbitals ϕ_i are then required to be the best possible ones, resulting in six variational equations

$$H_k \phi_k = \epsilon_k \phi_k \quad k = 1, 2, \dots, 6 \quad (6)$$

where

$$H_k = \frac{1}{2}\nabla^2 + U_k, \quad (7)$$

and U_k is analogous to U^{HF} in (3), except that the exchange terms are much more complicated.

The group operator G_i^γ is based on the Wigner projection operators for the symmetric group and involves only permutation operators for spatial and spin coordinates.⁸ The γ refers to the total spin (in this case singlet) and the i refers to the spin coupling. There are five independent ways to couple six electrons into a singlet state, each of which corresponds to a different G_i^γ operator. In the GI method we consider the first of these possible spin couplings and optimize all of the orbitals for that coupling.² In the spin-coupling optimized GI

(or SOGI) method,³ we optimize both the spin coupling and the orbitals. We have found for BH (as for LiH³) that the SOGI wavefunction is essentially identical with the G1 wavefunction, which is written as⁹

$$\begin{aligned}
 & G_1^\gamma [\phi_{1a} \phi_{1b} \phi_{2a} \phi_{2b} \phi_{3a} \phi_{3b} \alpha\beta\alpha\beta\alpha\beta] \\
 &= \frac{5}{8} \mathcal{Q} [\phi_{1a} \phi_{1b} \phi_{2a} \phi_{2b} \phi_{3a} \phi_{3b} (\alpha\beta - \beta\alpha)(\alpha\beta - \beta\alpha)(\alpha\beta - \beta\alpha)] \quad (8) \\
 &= \frac{5}{8} \mathcal{Q} [(\phi_{1a} \phi_{1b} + \phi_{1b} \phi_{1a})(\phi_{2a} \phi_{2b} + \phi_{2b} \phi_{2a})(\phi_{3a} \phi_{3b} + \phi_{3b} \phi_{3a})\alpha\beta\alpha\beta\alpha\beta]
 \end{aligned}$$

(here \mathcal{Q} is normalized so that $\mathcal{Q}\mathcal{Q} = \mathcal{Q}$).

If we set

$$\phi_{ia} = \phi_{ib} = \phi_i^{\text{HF}} \quad i = 1, 2, 3$$

in (8) we obtain the HF wavefunction as in (1). And if in (8) we set

$\phi_{1a} = \phi_{1b} = \text{B } 1s$, $\phi_{2a} = \phi_{2b} = \text{B } 2s$, $\phi_{3a} = \text{B } 2p_z$, and $\phi_{3b} = \text{H } 1s$, we obtain the valence bond wavefunction (4). Thus both the Hartree-Fock and valence bond methods are special cases of G1 in which restrictions are made upon the orbitals.

The SOGI wavefunction is a generalization of the G1 wavefunction in which the spin coupling is also optimized. The resulting wavefunction has a spin pairing different from that of (8); however, the SOGI wavefunction still involves just six orbitals, each of which is an eigenfunction of one of the variational one-particle equations (6) and (7). Consequently, these orbitals still lead to an interpretation of the many-electron wavefunction in terms of independent particle or self-consistent field orbitals.

III. CALCULATIONAL DETAILS

The G1 and SOGI differential equations, (6), were solved using a basis set expansion in terms of Gaussian basis functions. Three different basis sets were used.

The primitive basis for the first set (called the sp basis) consists of eleven¹⁰ 1s and five¹¹ 2p Gaussians centered on the boron and six¹¹ 1s Gaussians centered on the hydrogen (see Table I). For the G1 calculations we reduced this basis to a smaller number of contracted functions each of which is a linear combination of the primitive functions. This contracted basis consists of five s-functions, two p_x -functions, and two p_z -functions (z is the intermolecular axis) on the boron and two s-functions on the hydrogen; the contraction coefficients were selected from a series of G1 calculations on the separated atoms and the H_2 molecule. This sp basis was used for calculations at $R = 9.0, 7.0, 5.0, 4.0, 3.0, 2.336,$ and $2.0 a_0$. (The experimental¹² equilibrium distance for the ground state of BH ($X^1\Sigma^+$) is $2.3289 a_0$.)

A second basis (called the spd basis) was selected by adding polarization functions to the sp basis. The orbital exponents were based on the optimum Slater basis functions of Cade and Huo^{4a} and were fitted using a three-term Gaussian expansion.¹¹ The contraction coefficients for the spd basis were selected from an iterative series of G1 calculations at $R = 2.336 a_0$ involving nondisjoint contractions; the final contraction is given in Table I and the expansion coefficients of the G1 orbitals are given in Table II. A similar basis was used for calculations on the separated atoms.

TABLE I. The basis sets for the SOGI wavefunctions. Each (contracted) basis function is expressed as a linear combination of normalized primitive Cartesian Gaussian functions. The contracted basis functions are not necessarily normalized.

1s - primitive gaussians (Boron)								2p _z - primitive gaussians (Hydrogen)							
α_1	10224.65	1587.2834	356.64641	99.421167	31.516117	10.918521	4.0434363	1.6009069	0.42366713	0.16465811	0.06618283	α_1	3.89655	0.92283	0.28535
$\chi_1(\text{sp})$	0.0003046	0.0822779	0.0125034	0.0527374	0.2022619	0.4155042	0.3401305	0.1303975	0.0052250	0.0	0.0	$\chi_1^*(\text{spd})$	-0.0010782	-0.0055528	0.0007211
$\chi_2(\text{sp})$	0.0001887	0.0014885	0.0074021	0.0302514	0.0684721	0.2235100	0.5220507	0.2744027	0.0062519	0.0	0.0	$\chi_2^*(\text{spd})$	-0.0000619	-0.0003190	0.0016182
$\chi_3(\text{sp})$	0.0000125	0.0000977	0.0004877	0.0020511	0.0050574	0.0073860	-0.0300404	-0.0528426	0.3093856	0.0	0.0	$\chi_3^*(\text{spd})$	-0.0006115	-0.0041793	0.0136778
$\chi_4(\text{sp})$	0.0	0.0	0.0	0.0	0.0	0.0	0.0	0.0	0.0	0.0	0.0	$\chi_4^*(\text{spd})$	-0.0068010	-0.0350256	-0.0225844
$\chi_5(\text{sp})$	0.0	0.0	0.0	0.0	1.0	0.0	0.0	0.0	0.0	0.0	0.0	$\chi_5^*(\text{spd})$	-0.0016340	-0.0084150	-0.0000966
$\chi_6^*(\text{spd})$	0.0003044	0.0022765	0.0124917	0.0527005	0.2020657	0.4151594	0.3398895	0.1302149	0.0065278	0.0003255	0.0003149	$\chi_6(\text{spd})$	0.0	0.0	1.0
$\chi_7^*(\text{spd})$	0.0001884	0.0014658	0.0073879	0.0302022	0.0683701	0.2232327	0.5208404	0.2745578	0.0076804	-0.0125313	-0.0002894	3d _{x²} - primitive gaussians (Boron)			
$\chi_8^*(\text{spd})$	0.0000099	0.0000749	0.0003329	0.0016089	0.0050075	0.0059821	-0.0248124	-0.0525371	0.2799750	0.5055603	0.2470722	α_1	1.23148	0.36952	0.13582
$\chi_9^*(\text{spd})$	0.0000060	0.0000402	0.0002498	0.0008109	0.0034793	0.006214	-0.0140086	-0.0587366	0.2954351	0.2488047	0.0095641	$\chi_1^*(\text{spd})$	-0.0000659	-0.0003186	-0.0001763
$\chi_{10}^*(\text{spd})$	0.0000027	0.0000173	0.0001191	0.0004377	0.0027748	0.0026277	-0.0041193	-0.0155601	0.0639273	0.0124424	-0.0346481	$\chi_2^*(\text{spd})$	-0.0000807	-0.0003901	-0.0003737
1s - primitive gaussians (Hydrogen)								3d _{yz} - primitive gaussians (Boron)							
α_1	82.4736	12.3983	2.83924	0.814717	0.271838	0.099482					α_1	1.23148	0.36952	0.13582	
$\chi_{10}(\text{sp})$	0.0034336	0.0259598	0.1216899	0.3587761	0.4920964	0.1431782					$\chi_1^*(\text{spd})$	-0.0000701	-0.0003388	-0.0001403	
$\chi_{11}(\text{sp})$	0.0020068	0.0154023	0.0740994	0.2495336	0.4637421	0.3358507					$\chi_2^*(\text{spd})$	-0.0000387	-0.0001868	-0.0002529	
$\chi_{12}^*(\text{spd})$	-0.0000010	0.0002015	-0.0000174	0.0017250	0.0008292	0.0000550					$\chi_3^*(\text{spd})$	-0.0008211	-0.0039671	-0.0034826	
$\chi_{13}^*(\text{spd})$	-0.0000405	0.0001433	-0.0013198	-0.0021274	-0.0042553	-0.0031692					$\chi_4^*(\text{spd})$	-0.0060481	-0.0292207	-0.0083737	
$\chi_{14}^*(\text{spd})$	0.0000054	0.0010376	0.0037375	0.0156775	-0.0368242	-0.0903977					$\chi_5^*(\text{spd})$	0.0003149	0.0015212	-0.0018321	
$\chi_{15}^*(\text{spd})$	0.0004383	0.0064230	0.0181037	0.0226302	0.1286214	0.0392976					$\chi_6^*(\text{spd})$	0.0	0.0	1.0	
$\chi_{16}^*(\text{spd})$	0.0022563	0.0184051	0.0915000	0.3431838	0.4792783	0.0972112					3d _{z²} - primitive gaussians (Boron)				
2p _x - primitive gaussians (Boron)								3d _{xy} - primitive gaussians (Boron)							
α_1	11.3413	2.43599	0.68358	0.21336	0.070114					α_1	1.23148	0.36952	0.13582		
$\chi_1(\text{sp})$	0.0155373	0.0734559	0.4049270	0.6467836	0.0					$\chi_1^*(\text{spd})$	0.0001361	0.0006574	0.0003166		
$\chi_2^*(\text{sp})$	0.0	0.0	0.0	0.0	1.0					$\chi_2^*(\text{spd})$	0.0001194	0.0005769	0.0006267		
$\chi_3^*(\text{spd})$	0.0059068	0.0324678	0.1344217	0.2571221	0.0370575					$\chi_3^*(\text{spd})$	-0.0015371	-0.0074204	-0.0056788		
2p _z - primitive gaussians (Boron)								3d _{xz} - primitive gaussians (Boron)							
α_1	11.3413	2.43599	0.68358	0.21336	0.070114					α_1	1.23148	0.36952	0.13582		
$\chi_4(\text{sp})$	0.0179827	0.1102108	0.3822327	0.6487911	0.0					$\chi_1(\text{spd})$	-0.0127843	-0.0061766	-0.0406598		
$\chi_5(\text{sp})$	0.0	0.0	0.0	0.0	1.0										
$\chi_6^*(\text{spd})$	0.0001032	0.0005594	0.0012943	0.0026546	0.0003392										
$\chi_7^*(\text{spd})$	0.0000958	0.0005190	0.0001120	0.0010935	0.0019192										
$\chi_8^*(\text{spd})$	-0.0053855	-0.0291768	-0.0906685	-0.1335387	-0.0784002										
$\chi_9^*(\text{spd})$	0.0121558	0.0658559	0.2974717	0.3325925	0.0879993										
$\chi_{10}^*(\text{spd})$	0.0028271	0.0153161	0.0460586	0.0561691	0.0398936										

* Denotes basis functions that make use of primitive functions of more than one symmetry type.

TABLE II. The SOGI orbitals of BH for $R = 2.336 a_0$. (The spd basis listed in Table I was used; note that these basis functions are not normalized; however, each molecular orbital is normalized.)

	ϕ_{1a}	ϕ_{1b}	ϕ_{2a}	ϕ_{2b}	ϕ_{3a}	ϕ_{3b}
χ_1	1.0001261	0.0001261	-0.0000638	-0.0000638	0.0010385	-0.0002896
χ_2	0.0000636	0.9993060	-0.0000109	-0.0000109	0.0023288	0.0033659
χ_3	0.0001369	0.0003552	1.0039542	1.0039542	0.0045312	-0.0124687
χ_4	0.0000000	0.0000000	1.0018131	-1.0018131	0.0000000	0.0000000
χ_5	0.0000000	0.0000000	1.0083903	-1.0083903	0.0000000	0.0000000
χ_6	-0.0009159	0.0025092	0.0002817	0.0002817	1.0062892	0.0046190
χ_7	-0.0007085	0.0012632	-0.0028962	-0.0028962	-0.0040385	0.9876702
χ_8	0.0002332	0.0001641	0.0016517	0.0016517	0.0105227	0.0061252
χ_9	-0.0000166	-0.0001936	-0.0016980	-0.0016980	0.0021755	0.0109834
χ_{10}	-0.0000154	-0.0001857	-0.0017375	-0.0017375	0.0022947	0.0107200
χ_{11}	-0.0000940	-0.0002490	-0.0024681	-0.0024681	-0.0028500	0.0131089
ϵ^a	-7.88231	-7.37286	-0.44705	-0.44705	-0.59130	-0.64956
SOGI angles	$\frac{1}{2}\Xi_A = 0.4302128, \frac{1}{2}\Xi_B = 90.00000, \frac{1}{2}\Xi_C = -90.00000, \frac{1}{2}\Xi_D = 54.73561$					
Expansion coefficient ^b	$C_1 = 0.999972, C_2 = 0.0, C_3 = 0.0, C_4 = 0.004360, C_5 = 0.006149$					

^a Orbital energy, see Eq. (6).

^b See Eq. (9).

A third set (called the spxy basis) was constructed by adding p_y functions (equivalent to the p_x functions) to the sp basis. This set was then contracted to the molecular orbitals obtained from the G1 sp calculation (at the same R). The projected G1 calculations discussed in Section V used this basis.

The SOGI and G1 calculations were carried out with the quadratically convergent SOGI program written by R. C. Ladner. The Gaussian molecular integrals were calculated using either the W.J. Hunt version of the Harold Basch Polyatom Integrals program or the M. Geller Moses Integrals program. The Gaussian properties integrals were carried out using the Neumann-Moskowitz NYU program. The contour plots were made using the Guberman-Parr Contour Plotting program. The nondisjoint integral transformations (required for the spd and spxy contractions), were carried out with the D. Huestis N^5 -transformation program.

IV. RESULTS

A. Orbital Description

In the Hartree-Fock description of boron atom , the configuration is $(1s)^2 (2s)^2 (2p)$, that is, the wavefunction has the form

$$a \phi_1 \phi_1 \phi_2 \phi_2 \phi_3 \alpha \beta \alpha \beta \alpha ,$$

where ϕ_1 and ϕ_2 are 1s and 2s orbitals and ϕ_3 is a p_z orbital. In the BH molecule the configuration is $(1\sigma)^2 (2\sigma)^2 (3\sigma)^2$, where 1σ corresponds to the B 1s, 2σ is mainly a bonding combination of B 2s and H 1s, and 3σ is mainly a B 2p orbital hybridized away from the H. Thus the HF description does not correspond to the intuitive idea that the BH should be mainly formed from (a hybridized) B p_z and H 1s orbitals. (Note that the HF wavefunction for BH does not dissociate into B and H atoms; thus it might well lead to a misleading description of the bonding orbitals.)

In the VB description of BH we start with the HF B atom and form a bond between the B p_z and H 1s. Thus all orbitals are σ orbitals (as in HF).

The G1 description differs in several ways. The G1 solution of the boron atom consists of five nonorthogonal orbitals. The ϕ_{1a} and ϕ_{1b} orbitals are B core states, somewhat similar to the HF 1s orbital but radially split (and coupled into a singlet). The unpaired orbital ϕ_{3a} is essentially the same as the HF $2p_z$ orbital. However the ϕ_{2a} and ϕ_{2b} orbitals are not s-like functions as in HF but split into $s + p_x$ and $s - p_x$ functions (we will denote these as s_x and $s_{\bar{x}}$, respectively) which

are coupled into a singlet pair. A contour plot of the s_x orbital is shown in Fig. 1a (this figure is actually for BH at $R = 5.0 a_0$, but there is essentially no change for larger R). The function $s\bar{x}$ is exactly the same but it is pointed in the $-x$ direction. The resulting many-electron wavefunction for boron is not exactly a 2P state but contains a small component of 2F (for the sp basis and small components of 2F , 2H , etc., for the spd basis). The question of spatial symmetry is investigated in Section V, where it is concluded that it is correct to consider these spatially unrestricted orbitals.

In forming the ground state of the BH molecule, we bring the H along the z -axis of the p_z orbital. At large R the B p_z orbital, ϕ_{3a} , hybridizes and begins to delocalize onto the H (as shown in Fig. 1b for $R = 5.0 a_0$). This orbital is coupled into a singlet with the H orbital, ϕ_{3b} , which for large R delocalizes only slightly onto the B (see Fig. 1c for the orbital at $R = 5.0 a_0$). These two orbitals comprise the bonding pair. For large R the two nonbonding orbitals are $\sigma\pi$ hybrids (see Fig. 1a for the orbital at $R = 5.0 a_0$) which are essentially unchanged from the form for the boron atom. Only these two nonbonding orbitals have any π -character, all other orbitals have only sigma character. As we will see in Section V the resulting many-electron wavefunction is nearly exactly $^1\Sigma$ but has a small component of $^1\Delta$ symmetry.

For $R < 4a_0$ greater changes occur in the orbitals. The B bonding orbital, ϕ_{3a} , is significantly hybridized into the bonding region (as indicated in Fig. 1b) and the H bonding orbital becomes more contracted with a nodal

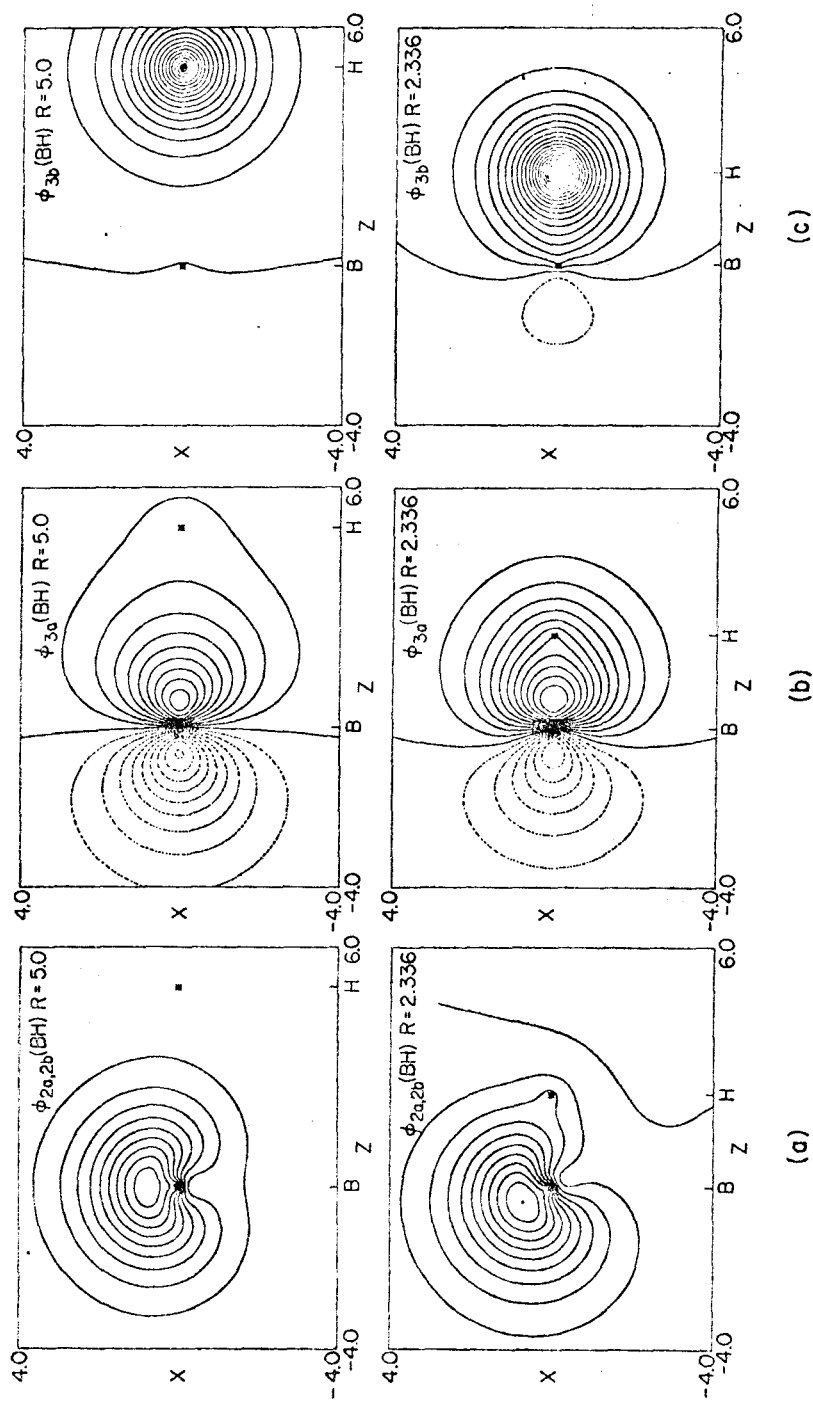


Fig. 1. Amplitude in the xz plane of the G1 valence orbitals for BH at $R = 5.0 a_0$ and $2.336 a_0$.

plane nearly passing through the B nucleus (see Fig. 1c). At the same time as the BH bond becomes stronger the nonbonding orbitals rotate out of the way of the bond until at R_e they point $\pm 116.5^\circ$ away from the bond axis (the angles are $\pm 90^\circ$ for $R = \infty$) as shown in Fig. 1a.

Following the changes in the orbitals as a function of internuclear distance, we find a very consistent behavior. As the hydrogen nucleus is brought up along the z-axis, the boron p_z orbital and the orbital centered on the hydrogen change so as to build up amplitude in the region between the two nuclei, and concomitantly the nonbonding orbitals bend away and stretch back from the bonding region. In Fig. 2 we show plots of the amplitude of the nonbonding orbital for various R, where for each R we show the amplitude along a line passing through the maximum in the orbital (90° for $R = 9a_0$, 95.1° for $R = 4a_0$, and 116.5° for $R = 2.336a_0$). We see that indeed the main effect is a rotation of this orbital. However for $R < 4a_0$ the nonbonding orbitals increase their amplitude behind the boron and decrease it in the region between the nuclei so that there is some distortion in the orbital as it rotates.

The amplitudes of the bonding orbitals along the bonding axis are shown in Fig. 3b, c for various R. Here we see the build up of amplitude in the bonding region as the atoms come together. Note that for $R > 4a_0$ the main change in ϕ_{3a} is a transfer of amplitude from behind the B to the H, with the lobe of ϕ_{3a} pointing toward the H only slightly changed. Below $4a_0$ this orbital increases rather uniformly in the B—H region. The ϕ_{3b} orbital changes only slightly for $R > 4a_0$, the main effect being the incorporation of a node just past the B. Larger

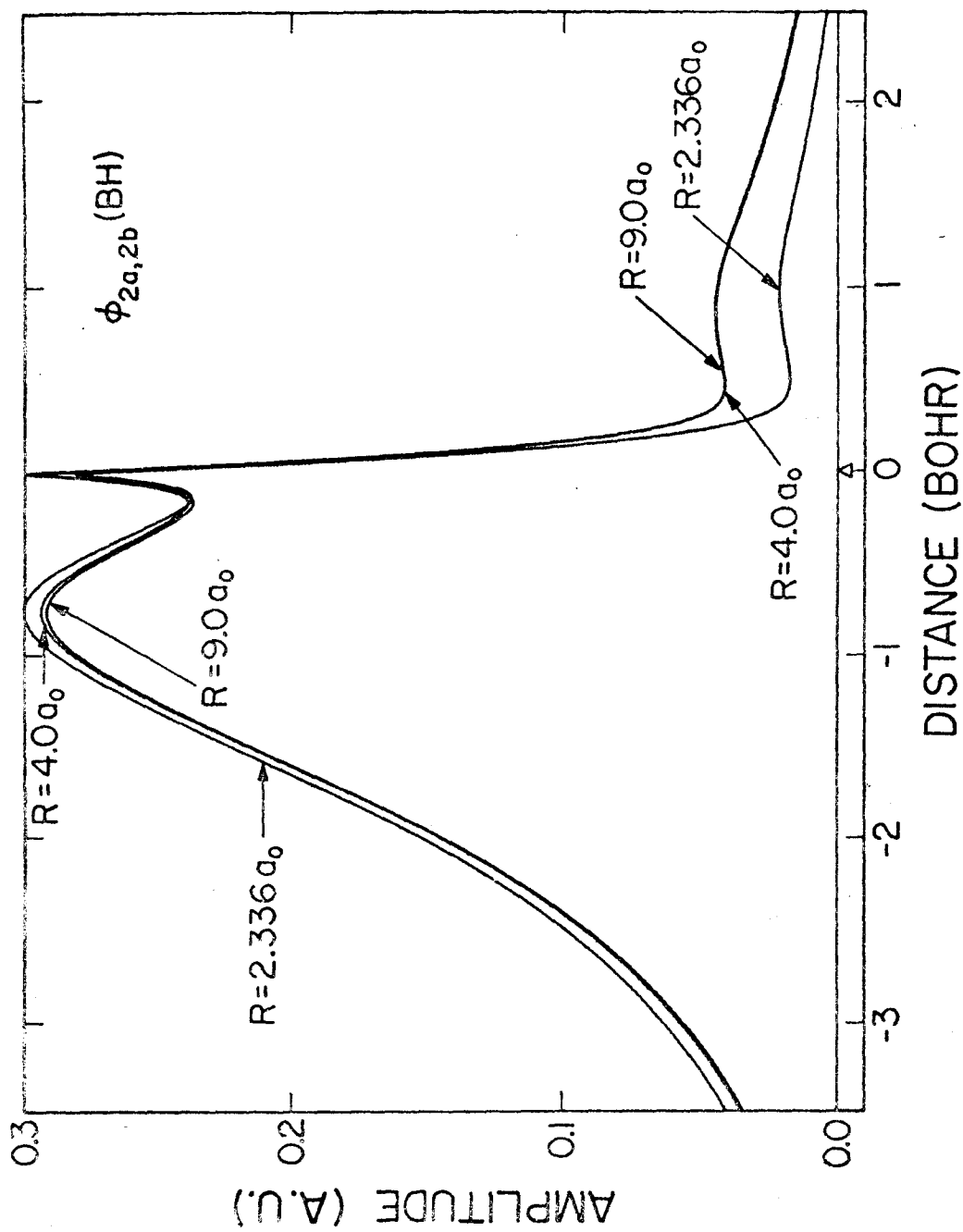


Fig. 2. Amplitude of one of the nonbonding orbitals along the axis of major amplitude.

changes occur for $R < 4a_0$, where the overlap between the atomic functions is more substantial and the nodal plane follows the H as R is decreased.

Further detail in the changes in $\phi_{2a, 2b}$ is given in Fig. 3a, which shows the amplitude along the bonding axis. For large R the σ part of this orbital is s-like with a slight hybridization into the bonding region. However at intermediate and short internuclear distances the rotation of the nonbonding orbitals out of the bonding region and into the area behind the boron nucleus leads to an effective hybridization away from the H. So that by $R = R_e$ the nonbonding orbital has significantly increased its amplitude behind the boron and decreased its amplitude in the bonding region.

The orbital energies (ϵ_i) as a function of the internuclear distance are shown in Fig. 4, where we see that they change smoothly as the atoms come together. For $R > 4a_0$, ϵ_{3a} decreases gradually as R decreases while for $R < 4a_0$, ϵ_{3a} decreases rapidly (approximately proportional to $\frac{1}{R}$). Concomitantly, ϵ_{3b} increases with decreasing R for $R > 4a_0$ and decreases with R for $R < 4a_0$ (approximately proportional to $\frac{1}{R}$). On the other hand, $\epsilon_{2a, 2b}$ decreases with decreasing R for $R > 4a_0$ and increases for smaller R. These changes may be qualitatively interpreted as follows: The slow drop in ϵ_{3a} for larger R (as R decreases) is due to the orbital being slightly bonding (it delocalizes onto the H). In this region the other orbitals change much less, but because of ϕ_{3a} delocalizing onto the H, it shields the proton from ϕ_{3b} a bit more and hence leads to an increasing ϵ_{3b} (for H^- the shielding

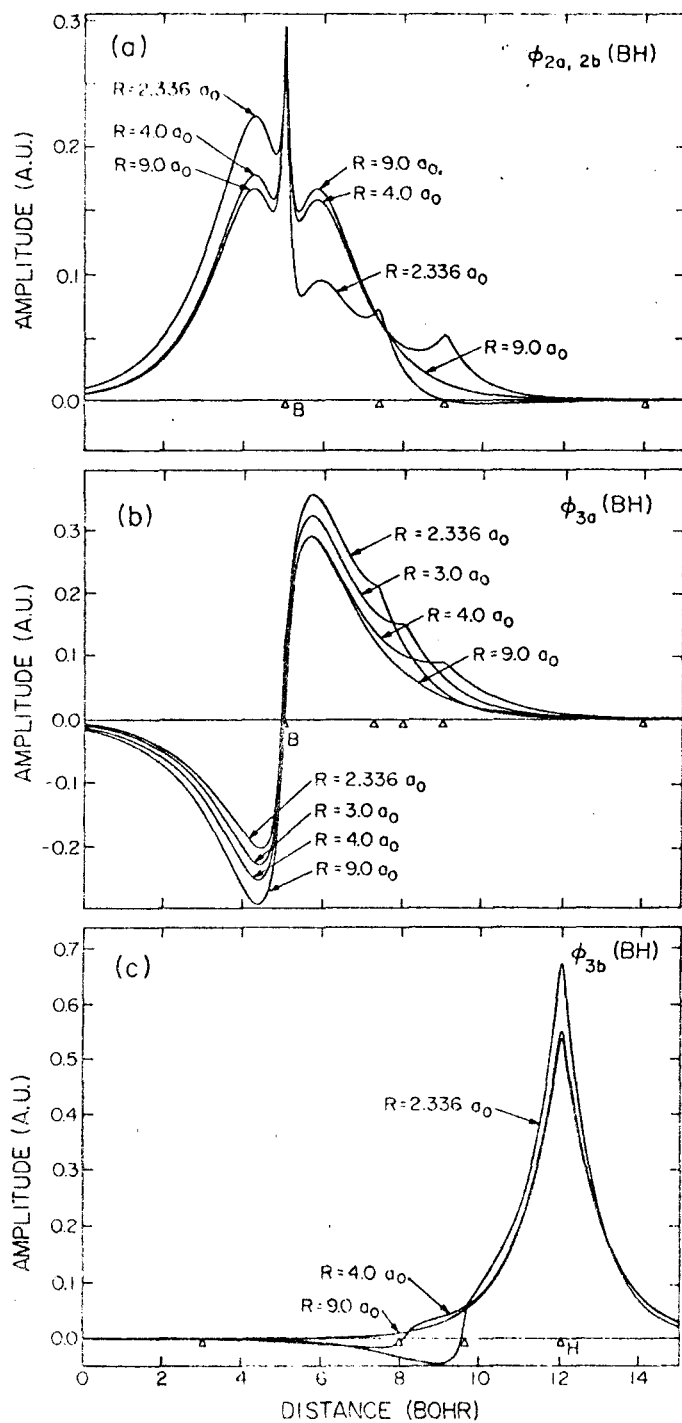


Fig. 3. Amplitude of the G1 valence orbitals along the bond axis for various inter-nuclear distances.

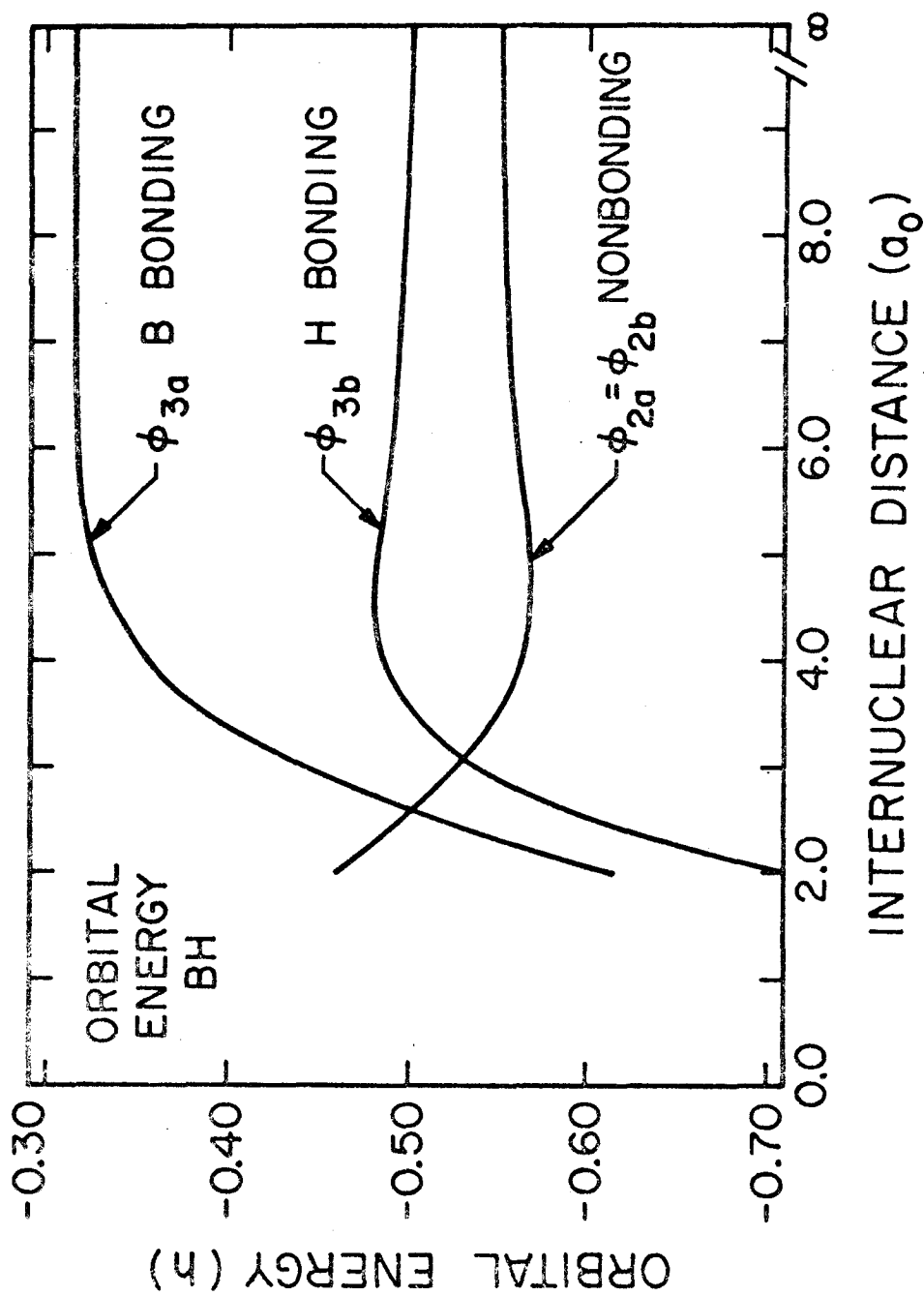


Fig. 4. The orbital energies of the G1 valence orbitals as a function of the internuclear distance.

due to the outer diffuse orbital increases the ϵ_{1s} from -0.500 to -0.268).¹³ At the same time since some of ϕ_{3a} is moved to the H, there is less on the B to shield the B nucleus from the nonbonding orbitals and so ϵ_{2a} and ϵ_{2b} drop. It is interesting to note in Fig. 3a that the nonbonding orbitals have a significant amplitude on the H, which is also a factor in the drop in ϵ_{2a} and ϵ_{2b} . Finally at $R = 4.0 a_0$ the H orbital, ϕ_{3b} , starts to delocalize onto the boron and the B orbital, ϕ_{3a} , begins building up uniformly throughout the bonding region. As a result the nonbonding orbitals start rotating back and since these orbitals are now more shielded from the B nucleus, ϵ_{2a} and ϵ_{2b} increase. As ϕ_{3b} and ϕ_{3a} tighten more and more about the nuclei, the orbital energies drop more and more.

B. Energies

The potential energy curve from the G1 calculations is shown in Fig. 5, where it is compared to the experimental, Hartree-Fock and VB-CI results. [In each case the bonding energy is plotted, so that the energy of the separated atoms (in the same approximation) is taken as the zero; an analytic form of each potential is given in Table III.] Of the theoretical curves, the G1 potential most nearly corresponds to the experimental potential. This G1 potential curve was obtained with the sp basis; however, Fig. 5 also shows the potential at $R = 2.336 a_0$ as obtained with the spd basis (properly correcting for the new spd energy at $R = \infty$). Thus the limiting G1 potential curve should correspond quite closely to the experimental potential curve. The experimental potential curve is somewhat in doubt because it is based only on the three lowest vibrational levels and a suggested dissociation energy ($D_0 = 3.43 \text{ eV}$);^{12b}

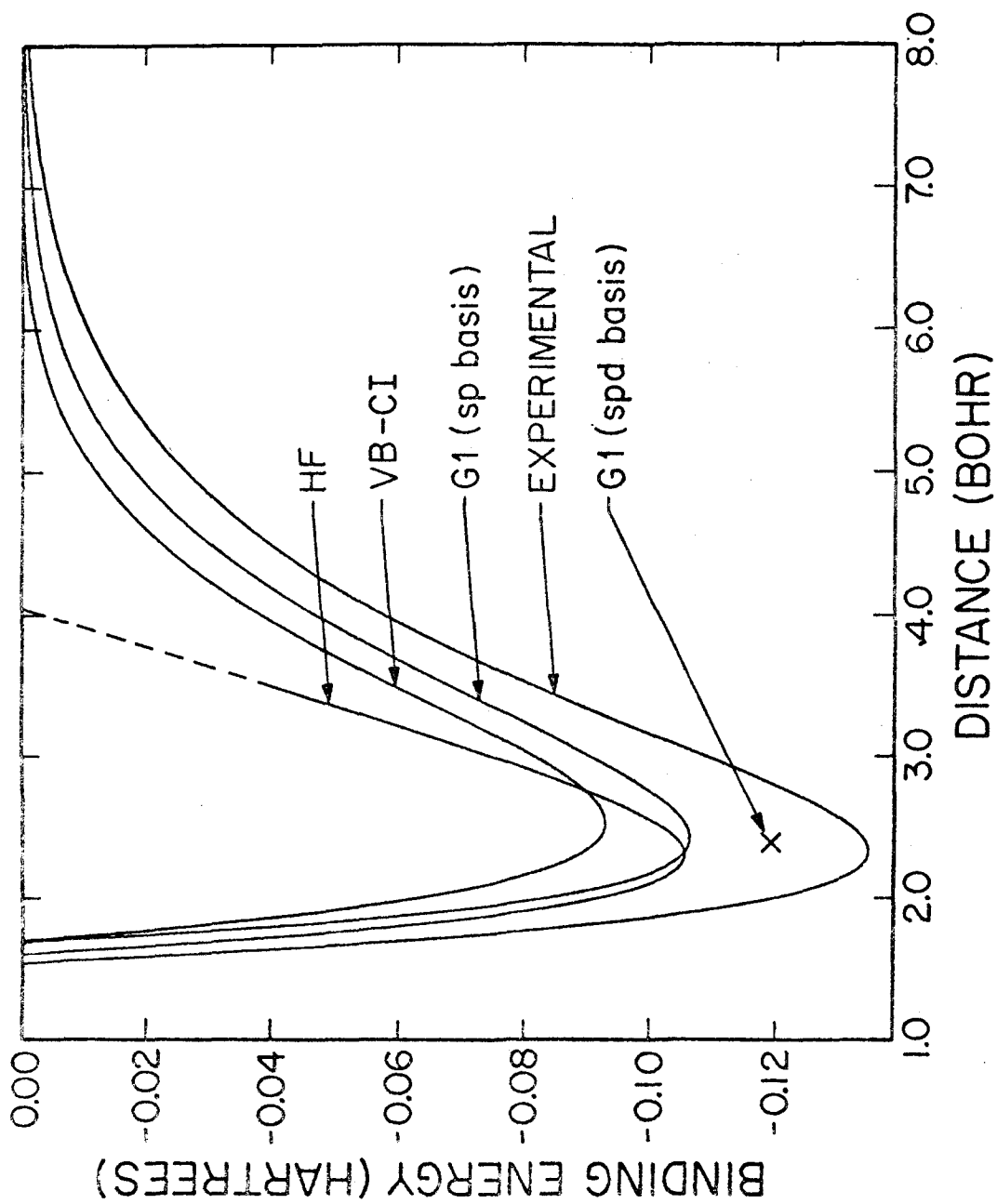


Fig. 5. The potential energy curves for BH(X¹Σ⁺). See Table III for details of the plot.

TABLE III. Parameters for the potential energy curves for BH. In each case the potential is fitted to the function

$$V(r) = V_0 + e^{-\alpha r}(a + br + cr^2 + dr^3 + er^4 + 10^{-4} \times fr^5),$$

where V_0 is the energy of the separated atoms (in the same approximation).

	HF ^a	VB-CI ^b	G1 ^c	Experimental ^d
α	0.851793	0.591160	1.66862	1.01109
a	6.41485	3.01561	31.2801	6.67969
b	-8.17126	-3.08386	-39.7969	-7.31967
c	3.06191	0.978177	19.5653	2.68847
d	-0.619426	-0.136729	-4.56791	-0.567444
e	0.0299847	0.00877808	0.260398	0.0585673
f	-0.00388294	-2.10395	48.4069	-22.0282

^aReference 4a, the dissociation limit was taken as the energy of B^+H^- (see Ref. 5).

^bReference 20.

^csp basis.

^dThe experimental curve was based on the reported spectroscopic constants¹² [including the suggested $D_e = 3.58$ eV (see Ref. 12b)] with an r^{-6} tail for large r and an r^{-12} tail for small r . RKR solutions (using the Zare program) with this potential were obtained and the points fitted to the above parametric form.

experimentally only an upper bound on the dissociation energy is known (due to a hump in the $A^1\Pi$ potential curve). It is then possible that the dissociation energy could be off by as much as 0.1 eV.

A more detailed comparison of the results from different approximations is given in Table IV. Here we see that the SOGI energy for B is 0.0321h (0.873 eV) lower than the HF value. Of this about 0.0139h is due to splitting in the core pair of orbitals,¹⁴ and hence about 0.0182h is due to splitting in the nonbonding pair of orbitals. For BH at $R = 2.336a_0$, the SOGI energy is 0.0488h (1.33 eV) lower than HF and thus SOGI accounts for 0.0166h = 0.453 eV more binding energy than HF. Hence for BH the energy improvement of SOGI over HF is nearly the same for each orbital pair split and in the range 0.014 to 0.018 (0.38 eV to 0.49 eV) per pair. In fact about the same improvement per pair was also observed for H_2 ($\Delta E = 0.0180$)² and LiH ($\Delta E_{\text{core}} = 0.0146$ ^{9c} and $\Delta E_{\text{bond}} = 0.0154$ ^{9b}).

The calculated binding energy for BH using G1 is 0.11896 as compared to the experimental value^{12b} of 0.131 ± 0.003 . Thus G1 accounts for 90.5% of the binding energy of BH; this is comparable to the value 86.8%,² obtained for H_2 , but somewhat higher than the percentage obtained for LiH, 75.5%.^{9b}

In calculating the binding energy for HF we cannot use the limiting energy of the molecular wavefunction as R goes to infinity since the wavefunction and energy dissociate improperly (the HF potential curve goes to a limiting value at $R = \infty$ about 8 eV above the energy of the Hartree-Fock B and H atoms). The conventional way of defining

TABLE IV. Energy properties for $B(^2P)$ and $BH(X^1\Sigma)$ at $R = 2.336 a_0$.

(All energies are in Hartrees.)

	$B(^2P)$				Experimental
	HF ^a	VB-CI	SOGI	CI	
Total Energy (E)	-24.52905	-24.56119 ^b	-24.639194 ^c	-24.658 ^d
Kinetic Energy (KE)	24.52826	24.55806	24.658
Virial Ratio (V/2E)	0.99999	0.99994	1.00000
	$BH(X^1\Sigma, R = 2.336 a_0)$				
	HF ^e	VB-CI ^f	SOGI	CI	Experimental
Total Energy (E)	-25.13137	-25.1426	-25.18014 ^g	-25.2621 ^h	-25.289 ⁱ
Kinetic Energy (KE)	25.11630	25.18879	25.289
Virial Ratio (V/2E)	1.00030	1.00017	1.00000
Binding Energy (D_e)	0.10232	0.0870 ^j	0.11896	0.1229 ^k	0.131 ^l
% Experimental Binding Energy	77.9	66.2	90.5	93.5	100.0

^a W. A. Goddard III, Phys. Rev. 182, 48 (1969).^b The G1 energy of B is -24.56118h, and the difference between G1 and SOGI is 0.000010.^c H. F. Schaeffer III and F. E. Harris, Phys. Rev. 167, 67 (1968).^d Reference 4a, Appendix I.^e P. E. Cade and W. M. Huo, Ref. 4a.^f J. F. Harrison and L. C. Allen, Ref. 20.

TABLE IV. (continued)

^g The G1 energy of BH is -25.18014, and the difference between G1 and SOGI is 0.000007h.

^h C. F. Bender and E. R. Davidson, Ref. 21.

ⁱ The total energy here is based on the energy of B and H atoms and the binding energy (D_e) from Ref. 12b.

^j Harrison and Allen obtained this binding energy by using the energy of BH at $R = 7.0 a_0$ as the energy of the separated atoms.

^k The boron calculation used 187 configurations, while the BH calculation used 1,123 configurations.

^l Based on the estimate due to Wilkinson, see Ref. 12b.

binding energy for HF is with respect to the HF energies of the separated atoms. This leads to 0.10232 or 77.9% of the experimental binding energy.

Table IV also shows the energy obtained from the G1 calculations. We see that for both B and BH the total SOGI energy is only 0.00001 lower than the G1 energy. The transformation angles are given in Table II. Expanding the SOGI wavefunction as

$$G_1^{\text{SOGI}} \Phi_\chi = \sum_i C_i G_i \Phi_\chi \quad (9)$$

in terms of the standard group operators G_i , we find that the normalized coefficient of the 1 representation is 0.99997 for BH (see Table II) and 0.99999 for B. Thus we see that for both B and BH the SOGI wavefunction is essentially equivalent to the G1 wavefunction. For this reason, the studies as a function of R were carried out for the G1 wavefunction.

V. SYMMETRY CONSIDERATIONS

In the GI and SOGI methods no spatial symmetry restrictions are made upon the orbitals. Thus for the ground states of H_2 , $^2 He_2$, 15b and Li_2^{15a} we found that the G1 orbitals are σ orbitals and do not have inversion symmetry, though the molecular symmetry is $D_{\infty h}$. Even so in each of these cases the G1 many-electron wavefunction has the correct symmetry under all molecular symmetry transformations. As discussed in Sec. IV(A), the BH nonbonding orbitals have mixed σ and π character and for the boron atom a pair of orbitals has mixed s and p character. Because of this the G1 many-electron wavefunction does not have exactly the correct spatial symmetry. Since similar behavior is expected in other systems, we will discuss this phenomenon in some detail.

A. Restricted GI Calculations

In order to preserve the correct symmetry of the total wavefunction exactly, we performed a series of calculations on BH in which each orbital was forced to have σ symmetry. This was accomplished by including only σ functions in the basis set. A similar calculation was performed on B in which the unpaired orbital was forced to have p symmetry and the paired orbitals were forced to be s functions.

The resulting orbitals for B are as follows: Two orbitals ϕ_{1a} and ϕ_{1b} (the B 1s core) are radially split, just as for the unrestricted calculations. For B atom ϕ_{2a} and ϕ_{2b} are singlet-paired, radially-split s functions and the unpaired valence orbital, —————|

$\phi_{3a'}$ is a pure p_z function. One would then expect that for large R the orbitals of BH would be as follows:

- (1) ϕ_{3a} and ϕ_{3b} (the bonding pair): ϕ_{3a} is essentially a B p_z function and ϕ_{3b} essentially an H $1s$ function, but with each orbital delocalized in a bonding way (no new nodes between B and H) onto the other center.
- (2) ϕ_{2a} and ϕ_{2b} (the nonbonding pair): both are essentially B s valence functions.

Instead we found that even at $R = 7a_0$ the G1 wavefunction has two pairs as follows (see Fig. 6):

- (1) ϕ_{3a} and ϕ_{3b} (the bonding pair): ϕ_{3a} resembles a B s orbital and ϕ_{3b} is essentially the H $1s$ orbital, but with each of these delocalized onto the other center.
- (2) ϕ_{2a} and ϕ_{2b} (the nonbonding pair): these are a B s function and a B p_z function which are delocalized a bit onto the H.

Although at this distance the BH wavefunction should be essentially that of a B atom plus an H atom, this coupling of the orbitals is incompatible with the coupling at $R = \infty$.

In addition we studied the wavefunctions at $R = 5a_0$, $3.5a_0$, $2.336a_0$, and $1.9a_0$. We found that between $R = 5a_0$ and $3.5a_0$ the character of some orbitals changed so that for $R \leq 3.5a_0$ the description of the orbitals is as follows:¹⁶

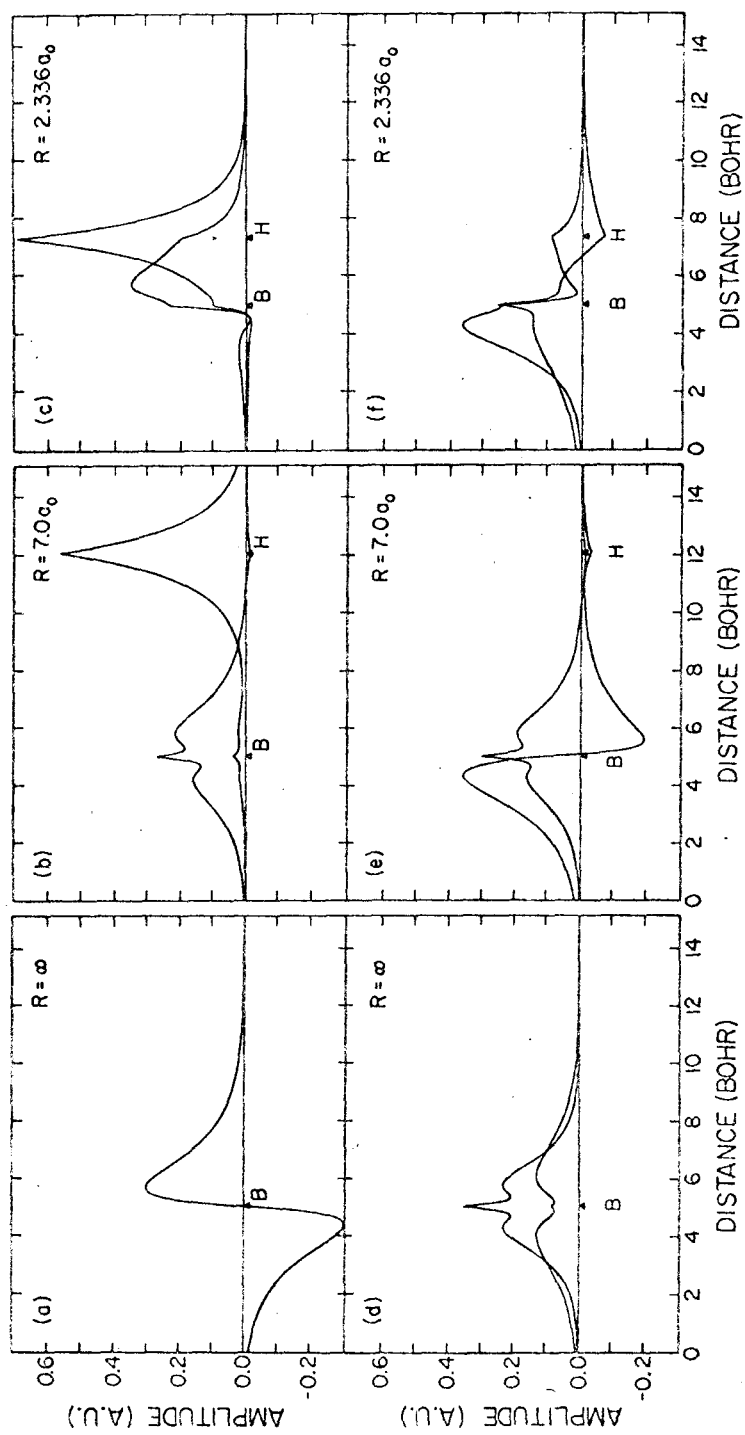


Fig. 6. The symmetry restricted G1 orbitals as a function of internuclear distance.

- (1) ϕ_{3a} and ϕ_{3b} (the bonding pair): ϕ_{3a} is essentially an sp hybrid on the B and ϕ_{3b} is essentially an H s function, both orbitals are delocalized in a bonding way onto the other center.
- (2) ϕ_{2a} and ϕ_{2b} (the nonbonding pair): one is an sp hybrid with positive amplitude on the hydrogen and high amplitude behind the behind the boron nucleus and the other is an sp hybrid with negative amplitude on the hydrogen and relatively diffuse behind the boron nucleus.

Thus the restricted GI orbitals do not behave at all smoothly as a function of R , but have at least two breaks, one between $3.5 a_0$ and $5 a_0$ and one above $7 a_0$. Upon reflection it appeared that these difficulties were due to the symmetry restrictions and we proceeded to carry out the unrestricted GI and SOGI calculations reported earlier. As we saw in Section IV(A), these unrestricted calculations lead to orbitals which change quite smoothly with R and have none of the difficulties associated with the symmetry restricted calculations. Our conclusion here is that the imposition of such nonvariational constraints as spatial symmetry restrictions upon a variational type of calculation (such as GI or UHF) can lead to very misleading results.

B. Symmetry Projected Wavefunctions

It is rather simple to project the proper molecular symmetry out of the GI (unrestricted) wavefunction. The GI wavefunction can

be written as

$$\Psi = G_1^\gamma \{ [\sigma \sigma' (\sigma'' + \pi_x) (\sigma'' - \pi_x) \sigma''' \sigma_H] \chi \}, \quad (10)$$

which is not a pure Σ state. [In (10) and below σ'' and π_x are not normalized functions; the relationship in (10) between ϕ_{2a} and ϕ_{2b} was not assumed but came out of the variational calculations.] We can rewrite this equation using Eq. (8) as

$$\Psi = \frac{5}{8} \mathcal{Q} \left\{ [(\sigma \sigma' + \sigma' \sigma) [(\sigma'' + \pi_x)(\sigma'' - \pi_x) + (\sigma'' - \pi_x)(\sigma'' + \pi_x)] (\sigma''' \sigma_H + \sigma_H \sigma''') \right\} \chi \quad (11)$$

which yields

$$\Psi = \frac{5}{8} \mathcal{Q} \{ [(\sigma \sigma' + \sigma' \sigma) (\sigma'' \sigma'' - \pi_x \pi_x) (\sigma''' \sigma_H + \sigma_H \sigma''')] \chi \} \quad (12a)$$

$$= G_1^\gamma [\sigma \sigma' \sigma'' \sigma'' \sigma''' \sigma_H \chi] - G_1^\gamma [\sigma \sigma' \pi_x \pi_x \sigma''' \sigma_H \chi]. \quad (12b)$$

If we replace the term $\pi_x \pi_x$ in (12b) by $\frac{1}{2} (\pi_x \pi_x + \pi_y \pi_y)$, then the wavefunction will have the correct spatial symmetry (${}^1\Sigma^+$). Thus from (12b) the symmetry-projected wavefunction can be written as

$$\Psi_p = \frac{1}{2} G_1^\gamma \Phi_x \chi + \frac{1}{2} G_1^\gamma \Phi_y \chi, \quad (13)$$

where the subscript x or y refers to the type of π function in the spatial nonbonding orbitals.¹⁷

The results from the projected and unprojected calculations are compared in Table V. We see the energy improvement is only 0.0080h

TABLE V. Comparison of energies of $B(^2P)$ and $BH(X^1\Sigma)$, $R = 2.336 a_0$) from G1, symmetry restricted G1, and spatially projected G1 calculations. The sp basis was used. (All energies are in Hartrees.)

	B		
	Symmetry Restricted	G1	Projected
Total Energy (E)	-24.54558	-24.56077	-24.56946
Kinetic Energy (KE)	24.53695	24.55906	24.55800
Virial Ratio (V/2E)	0.99982	0.99997	0.99977
	BH		
	Symmetry Restricted	G1	Projected
Total Energy (E)	-25.15372	-25.16337	-25.17136
Kinetic Energy (KE)	25.13385	25.16190	25.16066
Virial Ratio (V/2E)	0.99961	0.99997	0.99979

for BH at $R = 2.336a_0$ and 0.0089h for BH at $R = 4a_0$. In addition, we have found that even such symmetry-sensitive properties as the electric field gradient at the B, q_{zz}^B , are only slightly affected.

The equations for optimizing the orbitals of a GI wavefunction after spatial symmetry projection were indicated in Ref. 2, where the method was referred to as extended GI. A better name might be projected GI or PGI, where it is understood that the orbitals are optimized after projection. Such PGI calculations have been carried out for a number of excited states of H_2 and other two-electron systems;¹⁸ however, it has not yet been possible to apply this approach to BH. Based on the small changes in the GI energy and properties upon symmetry projection and based upon experience with spin projections,^{3,19} it is expected that the PGI orbitals of BH would be quite similar to the GI orbitals.

Thus our conclusion is that despite some symmetry contamination in the GI wavefunction for BH and B, the orbitals and properties may be relied upon.

VI. PROPERTIES

Several properties of the GI wavefunctions for the B atom and the BH molecule ($R = 2.336 a_0$) are listed in Table VI. These properties are based upon the spd basis. Also listed are the properties for the Hartree-Fock,⁴ VB-CI²⁰ and CI²¹ calculations. Changes in the GI properties with internuclear distance are shown in Figs. 7 and 8. The calculations as a function of R were carried out with the

TABLE VI. Comparison of properties for BH($X^1\Sigma^+$, $R = 2.336 a_0$) and $B(^2P)$ from various wavefunctions. Hartree atomic units are used.

	B		BH			
	HF ^a	GI	HF ^b	VB-CI ^c	GI	CI ^d
Dipole Moment (μ) ^e	0.0	0.0	0.6819 ^j	0.7021	0.59157	0.5784
Quadrupole Moment at B (Q_{ZZ}^B) ^f	-2.45908	-2.42552	-2.6667	-2.5041	-2.17651
$\langle r_B^2 \rangle$ ^g	15.853	15.71371	22.9380	22.35051	22.6146
Electric Field Gradient at B (q_{ZZ}^B) ^h	0.62042	0.57402 ^k	0.7467	0.5822	0.69315	0.6273
H (q_{ZZ}^H) ^h	0.0	0.0	-0.1689	-0.2471	-0.15845	-0.1704
$\langle 1/r_B \rangle$ ⁱ	11.37930	11.38220	11.8057	11.7671	11.81747	11.8296
$\langle 1/r_H \rangle$ ⁱ	1.0	1.0	3.2658	3.2437	3.28701	3.2688

^a W. A. Goddard III, Phys. Rev. 182, 48 (1969).

^b Reference 4c.

^c Reference 20.

^d Reference 21.

^e 1 a.u. = 2.54177 Debye.

^f 1 a.u. = 1.345047×10^{-26} esu cm².

^g Multiply by -0.7920187 to obtain diamagnetic susceptibility in ppm (cgs).

^h 1 a.u. = 3.241395×10^{15} esu/cm³.

ⁱ Multiply by 17.75044 to obtain diamagnetic shielding in ppm (cgs).

^j Reference 4b.

^k A CI result of 0.5466 is reported by H. F. Schaefer III, R. A. Klemm, and F. E. Harris, Phys. Rev. 181, 137 (1969).

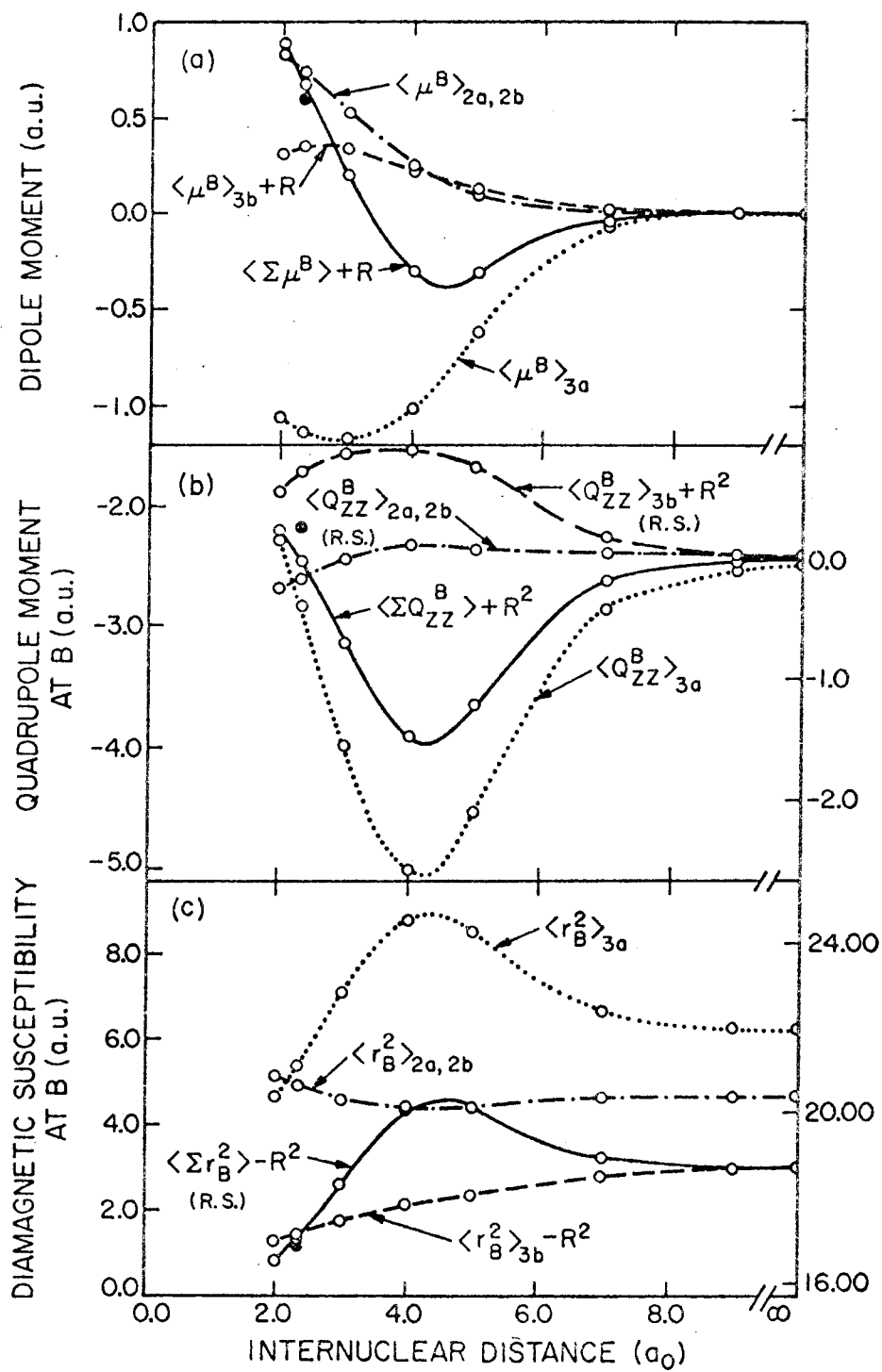


Fig. 7. The dipole moment (μ), the quadrupole moment at the boron (Q_{ZZ}^B), and $\langle \Sigma r_B^2 - R^2 \rangle$ are shown as a function of internuclear distance.

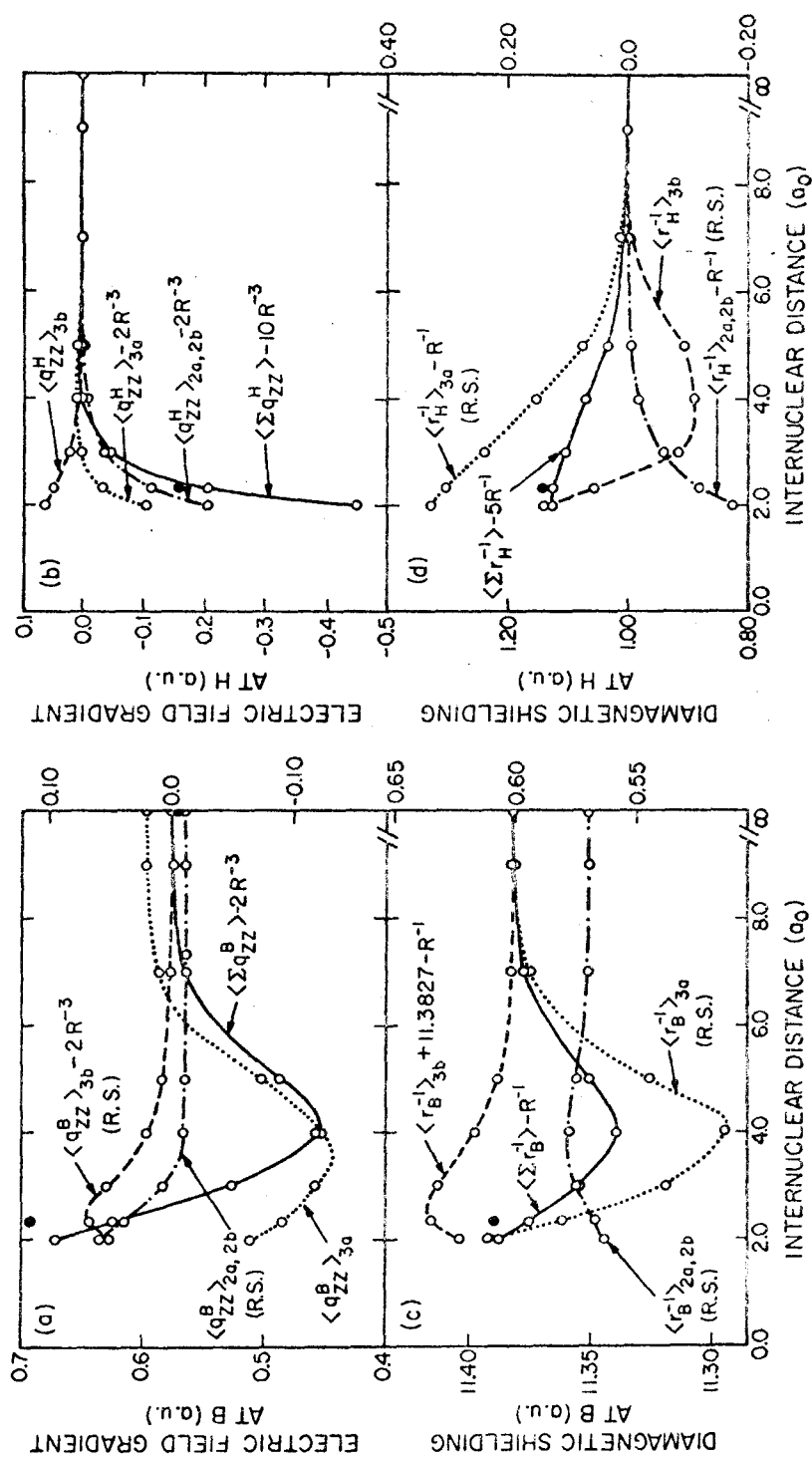


Fig. 8. The electric field gradient at both nuclei (q_{zz}) and $\langle \frac{1}{r} - \frac{Z}{R} \rangle$ properties as a function of internuclear distance.

sp basis; however, the changes in the property at R_e and $R = \infty$ upon going to the spd basis are indicated by the solid circles in Figs. 7 and 8 (see also the comparisons in Table VII). These properties are analyzed in terms of individual orbital contributions which are defined as

$$\langle P \rangle_i \equiv \langle \Phi P_i O_{11} \Phi \rangle / \langle \Phi | O_{11} \Phi \rangle, \quad (14)$$

where Φ is the product of spatial orbitals and P_i is the one-electron spatial operator associated with the property and operating only on electron index i . The total property $\langle P \rangle$ is then the sum of the orbital contributions,

$$\langle P \rangle = \sum_i \langle P \rangle_i. \quad (15)$$

The core orbitals ϕ_{1a} and ϕ_{1b} are centered almost entirely on the boron nucleus and make only a negligible or essentially unchanging contribution to most properties. The nonbonding orbitals are ϕ_{2a} and ϕ_{2b} and by symmetry these two orbitals always contribute equally to each property. It is important to note that in all of the plots only the contribution of one of the nonbonding orbitals is plotted so that it is necessary to double the value to obtain the full contribution of the nonbonding pair. The boron bonding orbital is ϕ_{3a} and the hydrogen bonding orbital is ϕ_{3b} (which at large R is essentially just a H 1s orbital).

The dipole moment (defined so that a positive dipole moment implies B^-H^+) as a function of R is shown in Fig. 7a. We see that the dipole moment, μ , is negative for large R , has a minimum around $4a_0$, and is positive at R_e . The orbital contributions to μ are also shown in

Fig. 7a (where the origin is taken _____) at the B nucleus and the hydrogen orbital contribution has the nuclear term, R , added to it so that it is zero at $R = \infty$). For large R , the most important contribution comes from the ϕ_{3a} orbital which delocalizes onto the H, resulting in a negative contribution to the dipole moment. As R decreases, ϕ_{3b} delocalizes onto the boron leading to a positive contribution to μ . As the H approaches, the nonbonding orbitals (which were perpendicular to the bonding axis at $R = \infty$) bend back away from the H resulting in a positive contribution to μ . The dipole moment changes sign because at large distances the boron bonding orbital contribution dominates (leading to negative μ) whereas at short distances the hydrogen bonding orbital and the B nonbonding orbital contributions dominate. Comparing the μ from the spd and sp bases we see that the polarization functions lead to a small drop in μ . The primary effect here is upon ϕ_{3a} whose contribution to μ becomes more negative. (This might be expected since the d-functions primarily aid in describing this orbital.) As indicated in Table VI, the G1 dipole moment is less than that from both the HF and the VB-DI methods.

The molecular quadrupole moment, Q_{ZZ}^B was evaluated with respect to the boron nucleus. A plot of Q_{ZZ}^B and its orbital contributions is shown in Fig. 7b. A negative quadrupole moment corresponds to an electron charge distribution which is prolate with the major axis being the bonding or z axis. We see that as R decreases from ∞ the wavefunction becomes increasingly prolate until $R \cong 4 a_0$, and becomes increasingly less prolate for shorter R . _____ The ϕ_{3a} orbital is the major contributor to Q_{ZZ}^B as shown in Fig. 7b. Orbital ϕ_{3b} makes a positive contribution (oblate) to Q_{ZZ}^B because this orbital is flattened as it delocalizes onto the boron nucleus. For

larger R , the nonbonding orbitals are oblate initially (a positive contribution to Q_{BB}^Z); however, as R decreases these orbitals bend back and make increasingly negative (prolate) contributions. The spd basis yields a less prolate wavefunction than the sp basis. The orbital contributions change as follows: the ϕ_{3a} contribution is less prolate, the nonbonding contribution is more prolate, and the hydrogen contribution is more oblate (see Table VII). In Table VI, we see that the quadrupole moment from the G1 wavefunction is more negative than that of either the VB-CI or the HF wavefunctions; this is expected since the G1 wavefunction is more contracted around the bond axis than either of the other two wavefunctions.

The expectation value of $(\Sigma r^2 - R^2)$ calculated with respect to the boron center is shown in Fig. 7c. All of the effects noted in the previous two properties are also found here. At infinity the property is equal to the sum of the expectation value of Σr^2 for the boron atom and the expectation value of r^2 for the hydrogen atom. This property increases as R decreases, reflecting the delocalization of ϕ_{3a} . A maximum occurs near $4a_0$ and the property decreases for smaller R as the wavefunction becomes more compact. The contribution from the boron bonding orbital again dominates these changes. The contribution due to the ϕ_{3b} starts out with the atomic expectation value and gradually dies off; this is due to a gradual tightening of the orbital as the nucleus is brought closer to the boron nucleus. The nonbonding orbital contributions are a minimum at the same point at which the boron bonding orbital contribution is a maximum; this is due to the slight contraction in the nonbonding orbitals as a result of the delocalization of ϕ_{3a} .

However, as ϕ_{3a} and ϕ_{3b} build up large amplitudes between the B and H for $R < 4a_0$, the nonbonding orbitals move away from the bond and hence from B. As expected, the spd basis leads to a more contracted wavefunction and hence a smaller value for this property.

Figure 8a is a plot of the electric field gradient at the boron nucleus, q_{ZZ}^B . In interpreting the contributions to q_{ZZ}^B note that a $2p_z$ function leads to a positive q_{ZZ} while a $2p_x$ function leads to a negative q_{ZZ} . We see that q_{ZZ}^B remains positive for all R shown; however, it does have a minimum near $4a_0$, due primarily to the boron bonding orbital, ϕ_{3a} . As can be seen in Fig. 3b, for $R > 4a_0$ the field gradient of ϕ_{3a} is smaller at $R = \infty$ due to transfer to the H, whereas for $R < 4a_0$ the gradient increases due to hybridization. The nonbonding orbitals initially lead to a small negative contribution to q_{ZZ}^B ; however, as they bend back, they take on $2p_z$ character and the contribution becomes positive. As can be seen from Fig. 3c, ϕ_{3b} builds in $2p_z$ character on the B as it transfers amplitude from the H and hence the contribution of ϕ_{3b} to q_{ZZ}^B is positive and increases as the internuclear distance decreases. Comparing the results for the sp and spd basis sets,²² we find that the polarization functions lead to an increase in q_{ZZ}^B . This is primarily due to changes in the nonbonding contribution to q_{ZZ}^B and results mainly from the incorporation of d_{xz} functions into the nonbonding orbitals (see Table VII). It appears that the HF value for the electric field gradient is greater than the G1 value primarily because of the lack of π character in the HF nonbonding orbitals.

The electric field gradient at the hydrogen nucleus, q_{ZZ}^H , is shown in Fig. 8b. At infinity q_{ZZ}^H is zero, and as R decreases from

TABLE VII. Basis set dependence of properties $\langle\langle P \rangle\rangle_T$ and partial properties $\langle\langle P \rangle\rangle_i$ for B and BH ($R = 2.336 a_0$). The upper value is for the spd basis and the lower is for the pd basis. (Hartree atomic units are used.)

	B			BH			
	$\langle P \rangle_{2a,2b}$	$\langle P \rangle_{3a}$	$\langle P \rangle_T$	$\langle P \rangle_{2a,2b}$	$\langle P \rangle_{3a}$	$\langle P \rangle_{3b}$	$\langle P \rangle_T$
$\langle \mu \rangle$	0.90818	-1.46662	0.24648	0.59157
	0.73514	-1.13474	0.34485	0.67806
$\langle Q_{ZZ}^B \rangle$	0.02780	-2.48137	-2.42552	-0.21755	-2.59224	0.85117	-2.17651
	0.02645	-2.47943	-2.42654	-0.16712	-2.81894	0.72040	-2.43242
$\langle \Sigma r_B^2 - R^2 \rangle$	1.52739	3.72205	15.71371	5.14522	5.04362	1.30479	16.89361
	1.52529	3.71914	15.71286	4.94351	5.41912	1.46624	17.02549
$\langle q_{ZZ}^B \rangle$	-0.01394	0.59885	0.57402	0.07810	0.47369	0.06499	0.69315
	-0.01107	0.59915	0.57702	0.03764	0.48489	0.06614	0.62449
$\langle q_{ZZ}^H \rangle$	-0.12129	0.02167	0.06182	-0.15845
	-0.11196	-0.02980	0.05022	-0.20276
$\langle \Sigma \frac{1}{r_B} - \frac{1}{R} \rangle$	0.57013	0.60141	11.38220	-0.56985	-0.59507	11.4206 ^a	11.38939
	0.57004	0.60158	11.38266	-0.56774	-0.58159	11.4157	11.37596
$\langle \Sigma \frac{1}{r_H} - \frac{5}{R} \rangle$	-0.14569	0.37079	1.06635	1.14660
	-0.11901	0.30431	1.05864	1.12532

$$^a \langle \Sigma \frac{1}{r_B} \rangle + 11.3827 - R^{-1}.$$

infinity, q_{ZZ}^H changes very little until $R = 4a_0$, at which point it starts dropping rapidly. The primary effect for $R < 4a_0$ seems to be the bending of the nonbonding orbitals behind the B, which allows the nuclear contributions to q_{ZZ}^H to dominate (resulting in $q_{ZZ}^H < 0$). Addition of the d functions to the basis set leads to a larger q_{ZZ}^H , primarily because of the increased polarization in the ϕ_{3a} orbital. The q_{ZZ}^H from the G1 wavefunction is more negative than that from the HF and the VB-CI wavefunctions.

The expectation value of $\Sigma \frac{1}{r_B} - \frac{1}{R}$ calculated at the boron center is shown in Fig. 8c. It has a minimum at about $4a_0$, primarily due to the contribution of the boron bonding orbitals, ϕ_{3a} . The decrease with R for large R is expected since the primary change at large R is the delocalization of ϕ_{3a} onto the hydrogen nucleus. For smaller R, the concentration of ϕ_{3a} and ϕ_{3b} in the B-H region leads to increases near the B and an increase in the property. The nonbonding contribution shows a slight maximum at the point at which the ϕ_{3a} contribution has a minimum; this results from the slight contraction in the nonbonding orbitals which occurs as the ϕ_{3a} orbital is delocalized onto the hydrogen. Note that the nonbonding contribution is less at R_e than at infinity indicating that the inner parts of the nonbonding orbitals do indeed move away from the nucleus as the orbitals bend back. The hydrogen bonding contribution increases as R decreases to R_e due to the delocalization of ϕ_{3b} onto the B. The addition of polarization functions leads to larger contributions to $\langle \Sigma \frac{1}{r} \rangle - \frac{1}{R}$ since they allow the wavefunction to be more contracted about the nucleus.

The expectation value of $\Sigma \frac{1}{r_H} - \frac{5}{R}$ calculated with respect to the hydrogen nucleus is shown in Fig. 8d. This property is 1.0 at infinity and rises gradually as R decreases. From the figure we see that the dominating term is due to ϕ_{3a} delocalizing onto the H as R decreases. Adding polarization functions leads to an increase in the property.

VII. DISCUSSION

A major objective in the ab initio study of the electronic wavefunctions of small molecules is to identify the significant factors which influence molecular formation. We saw in Sec. IV that the G1 orbitals of BH change in an orderly fashion as R decreases from to R_e and that the changes in the orbitals can be understood in terms of concepts such as hybridization and contraction of bonding orbitals and interaction of bonding and nonbonding pairs. In addition, the changes as a function of internuclear distance of the various properties of BH are simply explained in terms of the various orbitals. Thus the G1 orbitals would seem to be an accurate representation of the many-electron wavefunction. We might then ask if these orbitals can be used to predict the properties and structures of other related boron molecules. For example, if we bring up another H to BH to form BH_2 , what would we expect the structure of the ground state of BH_2 to be?

Since there are nonbonding orbitals of BH pointing at $\pm 116^\circ$ with respect to the BH axis (call it BH_p), we would expect the new H (call it H_q) to become paired with one of these lobes (say $+116^\circ$) leaving a

nonbonding unpaired orbital at -116° . As the second BH bond forms, one would expect an increase in the $\text{BH}_b\text{-BH}_a$ angle (bond-bond repulsions). In fact SOGI calculations on BH_2 lead to an equilibrium angle of 129° ²³ which compares favorably with the experimental angle of 131° .²⁴ Thus based on the orbitals of BH, we correctly predict BH_2 to be bent with an angle of about 120° . The valence orbitals of BH_2 are shown in Fig. 9. There are five valence orbitals of which two (ϕ_{2a} and ϕ_{2b} in Fig. 9) are singlet-coupled and involved in one BH bond, and two (ϕ_{3a} and ϕ_{3b}) equivalent to ϕ_{2a} and ϕ_{2b} , but concentrated in the other BH region.

—————|
|———— The other valence function is called the nonbonding orbital and is denoted as ϕ_{4a} in Fig. 9. This orbital is in the plane of the molecule but points away from the region of the bonds. The nodal plane of the nonbonding orbital nearly bisects each of the bonding pairs. As HBH angle is increased toward 180° the nonbonding orbital becomes more and more π -like and eventually is one component of the ${}^2\Pi$ state of linear BH_2 .

Thus we see that using the valence orbitals of the B atom on the premise that coupled pairs of orbitals repel each other somewhat, we can correctly arrive at the qualitative aspects of the electronic structure and geometries of BH, BH_2 , and BH_3 . This is the analog of Walsh's rules²⁵ but based on atomic SOGI orbitals rather than Hartree-Fock molecular orbital correlation diagrams.

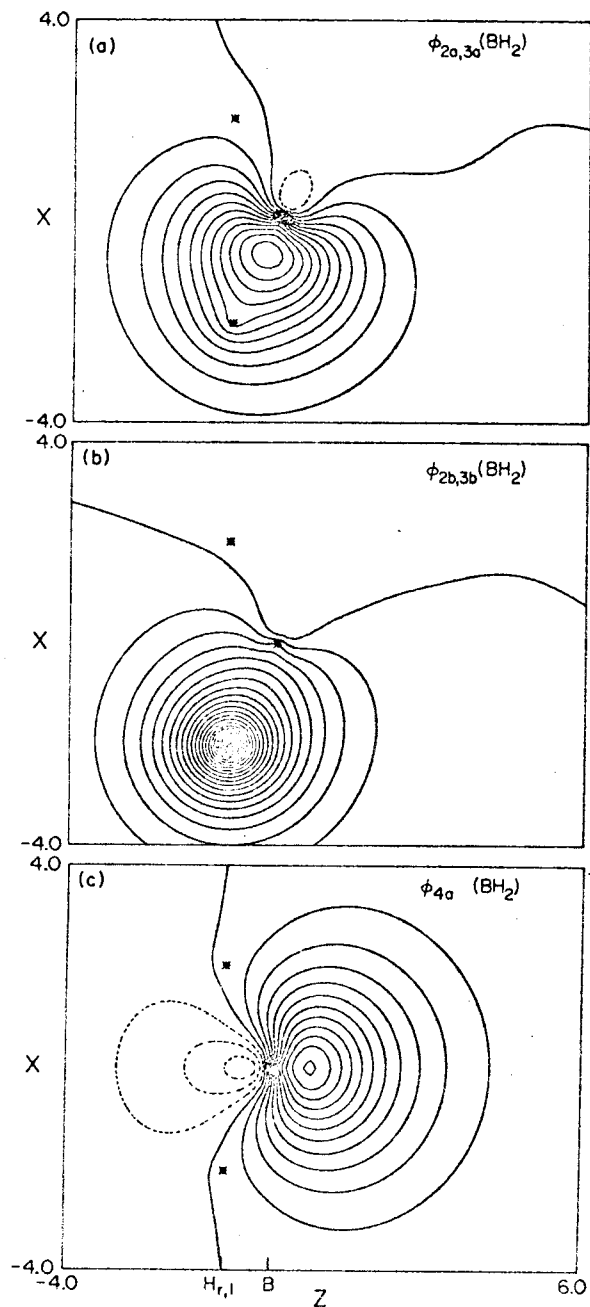


Fig. 9. The valence orbitals of BH_2 as obtained from SOGI calculations.

VIII. SUMMARY AND CONCLUSIONS

We find that the SOGI orbitals of BH lead to a perspicacious description of the structure and properties of BH. In addition, using the orbitals of B and BH, it is easy to understand the geometries of other molecules such as BH₂ and BH₃. It appears that these results should apply to a number of other molecules and thus the SOGI method may lead to a qualitative understanding of the structure and properties of a number of molecules.

We also find that the inclusion of symmetry restrictions upon the orbitals does not allow a consistent, continuous description of BH as R is reduced from infinity to R_e.

FOOTNOTES

1. D. R. Hartree, The Calculation of Atomic Structures (John Wiley & Sons, Inc., New York, 1957).
2. W. A. Goddard III, Phys. Rev. 157, 81 (1967).
3. R. C. Ladner and W. A. Goddard III, J. Chem. Phys. 51, 1073 (1969).
4. (a) P. E. Cade and W. M. Huo, J. Chem. Phys. 47, 614 (1967); (b) ibid. 45, 1063 (1966); (c) P. E. Cade, private communication.
5. From the usual orbital diagram, one would expect that the Hartree-Fock orbitals at $R = \infty$ would be B1s, B2s and H1s; that is, we would expect B^+ and H^- . In fact, a self-consistent calculation would probably lead to a third function partly on the B and mostly on the H. The resulting wavefunction would lead to an energy less than that of B^+ and H^- but far above that of B and H.
6. The configuration interaction based on VB configurations (4) is often also called VB. We will call this VB-CI and reserve the term VB for a single configuration of the form (4).
7. W. A. Goddard III, J. Chem. Phys. 48, 5337 (1968).
8. W. A. Goddard III, Phys. Rev. 157, 73 (1967); Int. J. Quant. Chem. 3S, 593 (1969).
9. (a) W. A. Goddard III, Phys. Rev. 169, 120 (1968); (b) W. E. Palke and W. A. Goddard III, J. Chem. Phys. 50, 4524 (1969); (c) W. A. Goddard III, J. Chem. Phys. 48, 1008 (1968).
10. S. Huzinaga and Y. Sakai, J. Chem. Phys. 50, 1371 (1969).
11. S. Huzinaga, J. Chem. Phys. 42, 1293 (1965).

12. (a) S. H. Bauer, G. Herzberg, and J.W.C. Johns [J. Mol. Spectrosc. 13, 256 (1964)] report $B_e = 12.016 \text{ cm}^{-1}$ and $R_e = 1.236 \text{ \AA}$ ($= 2.336 a_0$). However, $R_e(\text{\AA}) = c/(\mu B_e)^{\frac{1}{2}}$ where $c = 4.105853$ (from Ref. 12c) which leads to $R_e = \frac{4.105853}{\sqrt{\mu \cdot 12.016}} = 1.233 \text{ \AA} = 2.329 a_0$. This conversion constant c is nearly equal to the one using the older values of the fundamental constants, and hence the value of R_e quoted in Bauer et al. was probably a misprint. The more recent work by J.W.C. Johns, F.A. Grimm, and R. F. Porter [J. Mol. Spectrosc. 22, 435 (1967)] report $B_e = 12.021 \text{ cm}^{-1}$, which gives $R_e = 1.2324 \text{ \AA} = 2.3289 a_0$. The value of $R_e = 2.336 a_0$ was used in most other theoretical calculations of BH and we have used it also. (b) From predissociation in the $A^1\Pi \leftarrow X^1\Sigma$ transitions, G. Herzberg and L.G. Mundie [J. Chem. Phys. 8, 263 (1940)] find an upper limit of $28,350 \text{ cm}^{-1}$ to $D_0(X^1\Sigma)$. This is an upper limit due to a hump on the $A^1\Pi$ potential curve at large R . A.C. Hurley [Proc. Roy. Soc. (London) A261, 237 (1961)] has estimated this hump as 0.155 eV , leading to a D_0 of $3.39 \pm 0.04 \text{ eV}$, but P.G. Wilkinson [Astrophys. J. 138, 778 (1963)] has recommended a D_0 of 3.43 ± 0.08 . Converting to D_e we obtain $D_e = 3.58 \text{ eV} = 0.131 \text{ h}$. (c) B.N. Taylor, W.H. Parker, and D.N. Langenberg, The Fundamental Constants and Quantum Electrodynamics (Academic Press, N.Y., 1969).
13. W. A. Goddard, Phys. Rev. 172, 7 (1968).
14. The GI energy of B^{+++} is -22.00015 and the HF energy of B^{+++} is -21.98623 [from C.C.J. Roothaan, L.M. Sachs, and A.W. Weiss, Rev. Mod. Phys. 32, 186 (1960)].

15. (a) R. J. Blint, W.E. Palke, and W.A. Goddard III, unpublished work; see L.R. Kahn and W.A. Goddard III, *Chem. Phys. Letters* 2, 667 (1968); (b) W.E. Palke and W.A. Goddard III, unpublished work.
16. R. J. Blint, W. A. Goddard III, R. C. Ladner, and W. E. Palke, *Chem. Phys. Letters* 5, 302 (1970).
17. For the B atom the wavefunction (13) does not have 2P symmetry unless a similar component $G_1^{\gamma} \Phi_Z X$ is added.
18. D. L. Huestis, *Bull. Am. Phys. Soc.* 14, 1192 (1969).
19. W. Marshall, *Proc. Phys. Soc. (London)* 78, 113 (1961).
20. J. F. Harrison and L. C. Allen, *J. Mol. Spectrosc.* 29, 432 (1969).
21. C. F. Bender and E. R. Davidson, *Phys. Rev.* 183, 23 (1969).
22. Note that our basis does not include d functions tight enough to describe completely the quadrupolar distortion in the 1s (core) orbitals. Inclusion of such functions could change q by several per cent.
23. (a) R. J. Blint, L. R. Kahn, and W. A. Goddard III, unpublished results. These calculations made use of the ab initio G1 effective potential to replace the two B core orbitals, reducing the SOGI calculation to a five-electron problem. (b) C. F. Bender and H. F. Schaefer III (private communication) have recently carried out a CI calculation on BH_2 and find an optimum angle of 129.4° .
24. G. Herzberg, Molecular Spectra and Molecular Structure. III. Electronic Spectra and Electronic Structure of Polyatomic Molecules (D. Van Nostrand Co., Inc., Princeton, New Jersey, 1967).
25. A. D. Walsh, *J. Chem. Soc.* 2260 (1963).

References

1. A. D. Walsh, J. Chem. Soc. (1953) 2260, 2266, 2288, 2296, 2301, 2306, 2321, 2325.
2. R. S. Mulliken, Phys. Rev., 32 (1928) 186, 761; idem., Rev. Mod. Phys., 4 (1932) 1; F. Hund, Z. Physik., 40 (1927) 742; ibid., 42 (1927) 93; ibid., 51 (1928) 759; ibid., 63 (1936) 719.
3. R. B. Woodward and R. Hoffman, "The Conservation of Orbital Symmetry," Verlag Chemie, Germany, 1970.
4. W. A. Goddard III, Phys. Rev., 157, 73 (1967).
5. R. C. Ladner and W. A. Goddard III, J. Chem. Phys., 51, 1073 (1969).
6. H. F. King and R. E. Stanton, J. Chem. Phys., 50, 3789 (1969).
7. W. A. Goddard III, Phys. Rev., 157, 81 (1967).
8. Density matrices are the factors multiplying a term in the Hamiltonian which are a series of orbital overlaps and coefficients corresponding to all the permutations of the orbitals which are not involved in the Hamiltonian term.
9. Slater properties integrals program was written by L. R. Kahn; Gaussian properties were calculated using the Neumann-Moskowitz NYU program.
10. C. C. J. Roothaan, Rev. Mod. Phys., 23, 69 (1951); W. A. Goddard III, Class Notes, 1968.
11. P. K. Pearson, C. F. Bender, and H. F. Schaefer III, to be published.
12. R. Thomson and F. W. Dalby, Can. J. Phys., 47, 1155 (1969).

II. GAS PHASE REACTIONS OF FLUOROMETHYL CATIONS
WITH ETHYLENE AND BENZENE

A. Introduction

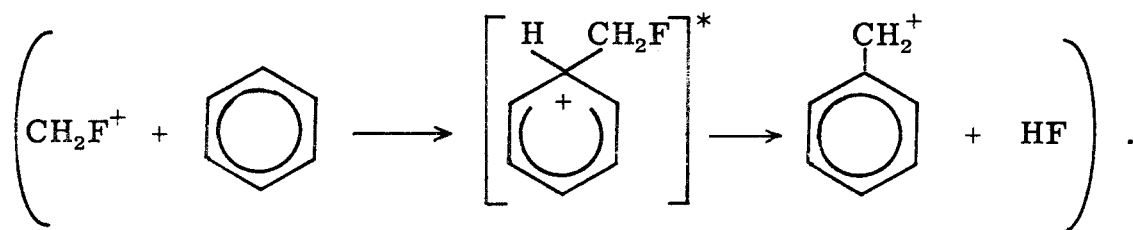
In electrophilic addition the rate and mechanism of reaction are significantly influenced by the stability of the attacking carbonium ion, the reaction intermediate and the leaving group. The high electronegativity of fluorine with respect to hydrogen causes a significant readjustment in the stability of the fluoromethyl cations. Consequently we have chosen to study the addition of fluoromethyl cations to ethylene and benzene as model systems for electrophilic addition reactions in which chemically activated intermediates are formed and subsequently decompose.

The gas phase ion chemistry of fluoromethanes, which are convenient sources of the desired ionic reactants, is discussed in Section C where the predominate reaction observed in the interaction of fluoromethyl cations with their parent neutrals is an apparently general fluoride transfer process. With available thermochemical data we have constructed and experimentally verified a relative ordering for the fluoride affinities of the fluoromethyl cations ($\text{CF}_3^+ > \text{CH}_3^+ > \text{CH}_2\text{F}^+ > \text{CF}_2\text{H}^+$). Utilizing this same thermochemical data we have also calculated the relative hydride affinities of the fluoromethyl cations ($\text{CH}_3^+ > \text{CF}_3^+ > \text{CH}_2\text{F}^+ > \text{CF}_2\text{H}^+$). These orderings which are discussed in detail are direct measures of carbonium ion stabilities and differ only in the relative orders of the CH_3^+ and CF_3^+ ions.

In Section D the reactions of fluoromethyl cations with ethylene are described. The reactions (e.g., $\text{CH}_2\text{F}^+ + \text{C}_2\text{H}_4 \rightarrow [\text{CH}_2\text{FCH}_2\text{CH}_2^+]^* \rightarrow$

$C_3H_5^+ + HF$) very likely involve a substituted propyl cation as an intermediate which undergoes a 1,2 elimination to form a propenyl (allyl) cation. The clear preference for HF elimination is attributed to the stability of the leaving group and the removal of unfavorable interactions of the carbonium ion center with fluorine substituents in the chemically activated intermediate. Isotopic product distributions observed in the reactions of fluoromethyl cations with ethylene- d_4 do not unambiguously reveal details of the proposed reaction mechanism.

Similar reactions with benzene are discussed in Section E with the exception that isotopic product distributions are consistent with the proposed reaction mechanism



B. Experimental Methods

Ion cyclotron resonance spectroscopy¹ was used to study these reactions. The instrumentation and experimental techniques have been discussed in detail elsewhere.² Reaction rate constants and equilibrium constants were determined by trapped ion methods using a slightly modified standard icr cell.³ Product distributions were determined by source ion ejection technique.^{2,4} All experiments were performed at ambient temperatures. All reagents were obtained from commercial sources and were used as supplied except for degassing

with multiple freeze-pump-thaw cycles. Purities as ascertained by mass spectrometric analysis were acceptable. Pressure measurements were effected through the use of a Schulz-Phelps gauge⁵ and a MKS Baratron. The Schulz-Phelps gauge was mounted in the pressure chamber just adjacent to the icr cell and within the field of the magnet. Pressure determinations were found to be linear with ion current from 10^{-7} to 10^{-4} torr; the absolute pressure measurements were made with the MKS Baratron.

C. Gas Phase Ion Chemistry of the Fluoromethanes

The entire range of the fluoromethanes from CH_3F to CF_4 have been studied. It is generally observed for these neutrals that the ion chemistry becomes progressively simpler with successive substitution of fluorine for hydrogen. The gas phase ion chemistry of methyl fluoride is reasonably complicated involving several different reaction types and products. In contrast only one simple fluoride ion transfer reaction characterizes the gas phase ion chemistry of tetrafluoromethane. The necessity for studying these reactions in detail arises because they are competitive reactions in the binary mixture reaction studies discussed in Sections D and E.

CH_3F . The gas phase ion chemistry of CH_3F has been discussed in detail elsewhere;⁶ however these reactions are reinvestigated using the trapped ion cell. The variation of ion abundance with time is shown in Fig. 1 at a pressure of 1.25×10^{-6} torr and an electron energy of 70 eV. The initial reaction is the combination of the parent ion and the

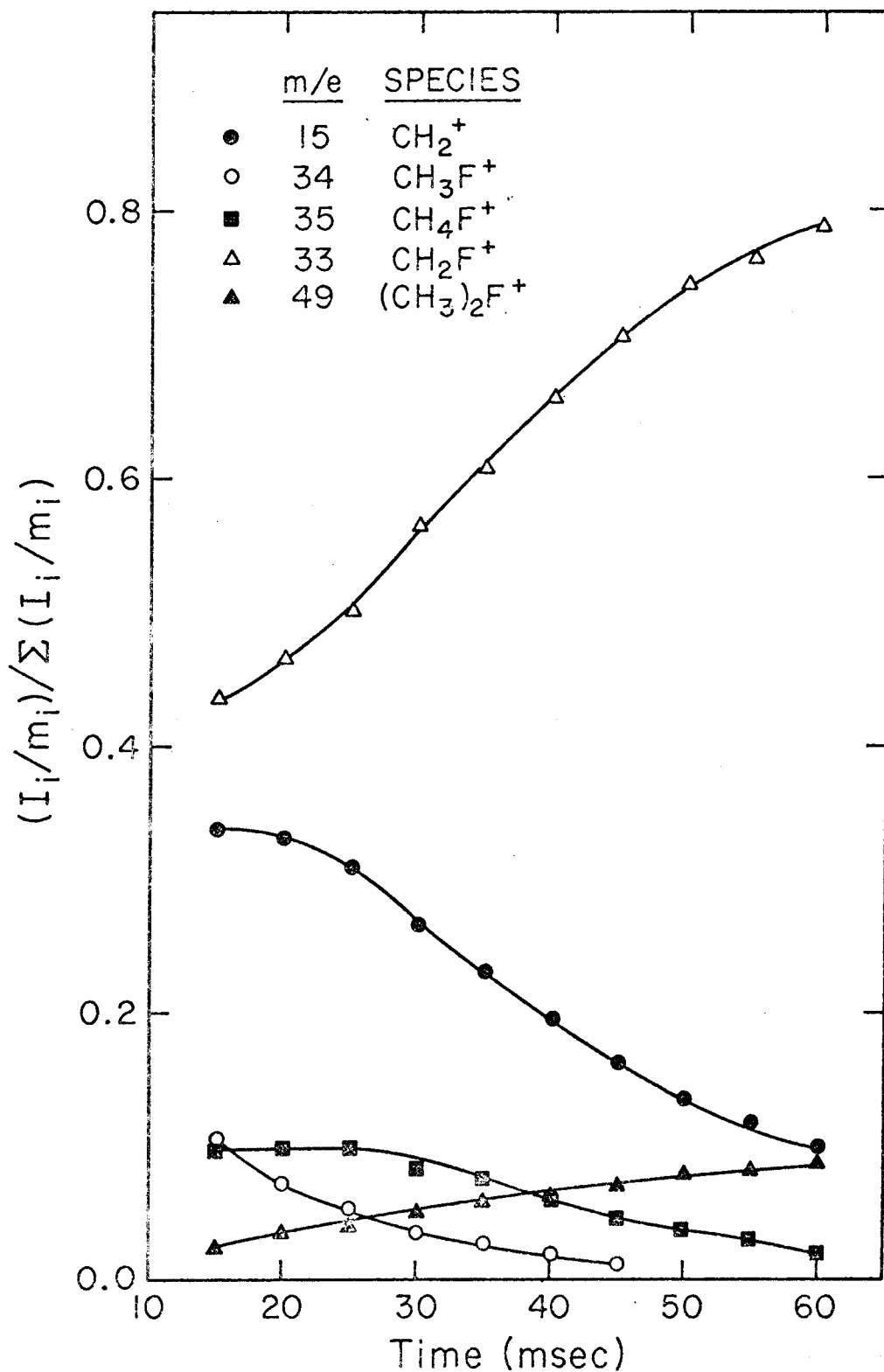
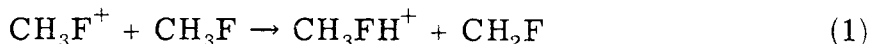
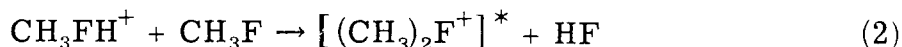


Fig. 1. Typical trace of variation of ion intensity with time for ions observed in methylfluoride at 70 eV and 1.25×10^{-6} torr.

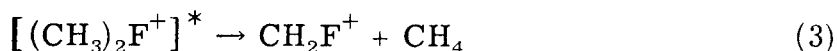
parent neutral (reaction 1) to form the protonated parent ion.



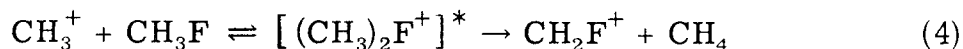
The protonated parent reacts in turn with the neutral to give the dimethyl fluoronium ion (reaction 2) which is formed.



in a highly excited state and partially decomposes eliminating CH_4 (reaction 3).^{6a} The predominate product, CH_2F^+ (see Fig. 1) is also



formed in the interaction of the remaining fragment ion CH_3^+ with CH_3F (reaction 4). Although this reaction formally involves a hydride



transfer, the reaction has been shown to proceed through a fluoronium ion intermediate. It is important that CH_2F^+ is found to be unreactive to the methyl fluoride neutral.

Kinetics. Rate constants for fluoromethane reactions have been determined by analysis of the ionic abundance of each species as a function of trapping time. A solution to the kinetic equations for a primary (P), secondary (S) and tertiary (T) ion system such as reaction 2 to 3 yields the abundances of the various ions as a function of time as

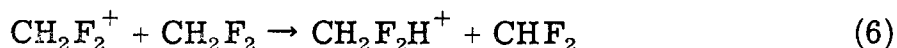
$$P = P(0) e^{-nk_1t} \quad (5a)$$

$$S = \frac{k_2}{k_2 - k_1} P(0) (e^{-nk_1 t} - e^{-nk_2 t}) \quad (5b)$$

$$T = \frac{k_1 k_2}{k_2 - k_1} P(0) \left(\frac{1 - e^{-nk_1 t}}{k_1} + \frac{e^{-nk_2 t} - 1}{k_2} \right) \quad (5c)$$

where $P(0)$ represents the initial concentration of primary ions. A plot of \log_{10} (relative ion abundance) versus time for each of the ions in Fig. 1 is shown in Fig. 2. The slope of the relative abundances of the two primary ions (CH_3F^+ and CH_3^+) is equal to $-nk_1$ which with knowledge of the pressure specifies the rate constant for the reaction. The determination of the rate constant requires an accurate knowledge of both the pressure and the slope of the plot in Fig. 2. The rate constant determined using this method compares favorably with the rate constants shown in Table I. All rate constants discussed in the following were similarly determined.

CH_2F_2 . The reactions of CH_2F_2 are similar in type to those of CH_3F where again the principle product observed at high pressures is CH_2F^+ . The important ions observed at 70 eV and 8×10^{-5} torr are CH_2F^+ (71.0%), CF_2H^+ (26.6%), $(\text{CH}_2\text{F})_2\text{F}^+$ (1.3%) and CH_2F_2 (1.1%), where the high percentage of CH_2F^+ product indicates some reaction (reaction 8) has already taken place. Two reactions are observed; the one involving the two most prevalent ions and the other (reaction 6) is analogous to reaction 1 involving formation of the protonated parent ion. The protonated parent in turn reacts with the neutral



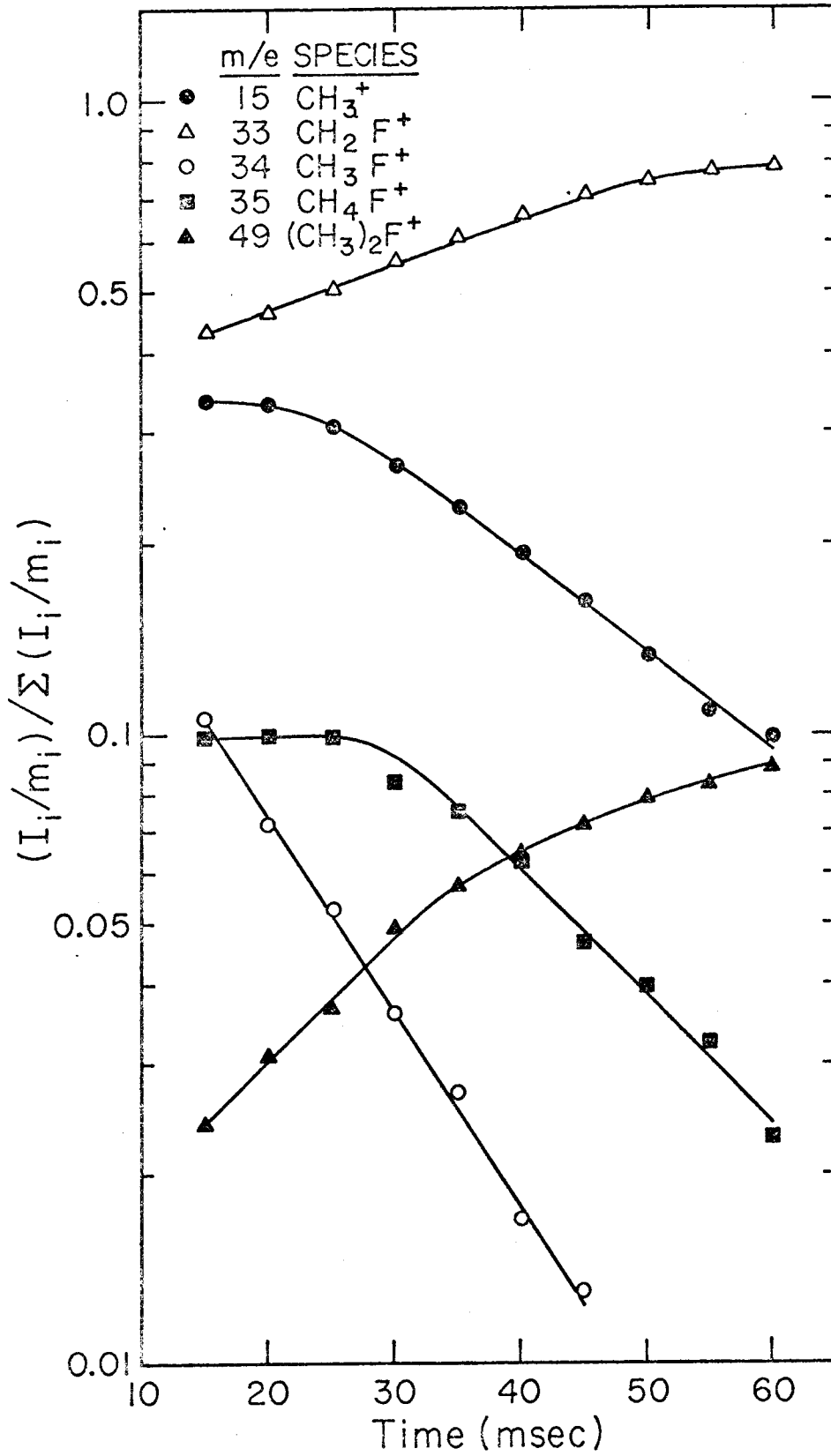


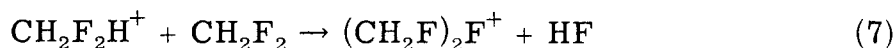
Fig. 2. Plot of \log_{10} (relative ion abundance) vs. time for each of the ions in the CH_3F reaction.

TABLE I. Several other determinations of the rate constant for reaction 1 are shown here. The value which was experimentally determined is shown both here and in Table II.

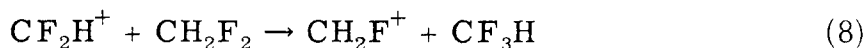
k_{total} (10^{-10} cm ³ molecule ⁻¹ seconds ⁻¹)	Ref.
13.6	6b
22.	6c
20.1 ^a	6d
13.9	6a
17.	b
17.3	this work

a) This value is an average of the tabulated experimental results.

b) P. Miasek and J. L. Beauchamp (private communication) determined this value using a high pressure trapped ion source analyzed by a quadrupole mass spectrometer.



to produce a substituted fluoronium ion. Reactions (6 and 7) were briefly examined by varying pressure in the drift mode of operation. The abundance of the parent and protonated parent ions did not permit their observation in trapped ion experiments. The reaction involving the two most prevalent ions is the fluoride transfer reaction 8.



Again CH_2F^+ is found to be unreactive toward the parent neutral.

Reaction 8 is endothermic by 0.8 kcal (see Table III) and is the slowest of the observable fluoromethane reactions.

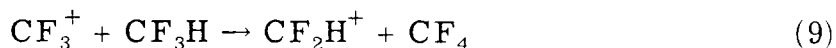
TABLE II. Experimental rate constants determined for the gas phase reactions of the fluoromethanes.

Species	Reactions Observed	k_{total} (10^{-10} cm ³ molecule ⁻¹ second ⁻¹)
	$\text{CH}_3\text{F}^+ + \text{CH}_3\text{F} \rightarrow \text{CH}_4\text{F}^+ + \text{CH}_2\text{F}$	17.3 ± 5.2
<u>CH₃F</u>	$\text{CH}_3^+ + \text{CH}_3\text{F} \rightarrow \text{CH}_2\text{F}^+ + \text{CH}_4$	10.2 ± 1.1
	$\text{CH}_4\text{F}^+ + \text{CH}_3\text{F} \begin{cases} \rightarrow (\text{CH}_3)_2\text{F}^+ + \text{HF} \\ \rightarrow \text{CH}_2\text{F}^+ + \text{CH}_3 + \text{HF} \end{cases}$	9.9^{b}
	$\text{CF}_2\text{H}^+ + \text{CH}_2\text{F}_2 \rightarrow \text{CH}_2\text{F}^+ + \text{CF}_3\text{H}$	$1.9 \pm .3$
<u>CH₂F₂</u>	$\text{CH}_2\text{F}_2^+ + \text{CH}_2\text{F}_2 \rightarrow \text{CH}_2\text{F}_2\text{H}^+ + \text{CF}_2\text{H}$	- - - - ^c
	$\text{CH}_2\text{F}_2\text{H}^+ + \text{CH}_2\text{F}_2 \rightarrow (\text{CH}_2\text{F})_2\text{F}^+ + \text{HF}$	- - - - ^c
<u>CF₃H</u>	$\text{CF}_3^+ + \text{CF}_3\text{H} \rightarrow \text{CF}_2\text{H}^+ + \text{CF}_4$	$2.1 \pm .4$
<u>CF₄</u>	$\text{CF}_2^+ + \text{CF}_4 \rightarrow \text{CF}_3^+ + \text{CF}_3$	- - - - ^c

- a) Error estimates are the widest experimental variation from the reported value.
- b) No error estimate available for this value although a rate constant of 7.1 was determined in Ref. 6a.
- c) The abundance of these ions did not permit their observation in trapped ion experiments.

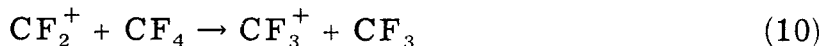
CF₃H. The principle fragment ions derived from CF₃H at a pressure 1.7×10^{-6} torr and 70 eV are CF₃⁺ (41.9%) and CF₂H⁺ (58.1%) which are the principle ions found at all electron energies. Although the parent ion has been previously reported,⁷ the sensitivity of the equipment did not

permit its detection under any circumstances. Only the fluoride transfer reaction 9 is observed,



where the product CF_2H^+ is unreactive toward CF_3H . Reaction 9 is exothermic by 17.3 kcal/mole. Interestingly this difference is not reflected by a rate constant which is significantly greater than that of the endothermic reaction 8.

CF₄. Fragmentation of CF_4 produces no observable parent ion, at all electron energies a high ion abundance of CF_3^+ is found and a considerably smaller ion abundance of CF_2^+ is also observed. Reaction 10 of CF_4 which is surmized from the pressure plots, but was not observable in the trapped ion cell due to low reactant ion intensity formally



simulates a fluoride abstraction reaction, although it is not possible to clearly characterize it as such. The CF_3^+ ion is unreactive toward CF_4 .

Thermochemistry. The thermochemistry of the fluoromethanes and the attendant fluoromethyl cations has only recently become available. Table III gathers together all the thermochemical data available on the ions and molecules discussed here. $\Delta H_f(\text{CH}_3^+)$ is quite accurately known from the ionization potential of the planar CH_3 radical.⁸ In a study of the thermal elimination of HF from 1,2 difluoroethane Kerr and Timlin have determined that $\Delta H_f(\text{CH}_2\text{F}) = -7.8$ kcal/mole.⁹ From

TABLE III. Thermochemical values of the reactants and products.
(All values are in kcal mole⁻¹).

Neutral Species	ΔH_f	Ref.	Ionic Species	ΔH_f	Ref.
CH ₄	- 17.88	a	- - -	- - -	- -
CH ₃	33.2	a	CH ₃ ⁺	260.8	8
CH ₃ F	- 55.9	9	- - -	- - -	- -
CH ₂ F	- 7.8	9	CH ₂ F ⁺	200.2	10
CH ₂ F ₂	-108.1	9	- - -	- - -	- -
CF ₂ H	- 59.2	9	CF ₂ H ⁺	141.2	b
CF ₃ H	-166.3	9	- - -	- - -	- -
CF ₄	-222.0	c	- - -	- - -	- -
CF ₃	-112.6	c	CF ₃ ⁺	98.9	12
CF ₂	- 39.0	c	- - -	- - -	- -
CFH	[30 ± 7]	d	- - -	- - -	- -
C ₂ H ₄	12.49	a	C ₂ H ₄ ⁺	255	16a
HF	- 64.8	a	- - -	- - -	- -
F	18.9	a	F ⁻	- 64.7	a
H	52.1	a	H ⁻	33.4	a
- - -	- - -	-	C ₃ H ₅ ⁺	226	16a

- a) J. L. Franklin, J. G. Dillard, H. M. Rosenstock, J. T. Herron, K. Drapl, and F. H. Field, "Ionization Potentials, Appearance Potentials, and Heats of Formation of Gaseous Positive Ions", NSRDS-NBS 26, U. S. Government Printing Office, Washington, D. C.
- b) This work see "Equilibrium Constant" and Table VI.
- c) J. Heicklen, Advan. Photochem., 7, 57 (1969).
- d) D. R. Shull and H. Prophet, "JANAF Thermochemical Tables", NSRDS-NBS 3, U. S. Government Printing Office, Washington, D. C.

photoionization experiments the ionization threshold of 13.37 eV for the reaction $\text{CH}_3\text{F} + h\nu \rightarrow \text{CH}_2\text{F}^+ + \text{H} + \text{e}^-$ the $\Delta H_f(\text{CH}_2\text{F}^+)$ is 200.2 kcal/mole. Experimentally the heat of reaction for reaction 8 is found to be 0.8 kcal/mole. Using this value and the previously determined $\Delta H_f(\text{CH}_2\text{F}^+)$ the $\Delta H_f(\text{CF}_2\text{H}^+) = 141.2$ kcal/mole. Identification of the adiabatic potential of CF_3 radical is difficult because the radical is nonplanar.¹¹ After a complete analysis of all previous work^{7, 12} Walter et al. estimated an ionization potential of 9.17 ± 0.08 eV for the CF_3 radical. Using $\Delta H_f(\text{CF}_3) = -112.6$ kcal/mole¹⁴ and the ionization potential $\Delta H_f(\text{CF}_3^+)$ is found to be 98.9 kcal/mole.

Fluoride Affinities. The thermochemical data contained in Table III allows the determination of the fluoride and hydride affinities of the fluoromethyl cations as is shown in Table IV.

TABLE IV. Fluoride and hydride affinities of the fluoromethyl cations.^a

R	IP(R) eV	$\Delta H_f(\text{R}^+)$ kcal/mole	$\Delta H_f(\text{RH})$ kcal/mole	$\Delta H_f(\text{RF})$ kcal/mole	$D(\text{R}^+ - \text{H}^-)$ kcal/mole	$D(\text{R}^+ - \text{F}^-)$ kcal/mole
CH_3	9.84	260.8	- 17.88	- 55.9	312.1	252.0
CH_2F	9.02	200.2	- 55.9	-108.1	289.5	243.6
CF_2H	8.68	141.2	-108.1	-166.3	282.5	242.8
CF_3	9.17	98.9	-166.3	-222.0	298.6	256.2

a) All thermochemical quantities are discussed in Table IV.

The relative fluoride affinities are found to be $\text{CF}_3^+ > \text{CH}_3^+ > \text{CH}_2\text{F}^+ > \text{CF}_2\text{H}^+$, while the relative hydride affinities are $\text{CH}_3^+ > \text{CF}_3^+ > \text{CH}_2\text{F}^+ >$

CF_2H^+ . The reversal in the ordering of the former two ions is discussed in detail in Section F. Experimentally the relative ordering of the fluoride affinities has been determined by the use of double resonance techniques on mixtures of the fluoromethane neutrals. In Table V we have summarized the results of the reactions of the mixtures together with dk/dE as determined by double resonance. In general a positive value for dk/dE indicates an endothermic reaction; while a negative value implies an exothermic reaction. Reactions in the $\text{CH}_3\text{F}:\text{CF}_4$ mixture show the ordering to be $\text{CF}_3^+ > \text{CH}_3^+$, $\text{CH}_3^+ > \text{CH}_2\text{F}^+$, and $\text{CF}_3^+ > \text{CH}_2\text{F}^+$. The reactions of $\text{CH}_4:\text{CH}_2\text{F}_2$ and $\text{CH}_4:\text{CF}_3\text{H}$ also basically affirm this order with the exception of the reaction $\text{CH}_3^+ + \text{CH}_2\text{F}_2 \rightarrow \text{CF}_2\text{H}^+ + \text{CH}_4$ which is only marginally observable. Reactions of CH_2F_2 , CF_3H and the mixture of these two ions also confirm this ordering. Consequently the only doubt in the fluoride affinity ordering arises from the closeness of the fluoride affinities of CF_2H^+ and CH_2F^+ .

Equilibrium Constant. To clearly establish the relative fluoride affinities for CF_2H^+ and CH_2F^+ the equilibrium constant for reaction 8 was determined using trapping techniques. In Fig. 3 is a plot of the relative ion abundances of the ions at an electron energy of 70 eV as a function of time. In the region from 60 msec to 80 msec all three ions seem to have reached equilibrium; that is, there is no significant indication that the system is in the process of a slow but steady adjustment to another equilibrium point. The ratio of the pressures of the neutral molecules is one-to-one and we find the ratio of the two ion abundances

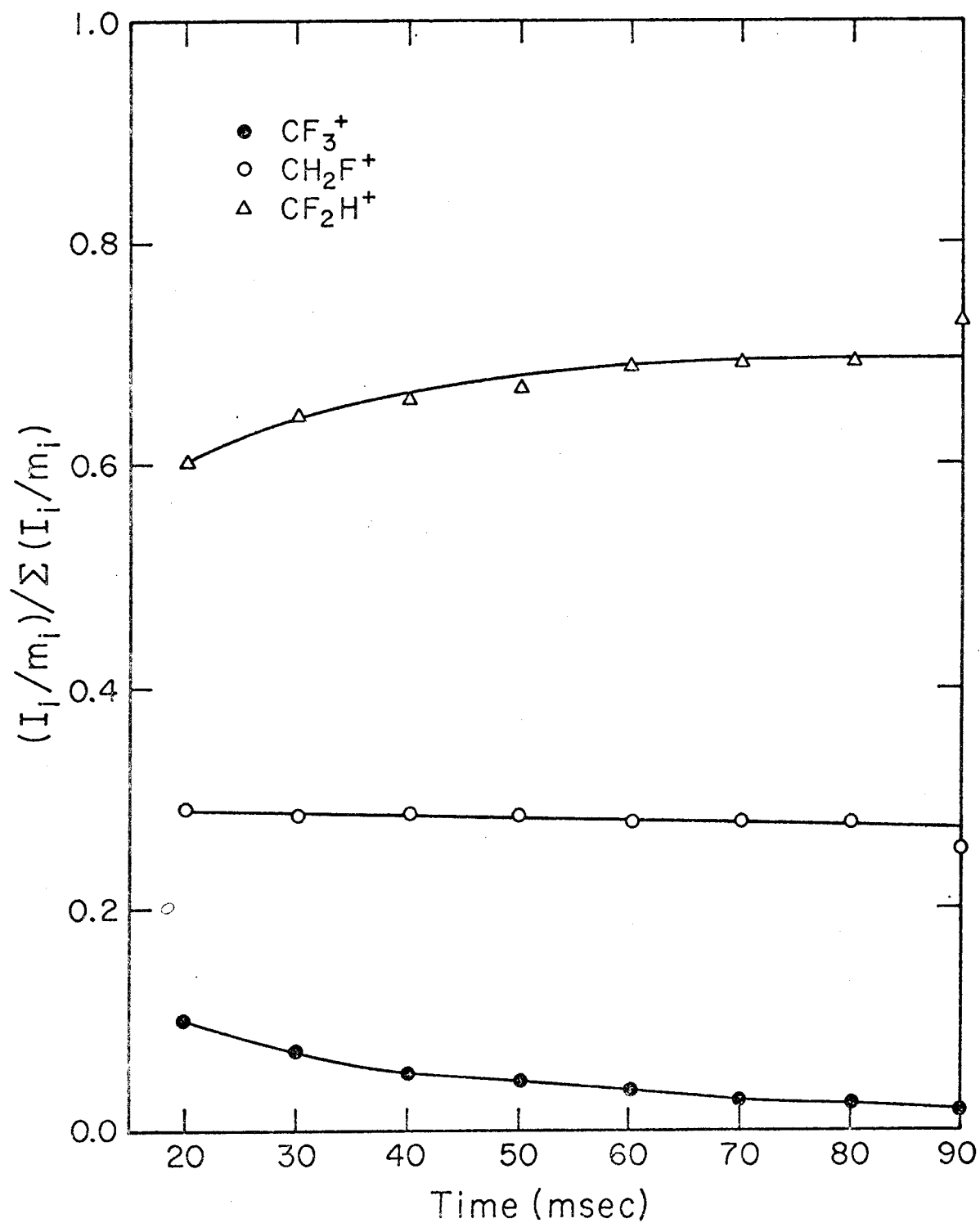


Fig. 3. Plot of the normalized intensities vs. time as the three ionic species attain equilibrium.

TABLE V. Summary of the F^- ion transfer reactions.

Mixture	Reaction	dk/dE ^a	ΔH_f kcal/mole
	$CF_3^+ + CH_3F \rightarrow CF_4 + CH_3^+$	-	- 4.2
	$CH_3^+ + CH_3F \rightarrow CH_2F^+ + CH_4$	-	-22.6
$CH_3F : CF_4$	$CF_3^+ + CH_3F \rightarrow CH_2F^+ + CF_3H$	- ^b	- 9.1
	$CH_2F^+ + CF_4 \rightarrow CF_3^+ + CH_2F_2$	+	12.6
	$CH_3^+ + CF_4 \rightarrow CF_3^+ + CH_3F$	+	4.2
$CH_4 : CH_2F_2$	$CH_3^+ + CH_2F_2 \rightarrow CH_2F^+ + CH_3F$	-	- 8.4
	$CH_3^+ + CH_2F_2 \rightarrow CF_2H^+ + CH_4$	+ ^c	-29.4
$CH_4 : CF_3H$	$CH_3^+ + CF_3H \rightarrow CH_4 + CF_3^+$... ^d	-13.5
	$CH_3^+ + CF_3H \rightarrow CF_2H^+ + CH_3F$	-	- 9.2
CH_2F_2	$CF_2H^+ + CH_2F_2 \rightarrow CH_2F^+ + CF_3H$	+	0.8
CF_3H	$CF_3^+ + CF_3H \rightarrow CF_2H^+ + CF_4$	-	-13.4
$CH_2F_2 : CF_3H$	$CF_2H^+ + CH_2F_2 \rightarrow CH_2F^+ + CF_3H$	+	0.8

a) A positive response corresponds to an increase in the single resonance intensity and a negative response indicates a decrease.

b) This reaction is ambiguous due to the first reaction.

c) Experimentally only a very small positive peak was observed.

d) Reaction not seen.

($\text{CH}_2\text{F}^+/\text{CF}_2\text{H}^+$) to be 0.400. From 11 we see that 1 : 1 ratio of the neutral gases makes the equilibrium constant

$$K = \frac{[\text{CFH}_2^+][\text{CF}_3\text{H}]}{[\text{CF}_2\text{H}^+][\text{CH}_2\text{F}_2]} = \frac{k_f}{k_r} \quad (11)$$

just the ratio of the two ion abundances. Using this equilibrium constant both the reverse rate constant (k_r) of reaction 8 and the free energy (ΔG_{298}) and enthalpy (ΔH_{298}) change of the reaction can be calculated.

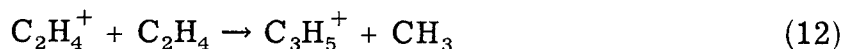
The free energy for this reaction is given by $-RT \ln K$ and using $T = 298^\circ\text{K}$ the free energy change for this reaction is calculated to be 543 cal/mole. The ΔS (change in entropy) for this reaction can be estimated to be $R \ln 3/2 = 240$ cal/mole through the use of symmetry numbers.¹⁵ Consequently the enthalpy change for this reaction is 783 cal/mole and will be taken to be 0.8 kcal/mol (within the error of the measurement). Clearly then CF_2H^+ has a lower fluoride affinity than does CH_3F^+ . The reverse rate constant for this reaction is given as $k_r = 2.5 k_f$ and from Table II $k_f = 1.9$ so $k_r = 4.75 (10^{-10} \text{ cm}^3 \text{ molecule}^{-1} \text{ sec}^{-1})$. In Table VI are the results from the two experimental determinations of the rate constant; the last row contains the average values.

TABLE VI. Experimental equilibrium constants and accompanying thermochemical and rate constants.

Ratio	K	ΔG_{298} (cal/mole)	ΔH_{298} (cal/mole)	k_r (10^{-10} cm ³ molecule ⁻¹ sec ⁻¹)
1 : 1	0.400	543	783	4.8
2 : 1	<u>0.445</u>	<u>480</u>	<u>720</u>	<u>4.3</u>
Avg.	0.4225	512	752	4.5

D. Fluoromethyl Cation Reactions with Ethylene

The condensation reaction (reaction 12) of ethylene is the primary reaction¹⁶ of the parent ion of ethylene. It experimentally has a



rate constant (7.9×10^{-10} cm³ molecule⁻¹ sec⁻¹)¹⁷ which is comparable to rate constants derived for prominent reactions of the fluoromethanes. Reaction (12) is exothermic by 8.3 kcal/mole. The rate constant for this reaction was determined as in Section C.

CH₃F + C₂H₄. In a binary mixture both the reactions of the isolated neutrals and cross reactions will take place. In this system and each of the following systems the change in concentration of the fluoromethyl cation which was unreactive to its parent neutral is monitored. In Fig. 4 are log₁₀ (unnormalized ion abundances) vs. time plots of the principle products of the binary mixture of CH₃F and C₂H₄ at 70 eV. From the plot it is seen that C₃H₅⁺ is the major product and that

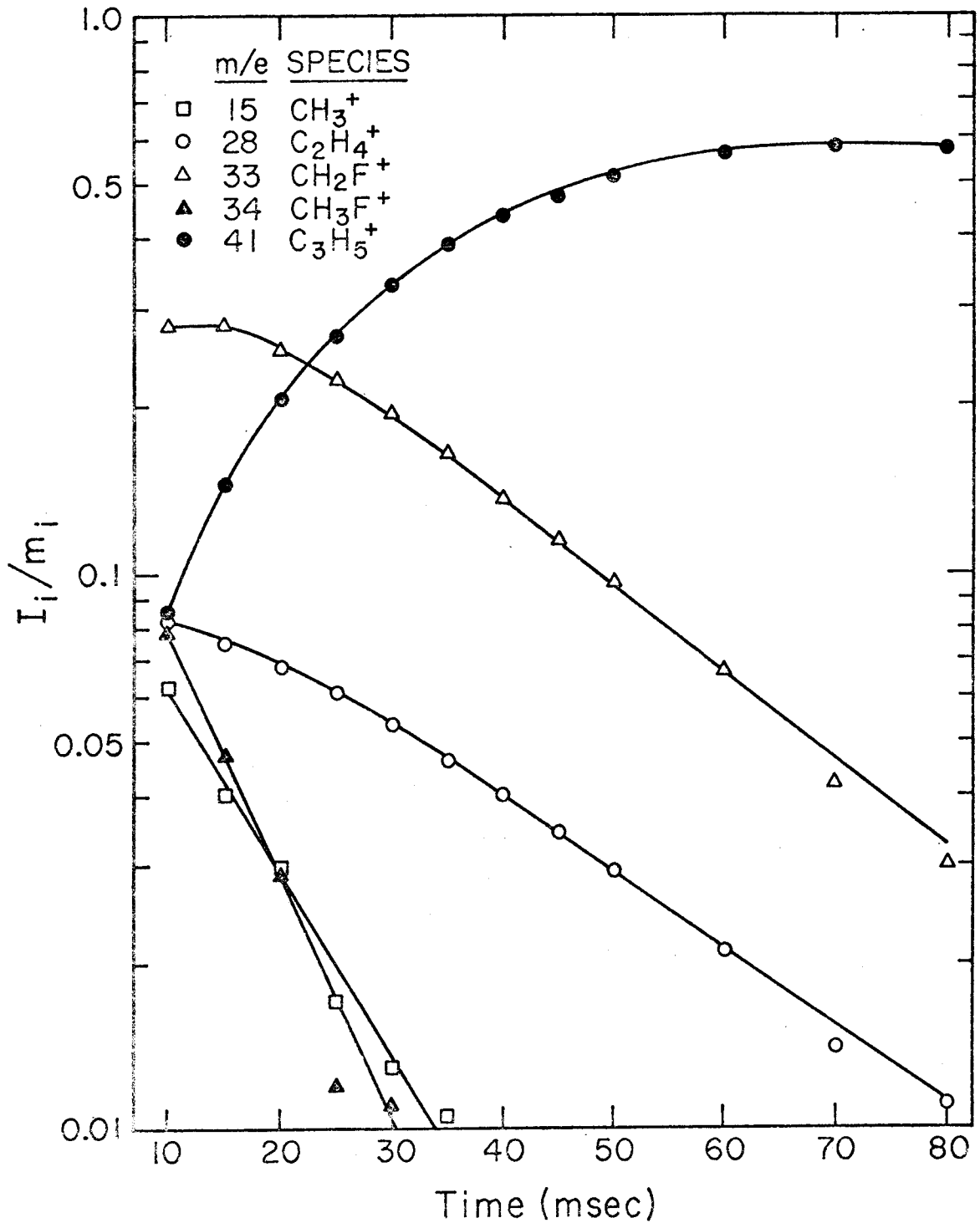
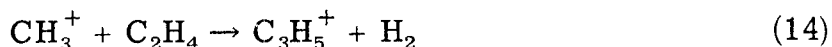


Fig. 4. Reactants and products in the mixture $\text{CH}_3\text{F}:\text{C}_2\text{H}_4$ are plotted as \log_{10} (unnormalized ion abundances) vs. time at 70 eV.

$C_2H_4^+$ and CH_2F^+ are the major reacting ions. CH_2F^+ is undergoing a condensation reaction with ethylene as shown in reaction 13. From the slope of linear portion of the CH_2F^+ ion abundance the rate constant for this



reaction is determined using the methods developed in Section C where the pressure used is the partial pressure of ethylene. Table VII contains the rate constants which were determined from these reactions. The rate constant for this reaction is $8.9 \times 10^{-10} \text{ cm}^3 \text{ molecule}^{-1} \text{ sec}^{-1}$ and is exothermic by 51 kcal/mole. Another possible reaction is that of CH_3^+ with



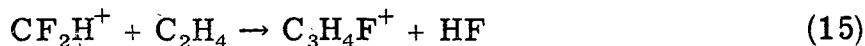
ethylene (reaction 14); however it was not possible to detect this reaction nor was it detected by Munson and Field.¹⁸ This reaction is exothermic by 47.3 kcal/mole; however the relative ion abundance of CH_3^+ is so low at all pressures and electron energies that reaction 14 is undetectable.

$CH_2F_2 + C_2H_4$. The reactions of CH_2F_2 with ethylene are very similar to those of CH_3F with ethylene. CH_2F^+ is the major product formed as is shown in reaction 8 and it undergoes the same condensation as reaction 13. The rate constant for the reaction is shown in Table VII and is smaller than that obtained from the CH_3F reaction; however it differs by about 17% which is within the error limits of the experiment. A secondary reaction which occurs in this experiment is reaction 15

TABLE VII. Experimental rate constants for the reactions of fluoromethyl cations with ethylene.

Species	Reaction	k_i (10^{-10} cm ³ molecule ⁻¹ sec ⁻¹)	k_{total} (10^{-10} cm ³ molecule ⁻¹ sec ⁻¹)
C ₂ H ₄	C ₂ H ₄ ⁺ + C ₂ H ₄ → C ₃ H ₅ ⁺ + CH ₃	7.9 ± 1.2	7.9 ± 1.2
CH ₃ F	CH ₂ F ⁺ + C ₂ H ₄ → C ₃ H ₅ ⁺ + HF	9.4 ± 1.2	9.4 ± 1.2
	CH ₃ ⁺ + C ₂ H ₄ → C ₃ H ₅ ⁺ + H ₂	- - - - ^a	15.4 ± 2.0
CH ₂ F ₂	CH ₂ F ⁺ + C ₂ H ₄ → C ₃ H ₅ ⁺ + HF	7.3 ± 1.8	7.3 ± 1.8
	CF ₂ H ⁺ + C ₂ H ₄ → C ₃ H ₄ F ⁺ + HF	6.3 ^b	8.3 ^b
CF ₃ H	CF ₂ H ⁺ + C ₂ H ₄ → C ₃ H ₄ F ⁺ + HF	5.4 ± 1.5	5.4 ± 1.5
	CF ₃ ⁺ + C ₂ H ₄ → C ₃ H ₄ F ⁺ + F ₂	5.2 ± 0.7 ^c	7.3 ± 0.4

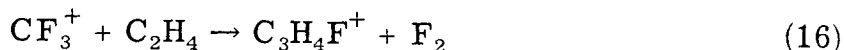
- a) There is no definite indication that this reaction actually occurs; however, the rate constants determined in ethylene did not overlap with those determined in CH₃F only.
- b) No error estimate available; this number was obtained by subtracting two rate constants.
- c) This number was obtained from subtracting the two rate constants.



which is the analogous condensation reaction which leaves the fluoropropenyl (fluoroallyl) cation.

CF₃H + C₂H₄. The primary reactant ion in the binary mixture of CF₃H and ethylene is CF₂H⁺. It undergoes reaction 15 as the major cross

reaction. The rate constant for this reaction is shown in Table VII and it includes the rate constant found in the $\text{CH}_2\text{F}_2 + \text{C}_2\text{H}_4$ reaction within its limits. Some evidence for the occurrence of reaction 16 is evidenced by a double resonance peak and a difference in rate constant for the



reactions with and without ethylene (the rate constant spreads do not overlap). However this reaction seems unlikely because it will require a 1,1 F_2 elimination.

C_2D_4 . Fluoromethyl cation reactions with ethylene- d_4 result in a range of deuterated products which indicate the possibility of a long intermediate lifetime and quite likely an isotope effect. Table VIII gathers together the different reactants, reactions and products.

CH_2F^+ reacting with ethylene exhibits almost equal probability to eliminate HF or DF which is not consistent with the statistical distribution for the system. A calculation of the isotope effect gives a value of 1.6. Using the results of Abramson and Futrell¹⁹ who find an isotope effect of 2.0 ± 0.3 for proton abstraction in methane, the product distribution seems to exhibit a statistical distribution corrected by an appropriate isotope effect. Reaction of CH_2F^+ plus ethylene to eliminate H_2 or HD is extremely weak compared to all the other reactions; however it too seems to obey a statistical distribution with an isotope effect. The product corresponding to H_2 elimination simply could not be observed.

Electrophillic attack by CF_2H^+ on ethylene- d_4 also shows a product distribution which favors HF elimination; however a calculation

TABLE VIII. Product distributions for the reactions of fluoromethyl cations with ethylene-d₄.

Species	Reactions Observed	Product Dist.	Statistical Dist.	Isotope Effect
<u>CH₃F</u>	CH ₂ F ⁺ + C ₂ D ₄ → C ₃ D ₃ H ₂ ⁺ + DF → C ₃ D ₄ H ⁺ + HF	55.0 45.0	66.7 33.3	1.6
<u>CH₂F₂</u>	CH ₂ F ⁺ + C ₂ D ₄ → C ₃ D ₃ H ₂ ⁺ + DF → C ₃ D ₄ H ⁺ + HF	55.0 45.0	66.7 33.3	1.6
	CH ₂ F ⁺ + C ₂ D ₄ → C ₃ D ₂ H ₂ F ⁺ + D ₂ → C ₃ D ₃ HF ⁺ + HD → C ₃ D ₄ F ⁺ + H ₂	23.2 76.8 0.0	40.0 53.3 6.7	2.5
	CF ₂ H ⁺ + C ₂ D ₄ → C ₃ D ₃ HF ⁺ + DF → C ₃ D ₄ F ⁺ + HF	62.5 37.5	80.0 20.0	2.4
<u>CF₃H</u>	CF ₂ H ⁺ + C ₂ D ₄ → C ₃ D ₃ HF ⁺ + DF → C ₃ D ₄ F ⁺ + HF	69. ^a 31. ^a	80.0 20.0	1.8

a) Experimental difficulties were encountered causing higher expectations of error for these result.

of the isotope effect for this reaction is consistent with the previous two reactions.

Each of these three reactions exhibit a product distribution and isotope effect which is consistent with complete scrambling of the hydride and deuteride species. This reaction and these effects will be discussed in Section F.

E. Fluoromethyl Cation Reactions with Benzene

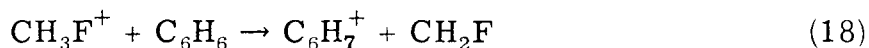
C₆H₆. Mass spectral analysis of benzene ion-molecule reactions observe fragmentation and dimerization. Fragmentation of benzene at 70 eV produces at least fifteen different species of which the most prominent are C₆H₆⁺, C₆H₅⁺, C₄H₄⁺, C₄H₃⁺, C₄H₂⁺, and C₃H₃⁺.²⁰ Dimerization products observed are C₁₂H_{9,10,11}⁺, C₉H₇⁺ and C₁₀H₈⁺.²⁰ At higher pressures (10⁻³ to 0.32 torr) C₆H₇⁺ and C₁₂H₁₂⁺ are among the products of the ion molecule reactions.²¹ And at pressures (0.025 to 1.0 torr) primarily the C₁₀ and C₁₂ dimerization products are found.²² Clearly the C₇ adduct formed from electrophilic attack is not a primary product of the benzene ion-molecule reactions.

In a binary mixture of methyl iodide and benzene Theard and Hamill²³ report the electrophilic addition reaction 17 of methyl cation



to benzene. A product distribution from the reaction of CD₃I and C₆H₆ at 18 eV shows the elimination products to the D₂ (15%), HD (72%) and H₂ (13%)²⁰ which favorably compares with the equivalent experiment of Theard and Hamill.²³ Field, Hamlet and Libby²⁴ observe the proton transfer reaction CH₅⁺ + C₆H₆ → C₆H₇⁺ + CH₄ in a methane-benzene mixture and also observe the dimerization reaction.

CH₃F + C₆H₆. Similar reactions occur for a mixture of fluoromethane and benzene. An effective proton transfer reaction (reaction 8) occurs between the parent ion of methyl fluoride and benzene.

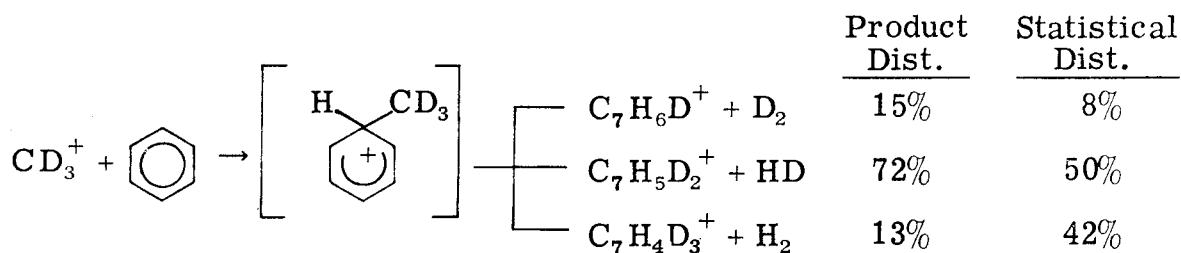


Electrophillic addition to benzene (reaction 19) of the fluoromethyl cation is analogous to the reaction observed by Theard and Hamill.²³ Essential total HF elimination is observed in this reaction producing

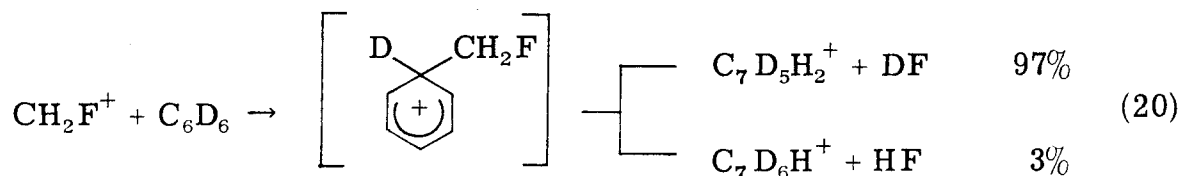


a benzyl cation.

$\text{CH}_3\text{F} + \text{C}_6\text{D}_6$. Significant isotopic scrambling was observed in the reaction of deuteromethyl cation with benzene. In contrast reaction



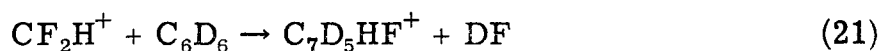
19 preferentially eliminates DF (reaction 20) in the reaction with



benzene-d₆. A definite reaction mechanism probably accounts for this result. The single fluoride substituent has altered the characteristics of the methyl cation reaction. Also the protonation reaction 18 is observed to occur.

$\text{CH}_2\text{F}_2 + \text{C}_6\text{D}_6$. Again we find reaction 20 as the predominant reaction with a similar product distribution. Double resonance

experiments confirm that this is indeed reaction 20 where the reactant ion CH_2F^+ is produced from reaction 8. Difluoromethyl cation also reacts with benzene- d_6 (reaction 21) evidencing no observable hydride scrambling.



$\text{CF}_4 + \text{C}_6\text{D}_6$. Reaction of CF_4 plus benzene- d_6 resembles reactions 20 and 21 in that a substituted benzyl cation is produced (reaction 22). It might be expected that this reaction would proceed through a



mechanism similar to that of reactions 20 and 21.

F. Relative Reactivities of the Fluoromethyl Cations

Fluoride and Hydride Affinities. The fluoride and hydride affinities (see Table IV) of the fluoromethyl cations have the relative ordering of the CF_3^+ and CH_3^+ ions reversed. In an effort to explain this effect and to explain the relative ordering as found, the heterolytic dissociation process is broken into two steps as shown in Table IX. The first step illustrates the energy necessary to rupture the bond and the second step is the electron transfer process. From Table IV the ordering of the ionization potentials of the radicals is found to be $\text{CH}_3 > \text{CF}_3 > \text{CH}_2\text{F} > \text{CF}_2\text{H}$. For the hydride affinities the ordering of the ionization potentials is clearly the determining factor because the RH bond energies are all essentially the same. In the case of the fluoride affinities

TABLE IX. Fluoride and hydride bond breaking.
(All values in kcal/mole.)

R	RF →	R + F →	R ⁺ + F ⁻	RH →	R + H →	R ⁺ + H ⁻
CH ₃	108.0	144.0		103.2	208.9	
CH ₂ F	119.2	124.4		100.2	189.3	
CF ₂ H	126.0	116.8		101.0	181.7	
CF ₃	128.4	127.9		105.9	192.8	

again the relative ionization potentials are a critical factor; however the reversal of the CH₃⁺ and CF₃⁺ ions is caused by the relative differences in the two CF bonds caused by successive fluorine substitution.

Ionization Potential. Planarity or nonplanarity of the respective radicals is a criterion which gives an ordering similar to that of the ionization potentials. The relative order of the substituent angle with the plane of the radical is CH₃ > CH₂F > CF₂H > CF₃ where CH₃ is planar.^{11,25} Significantly, successive substitution of fluorines onto the carbon atom induces a higher degree of nonplanarity of the molecule. This nonplanarity most likely arises from the repulsive interaction between the π orbitals on fluorine and the unpaired electron. Consequently the unpaired electron will become less bound as each fluorine atom is substituted onto the carbon and will incorporate σ character to minimize the interaction with the fluorine π orbitals. Fessenden and Shuler¹¹ employing esr techniques show that each additional fluorine substituent causes a greater degree of σ character incorporation into

the unpaired orbital [CF_2H (10% σ) and CF_3 (21% σ)]. However the significant nonplanarity of CF_3 (17.8° substituent angle with the plane) causes weakening of the CF bonds due to repulsive interactions which would allow a lowering of the energy of the unpaired orbital and an increase in the ionization potential. Essentially then the nonplanarity of the radical determines the ordering of the ionization potentials until bond-bond interactions cause bond weakening.

CF Bond Energies. The reversal in the ordering of the fluoride affinities is due to the stability of the $\text{F}_3\text{C-F}$ bond as compared to the $\text{H}_3\text{C-F}$ bond. The order of the strength of the CF bond is $\text{CF}_4 > \text{CF}_3\text{H} > \text{CH}_2\text{F}_2 > \text{CH}_3\text{F}$. Obviously the CF bond strength goes up with successive fluorine substitution. An important effect in determining this order is the repulsive interactions between the nonbonding orbitals on the fluorine atom and the adjacent σ bond. In terms of intramolecular distances the nonbonding fluorine orbitals and the adjacent σ bond should be the shortest as compared to the distance between nonbonding orbitals on adjacent fluorines. If the adjacent bond is a CH bond the repulsive interactions should be relatively high because the net charge on the carbon is negative; however an adjacent CF bond should provide a lower interaction effect because the net charge on the carbon from this bond is positive. In Hartree-Fock calculations on the fluoromethanes the net charge on the carbon is reported as -0.739, -0.140, 0.327, 0.665, and 0.936 for the series CH_4 , CH_3F , CH_2F_2 , CF_3H and CF_4 .²⁶ Consequently the CF bonds have the effect of withdrawing electron density while CH bonds enhance the electron density on the carbon atom. Therefore an

adjacent CH bond is detrimental to a CF bond while an adjacent CF bond has a much less disturbing effect. This suggests that the ordering of CF bond energies is dependent upon the number of CH (or CF) bonds on the carbon. Ultimately the interplay of the bonding effect with the change in ionization potential determines the order of fluoride and hydride affinities.

$\text{CH}_2\text{N}_3\text{F}^+$ The reaction intermediate is quite likely a substituted propyl cation which subsequently decomposes by way of a 1,2 elimination to form a propenyl (allyl) or substituted propenyl cation. The considerable isotopic scrambling and the calculated isotope effect indicate that the reaction intermediate is long lived enough to permit essentially complete (statistical) isotopic scrambling. In all of these reactions a 1,2 elimination process is most likely.

Given the 55:45 DF to HF elimination in reaction 13 an isotope effect of 1.6 is calculated which is consistent with previous determinations of isotope effects for protonation (and deuteration) of methane, and elimination from 2-propanol.¹⁹ Suggested as the mechanisms for isotopic scrambling are 1,3 isotope exchange allowed by rotation about the carbon-carbon single bonds and isomeric rearrangements characterized by hydride and deuteride shifts between nearest-neighbor carbon centers. A small contribution to the analogous $\text{C}_3\text{H}_4\text{F}^+$ peak by electrophillic attack of CH_2F^+ on ethylene shows almost 80% HD elimination.

The isotope effect determined for the reaction of CF_2H^+ and ethylene favors HF elimination with a resultant isotope effect of 2.6. Since 1,1 elimination would result in a highly unstable carbonium ion for the 1,1-difluoropropyl cation, isotopic exchange is probably the cause

for the existence of appreciable HF elimination. The high incidence of HF elimination strongly suggests a long-lived difluoropropyl cation which would allow migration of the single hydride to a preferential position on the middle carbon.

1,2 DF elimination is the most likely mechanism for the reaction of CF_3^+ with ethylene- d_4 ; however there is no direct evidence to support this conclusion. The relative instability of a carbonium ion with three fluorine substituents on the β carbon would suggest rapid DF elimination to form the unsaturated substituted allyl cation.

Rate Constants. The long-range interaction of an ion with a dipole is given by $V(r) = -\alpha e^2/2r^4 - \mu e \cos\theta/r^2$ where α is the polarizability of the neutral, e is the electronic charge, μ is the dipole moment of the neutral and θ is the angle of the dipole with r . The polarizabilities and dipole moments of the reactants have been experimentally determined (see Table X).²⁷ And the calculated dipole moments of the fluoromethanes (CH_3F , CH_2F_2 and CF_3H) compare favorably with these results.²⁶

The large relative polarizability of ethylene compared to methane and the fluoromethanes suggests a reason for the higher experimental rate constants associated with the electrophilic addition of the fluoromethyl cations to ethylene. The dipole term which is a much longer range effect seems to have a lower relative effect upon the rate constant because the rate constants for the fluoromethyl cations reactions with fluoromethane neutrals are less than the fluoromethyl cation-ethylene rate constants. Also presumed important is the dominance of the

polarizability term at short range compared to the dipole term.

TABLE X. Polarizabilities and dipole moments of the neutrals for which rate constants were determined.

Species	μ (D.)	$\alpha (\times 10^{-26} \text{ cm}^3)$
CH ₄	0.0	2.56
CH ₃ F	1.79	2.57
CH ₂ F ₂	1.96	2.69
CF ₃ H	1.64	2.77
CF ₄	0.0	2.82
C ₂ H ₄	0.0	4.10

Orientational effects in the reactions of the fluoromethyl cations with the fluoromethyl neutrals are important only within the effect of the dipolar term of the long-range interaction. It is expected that the dipole moment for the three fluoromethanes will line up the attacking positive ion on the fluoro-substituents of the neutral thereby enhancing the possibility of a fluoride exchange reaction. Much less important, although somewhat influential in the reactions with ethylene, is the orientation of the planar fluoromethyl cation to the neutral. If the plane of the attacking fluoromethyl cation is perpendicular to the attacked site, reaction is more likely than if the plane is parallel to the attacked site.

Table XI contains a comparison of the calculated Langevin rate constant²⁸ with the experimental rate constant for the reactions of the

fluoromethyl cations with ethylene. The Langevin rate constant is $k = 2\pi e(\alpha/\mu)^{\frac{1}{2}}$ where e is the electronic charge, α is the polarizability and μ is the reduced mass. The greater value of the Langevin rate constant as compared to the experimental rate constant indicates that a complex does not form or necessarily go to products on each collision. Similar results are observed for the fluoride transfer reactions.

TABLE XI. Calculated and experimental rate constants for fluoromethyl cation reactions. (All rates are $k \times 10^{-10} \text{ cm}^3 \text{ molecule}^{-1} \text{ sec}^{-1}$.)

Reaction	k_{exp}	k_{calc}
$\text{CH}_2\text{F}^+ + \text{C}_2\text{H}_4$	7.3	12.1
$\text{CF}_2\text{H}^+ + \text{C}_2\text{H}_4$	5.4	11.1
$\text{CF}_3^+ + \text{C}_2\text{H}_4$	5.2	10.6
$\text{CF}_2\text{H}^+ + \text{CH}_2\text{F}_2$	1.9	7.6
$\text{CF}_3^+ + \text{CF}_3\text{H}$	2.1	8.6

Once a complex has formed, the possibility of reverting to original reactants exists. In the case of ethylene no observable amount of deuterated fluoromethyl cation was observed indicating essentially complete conversion of each complex formed to products. For the reaction of fluoromethyl cation reactions with one of the fluoromethane neutrals a complex is formed which is essentially a fluoronium ion intermediate although the most likely path for this

reaction to follow is decomposition into products, reversion of the intermediate to reactants should be quite likely especially in the reaction $\text{CF}_2\text{H}^+ + \text{CH}_2\text{F}_2 \rightarrow \text{CH}_2\text{F}^+ + \text{CF}_3\text{H}$ where the two ions have such similar fluoride affinities.

Electrophillic Addition. Electrophillic addition of fluoromethyl cations to benzene exhibits no isotopic scrambling which is in direct contrast to the attack of both methyl cation on benzene and the reaction of the fluoromethyl cations with ethylene.

The relative stability of the products and reactants are shown in Fig. 5.²⁹ The effect of substituting a fluorine into the methyl cation has the effect of destabilizing the intermediate with respect to the products. While significant isotopic scrambling is observed in the electrophillic attack of fluoromethyl cation on ethylene, essentially no isotopic scrambling occurs in the reaction of this species with benzene. In contrast the reaction of methyl cation with benzene exhibits isotopic scrambling.

On the basis of the reactions of methyl and fluoromethyl cations with benzene it is suggested that the destabilizing effect of the fluorine substituent upon the reaction intermediate causes a rapid elimination of DF. For the methyl cation reaction with benzene the stability of the intermediate with respect to the products allows a much longer lived intermediate which can undergo isotopic scrambling, although reaction 17 does show a preference for HD elimination. The constraints imposed by the rigid ring system may mitigate against isotopic scrambling.

Fluoromethyl cation attack on ethylene exhibits a contrary effect

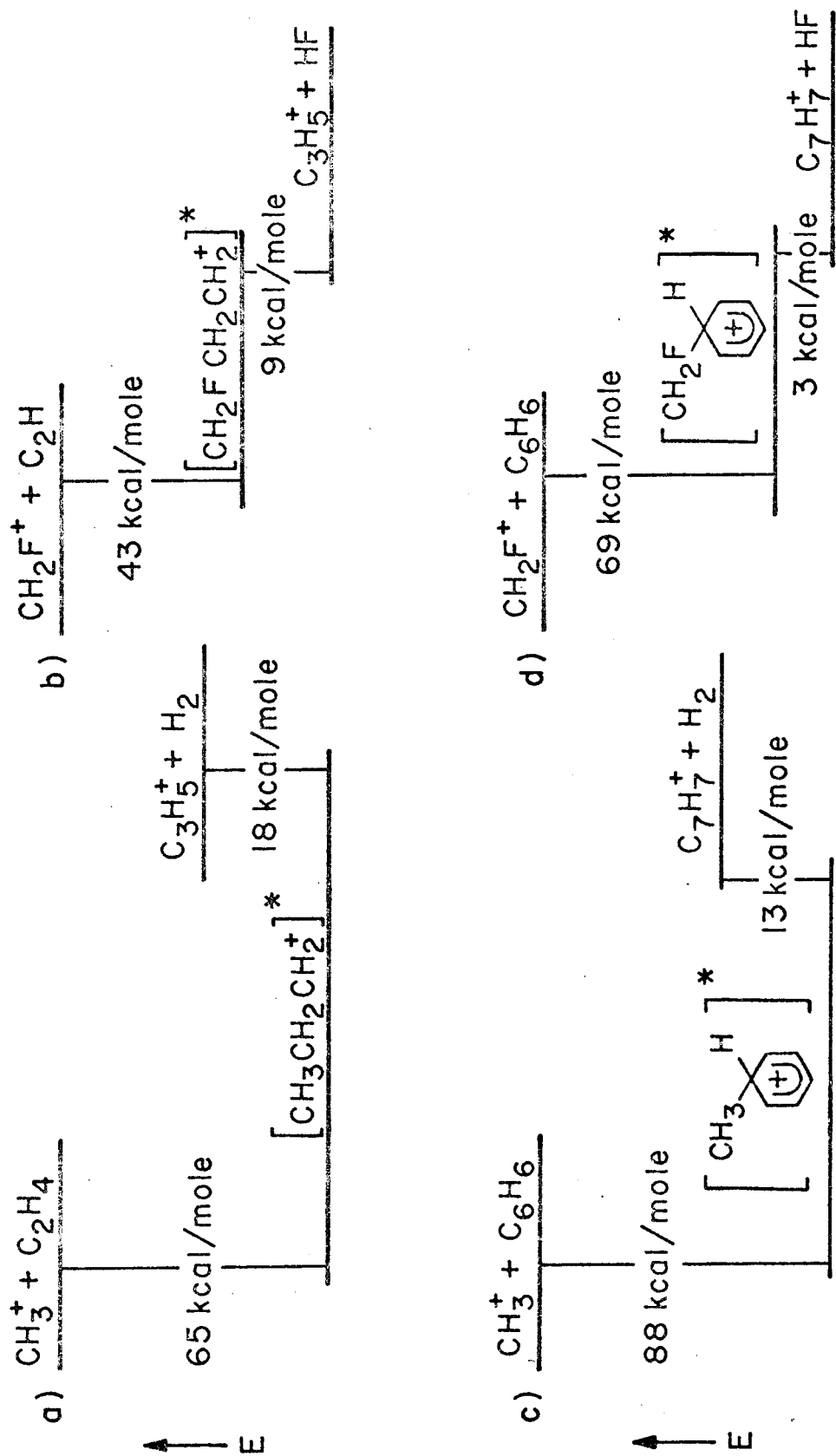


Fig. 5. Relative ordering of products, intermediates and reactants.

where, even though the reaction intermediate is again destabilized by the fluorine substituent, isotopic scrambling still occurs. If complete scrambling occurred, then the observed isotopic product distribution reflects an isotope effect favoring elimination of HF over DF by a factor of 1.6-2.5 (Table VIII). These results are consistent with isotope effects (1.7 favoring H₂O) for 1,2 elimination of HDO and H₂O from chemically activated CD₂CDOHCH₃.¹⁹ Structural rearrangements could explain this phenomenon where 1,3 isotopic exchange, 1,3 fluoride transfer and 2,3 hydride transfer could stabilize the intermediate and provide the isotopic scrambling observed. So, differences in the reactions of fluoromethyl cations are assumed to arise from structural rearrangements which cannot easily occur under the constraints imposed by a benzene ring.

To properly characterize this effect a second series of reactions are suggested; wherein the reactions of deuterated methyl and fluoromethyl cations with 1-cyclohexene and 1,3 cyclohexadiene would be investigated. The destabilizing effect of the fluorine substituent would still be a factor and the intermediate would be alkyl cation; however the structure of the substituted cyclohexane and substituted cyclohexene cations would significantly enhance the probability of HF elimination. It would be anticipated, if structural rearrangements are a significant factor, that 1,3 cyclohexadiene would exhibit almost complete HF elimination and that cyclohexene would also show a high degree of HF elimination.

G. Summary

Gas phase ion-molecule reactions provide a unique opportunity to study the factors which influence reactions in an environment which is totally devoid of all influences other than molecular ones. The relative stability of the fluoromethyl cations has been an interesting consequence of this. Carbonium ion stability is rather clearly shown to be dependent upon the nature of the nucleophile. The relative fluoride affinities ($\text{CF}_3^+ > \text{CH}_3^+ > \text{CH}_2\text{F}^+ > \text{CF}_2\text{H}^+$) of the fluoromethyl cations have been experimentally determined and contrasted with the calculated relative hydride affinities ($\text{CH}_3^+ > \text{CF}_3^+ > \text{CH}_2\text{F}^+ > \text{CF}_2\text{H}^+$). The differences in the orders of these ions have been discussed in detail and are related to the ionization potentials of the radicals and the relative CF and CH bond energies. Also the trapped ion mode of the icr has been employed to quantitatively determine the free energy (and enthalpy) for the reaction $\text{CF}_2\text{H}^+ + \text{CH}_2\text{F}_2 \rightarrow \text{CH}_2\text{F}^+ + \text{CF}_3\text{H}$ ($\Delta H_r = 0.8$ kcal).

Electrophillic addition to ethylene and benzene has been studied in some detail with the discovery of significant differences in reaction results for the neutrals. The rate constants of the fluoromethyl cation reactions with ethylene are compared to those of the fluoromethyl cations with the fluoromethanes and the factors which influence these rate constants have been discussed. Reactions with ethylene- d_4 evidence high isotopic scrambling and isotope effects which are comparable to another elimination reaction. The mechanism for this reaction is suggested to be electrophillic attack with subsequent 1,2 HF elimination from the substituted propyl cation.

Electrophilic addition of fluoromethyl cations to benzene-d₆ was also investigated with the somewhat startling result that preferential DF elimination occurs. The characteristics of these reactions as compared to the ethylene reactions are discussed and an explanation for the differences in product distributions is developed which is based upon the destabilizing effect of a fluorine substituent on the intermediate and geometrical considerations.

References

1. J. L. Beachamp, Ann. Rev. Phys. Chem., 22, 527 (1971).
2. D. Holtz, J. L. Beachamp, and J. R. Eyler, J. Amer. Chem. Soc., 92, 7045 (1970).
3. T. B. McMahon and J. L. Beachamp, Rev. Sci. Instrum., in press.
4. J. L. Beachamp and R. C. Dunbar, J. Amer. Chem. Soc., 92, 1477 (1970).
5. F. Rosenbury, "Handbook of Electron Tube and Vacuum Techniques," Addison-Wesley Publishing Company, Inc., Reading, Mass., 1965.
6. a) J. L. Beachamp, D. Holtz, S. D. Woodgate, and S. L. Patt, J. Amer. Chem. Soc., in press; b) A. G. Marshall and S. E. Buttrill, J. Chem. Phys., 52, 2752 (1970); c) N. A. McAskill, Aust. J. Chem., 23, 2301 (1970); d) A. A. Herod, A. G. Harrison and N. A. McAskill, Can. J. Chem., 49, 2217 (1971).
7. C. J. Noutary, J. Res. N.B.S., 72A, 479 (1968).
8. G. Herzberg, Proc. Roy. Soc. (London), A262, 291 (1961).
9. J. A. Kerr and D. M. Timlin, Int. J. Chem. Kinet., III, 427 (1971).
10. M. Krauss, J. A. Walker, and V. H. Dibeler, J. Res. N.B.S. 72A, 281 (1968).
11. R. W. Fessenden and R. H. Shuler, J. Chem. Phys., 43, 2704 (1965); M. T. Rogers and L. D. Kispert, J. Chem. Phys., 46, 3193 (1967).
12. C. Lifshitz and W. A. Chupka, J. Chem. Phys., 47, 3439 (1967).
13. T. A. Walter, C. Lifshitz, W. A. Chupka, and J. Berkowitz, J. Chem. Phys., 51, 3531 (1969).
14. J. Heicklen, Advan. Photochem., 7, 57 (1969).

15. S. W. Benson, "Thermochemical Kinetics," John Wiley and Sons, Inc., New York, 1968.
16. a) M. T. Bowers, D. D. Elleman, and J. L. Beauchamp, J. Phys. Chem., 72, 3599 (1968); b) J. M. S. Henis, J. Chem. Phys., 52, 282 (1970); c) A. A. Herod and A. G. Harrison, Int. J. Mass Spectrom. Ion Phys., 4, 415 (1970).
17. A rate constant of $8.5 \times 10^{-10} \text{ cm}^3 \text{ molecules}^{-1} \text{ sec}^{-1}$ was determined by Herod and Harrison (Ref. 16c) and $8.1 \times 10^{-10} \text{ cm}^3 \text{ molecule}^{-1} \text{ sec}^{-1}$ was obtained by P. Miasek and J. L. Beauchamp (private communication).
18. M. S. B. Munson and F. H. Field, J. Amer. Chem. Soc., 91, 3413 (1969).
19. a) F. P. Abramson and J. H. Futrell, J. Chem. Phys., 45, 1925 (1966); b) J. L. Beauchamp and M. C. Caserio, to be published.
20. J. L. Beauchamp, unpublished results.
21. S. Wexler and R. P. Clow, J. Amer. Chem. Soc., 90, 3940 (1968).
22. S. Wexler and L. G. Pobo, J. Amer. Chem. Soc., 91, 7233 (1969).
23. L. P. Theard and W. H. Hamill, J. Amer. Chem. Soc., 84, 1134 (1961).
24. F. H. Field, P. Hamlet, and W. F. Libby, J. Amer. Chem. Soc., 91, 2839 (1969).

25. G. Herzberg, "Molecular Spectra and Molecular Structure, III. Electronic Spectra and Electronic Structure of Polyatomic Molecules," Van Nostrand Reinhold Co., New York, 1966.
26. C. R. Brundle, M. B. Robin, and H. Basch, J. Chem. Phys., 53, 2196 (1970).
27. E. W. Rothe and R. B. Bernstein, J. Chem. Phys., 31, 1619 (1959).
28. G. Gioumousis and D. P. Stevenson, J. Chem. Phys., 29, 294 (1958).
29. J. L. Beauchamp (private communication).